Fluid velocity slip and temperature jump at a solid surface

Teo, Melvin Ji Bin

2013

Teo, M. J. B. (2013). Fluid velocity slip and temperature jump at a solid surface. Doctoral thesis, Nanyang Technological University, Singapore.

https://hdl.handle.net/10356/61997

https://doi.org/10.32657/10356/61997

NANYANG TECHNOLOGICAL UNIVERSITY

FLUID VELOCITY SLIP AND TEMPERATURE JUMP AT A SOLID SURFACE

TEO JI BIN MELVIN

SCHOOL OF MECHANICAL AND AEROSPACE ENGINEERING

2013

FLUID VELOCITY SLIP AND TEMPERATURE JUMP AT A SOLID SURFACE

TEO JI BIN MELVIN

School of Mechanical and Aerospace Engineering

A thesis submitted to the Nanyang Technological University
in partial fulfilment of the requirement for the degree of
Doctor of Philosophy

2013

Abstract

This thesis focuses on the discontinuous transport profiles across fluid-solid interfaces that are commonly encountered in micro and nano fluid systems. Despite the long history of the jump boundary conditions, most of the existing theoretical models for gas-solid and liquid-solid interfaces fail to provide satisfactory predictions of experimental findings.

We first develop an adsorption model for fluid-solid interactions that is applicable to both gases and liquids. The various adsorption processes that take place simultaneously depend on factors such as the molecular energies, surface chemistry and surface fraction of vacant adsorption sites. Fluid molecules in each of these adsorption states emerge from the surface with different momenta and energies. The net velocity and temperature of the near-wall molecules, equivalent to the slip velocity and temperature jump, can be evaluated by considering the relative rates of adsorption.

Our first theoretical model focuses on the subject of fluid slip over solid surfaces, where the corresponding velocities of various adsorbed fluid molecules are analysed based on the dynamics of the adsorption processes. The slip velocity expression is obtained through the overall velocity distribution of the near-wall molecules. Predictions from the new general model are compared with experimental results from the literature for gas and liquid systems.

The motion by which mobile adsorbed fluid molecules traverse across a solid substrate has been suggested to occur through hops between adsorption sites. However, the slip velocity from such a mechanism has been shown to be significantly lower than that

observed experimentally. Surface diffusion of adsorbed molecules may develop in several ways other than surface hopping. We propose two surface diffusion mechanisms by which molecular slip may take place. These alternative mechanisms are capable of producing elevated molecular slip velocities that are much closer to measured quantities.

Using the proposed adsorption framework of fluid-solid interactions, we derive an interfacial temperature jump expression for gas-solid and liquid-solid interfaces. In this model, the temperature jump is evaluated by considering the energies of fluid molecules that correspond to their adsorption states. Experimental data from the literature is used as corroboration for the new model, which addresses the inadequacies of current temperature jump theory in the prediction of observed temperature jump behaviour.

Acknowledgements

I would first like to thank my supervisors, Associate Professor Chan Weng Kong and Associate Professor Shu Jian Jun, for their patience and guidance.

Next, I would also like to express my appreciation to the technical staff, Mr Yap Pow Khim, Eric from the Fluid Mechanics Lab and Mr Yuan Kee Hock from the Thermal and Fluids Laboratory for providing technical support and assistance in equipment purchase.

Postgraduate life would not have been complete without the company of fellow research students, past and present, from the Thermal and Fluids Laboratory and Researcher Room 2, some of whom have since become dear friends who I can count on for help and advice. Memories of our fun times together will be deeply cherished.

Finally and most importantly, I thank my family for their unwavering support and encouragement, especially over the last year.

Table of Contents

List of Figures

List of Tables

List of Symbols

A	surface area
b	slip length
b_T	temperature jump coefficient
c_v	specific heat at constant volume
D	diffusion coefficient
E	energy of molecules
E_a	activation energy
$f(\theta)$	surface coverage factor
h	characteristic length, channel height
k	thermal conductivity
k_B	Boltzmann constant
Kn	Knudsen number
l	channel length
m	mass of particle
n	coordinate normal to wall
p	pressure
$p(u,t)$	velocity probability distribution function
p_i	probability
Pr	Prandtl number
$\dot{Q}$	heat current
q''	heat flux
r	reflectance
R	specific gas constant
R_i	adsorption rate
R_k	Kapitza resistance
t	sticking time, transmittance
T	temperature
u	tangential velocity
w	channel width

x, y, z	cartesian coordinates
Z	acoustic impedance

Greek symbols

α	transmission probability
γ	ratio of specific heats, damping coefficient
$\dot{\gamma}$	shear rate
ε	coefficient of restitution
η	dynamic viscosity
$\eta(t)$	noise
θ	contact angle
λ	mean free path
μ	coefficient of friction
ρ	fluid density
σ	tangential momentum accommodation coefficient
σ_t	thermal accommodation coefficient
τ	mean sticking time
ν	probability of change in direction per unit time
ν_0	rateprefactor
$\varphi(t)$	waiting time distribution

Subscripts

ads	adsorbed
av	average
B	backward
des	desorbed
$diff$	diffuse
e	elastic
eff	effective
F	forward
g	gas
i	incident particles

ie	inelastic
m	mobile adsorption state
p	precursor state
r	reflected
s	surface
sp	specular
w	wall
0	referring to fluid at wall

1 Introduction

The nature of the boundary condition at a fluid-solid interface has been a long-standing conundrum. Slip and temperature jump boundary conditions, representing a discontinuity in the transport variable in across the interface, were first proposed close to two centuries ago in place of the conventional 'no-slip' type boundary conditions. This is fundamentally unsurprising due to the abrupt transition in molecular structure. The modelling of gas-solid boundary conditions within a kinetic theory framework offered much insight based on molecular interactions at the surface and was supported by numerous experiments and numerical simulations. Though the possible existence of liquid slip was first reported in 1860 (von Helmholtz and von Piotrowski), the appreciably smaller order of magnitude relative to transport quantities renders the effect of the interfacial jump virtually unnoticeable in large-scale liquid systems, allowing the mathematically-straightforward conventional boundary conditions to be applied without major repercussions. As micro and nanoscale liquid systems became more commonplace, attention to the boundary condition was rekindled – studies were performed to investigate the effect it has on the overall behaviour as well as possible enhancements in device performance.

Micro and nanoscale transport phenomena require different treatment from the macroscopic case as interactions between solid and fluid particles become more pronounced due to higher surface to volume ratio and shorter length scales. In this regime, inertial forces can typically be neglected while effects such as rarefaction, compressibility, viscous dissipation and surface energy have to be considered. For gases, the continuum model and assumption of thermodynamic equilibrium start to break down when characteristic dimensions decrease as shown in Fig. 1.1 (Gad-el-Hak 2003).

The same boundaries are less straightforward for liquid systems but the poor agreement of the conventional models with experimental findings reveals the inadequacies of these assumptions. In fact, it should be highlighted that the no-slip boundary condition originated as an assumption without any fundamental basis (Lamb 1932).

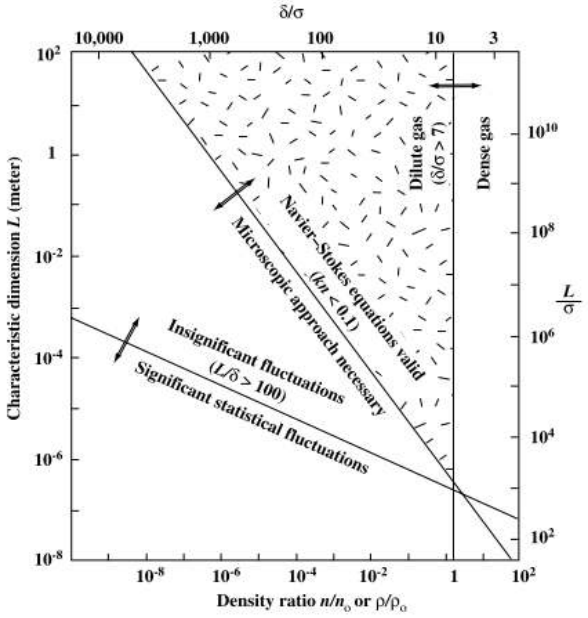

Fig. 1.1 Validity limits of flow models (Gad-el-Hak 2003)

Referring to Fig. 1.2, slip flow is characterised by a non-physical quantity termed as the slip length, which is a measure of the distance beyond the surface where velocity extrapolates to zero. This provides a convenient means of quantifying slip through experiments and the study of influencing factors such as surface roughness, wetting, electrical properties, dissolved gases and shear rates. Navier proposed the following linear slip model in (1823) which relates the tangential slip velocity, u_s, to the shear rate at the interface:

$$u_s = b \left. \frac{\partial u}{\partial x} \right|_s \tag{1.1}$$

Where b denotes the slip length, x is the normal from the surface pointing into the liquid. The subscript s refers to the value of the variable at the surface. This basic relation is employed in experimental models to link slip to measurable macroscopic quantities.

The temperature jump condition, sketched in Fig. 1.2, was postulated by Poisson in the form of Eqn. (1.2) in analogy with the slip boundary condition

$$T_f - T_w = b_T \left.\frac{\partial T}{\partial x}\right|_s \tag{1.2}$$

Where T_w and T_f refer to the temperatures of the wall and the gas immediately next to it, x is the coordinate normal to the wall directed towards the fluid, b_T represents the temperature jump coefficient or temperature jump length.

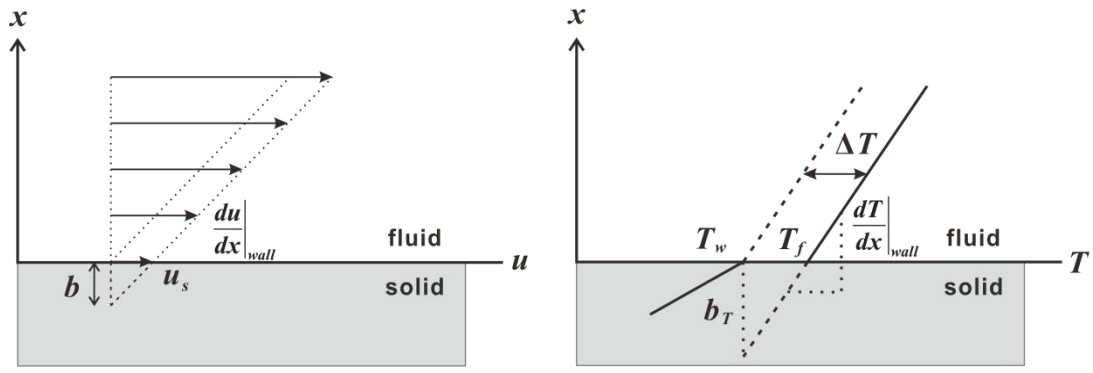

Fig. 1.2 Jump-type boundary conditions: (Left) Slip boundary condition -u_s: slip velocity, b: slip length. (Right) Temperature jump boundary condition - ΔT: temperature jump, T_w: wall temperature, T_f : surface fluid temperature, b_T: temperature jump length

In microscale gas systems, the extent of deviation from the quasi-equilibrium state is measured by the Knudsen number $Kn = \lambda / h$ which is defined as the ratio of the molecular mean free path λ to the characteristic domain length h. Typical MEMS and nanotechnology applications span the entire Knudsen regime. Kn physically represents the relative dominance of molecule-wall collisions over intermolecular collisions. Slip and temperature jump effects are expected to manifest macroscopically when Kn > 0.1. The

problem may be approached in two ways: solving the statistical Boltzmann equation or using the continuum transport equations coupled with slip or temperature jump boundary conditions. The continuum approach can provide accurate predictions in the slip regime ($10^{-3} < Kn < 0.1$). For free molecular conditions ($Kn > 10$), analytical solutions to the Boltzmann equation for simple geometries can be obtained (Fukui and Kaneko 1988) while molecular dynamics (MD) and direct simulation Monte Carlo (DSMC) can provide numerical solutions for complex geometries (Huang et al. 1997). Modelling of the transition regime ($0.1 < Kn < 10$) however, remains a problem by virtue of the equal importance of intermolecular and molecule-surface collisions. The theoretical models of gaseous slip and temperature jump are treated in the same vein - the latter is based on the exchange of momentum between the gas molecules and surface while the former considering energy balance of the gas molecules during the scattering process.

The mechanism of Newtonian liquid slip has yet to be ascertained but two models distinguishing between true slip and apparent slip have been hypothesised (Neto et al. 2005, Lauga et al. 2007). True slip refers to actual slipping of liquid molecules over the solid surface as opposed to apparent slip, where the sliding of liquid occurs over a less viscous layer that could be made up of a gas layer, surface coverage of nanobubbles, or even a density-depleted layer adjacent to the surface. For non-Newtonian fluids, slip has been attributed to adhesive failure of polymer chains and disentanglement of surface chains from the bulk chains (Léger et al. 1997).

The temperature jump at a liquid-solid interface was first discovered by Kapitza (1941) for superfluid helium at temperatures of around 2 K. Attempts at modelling the thermal boundary resistance using acoustic theory to describe phonon interactions at the interface have provided qualitative agreement at best. More recently, non-equilibrium

molecular dynamics simulations and time-domain thermoreflectance measurements have presented evidence of temperature jump across an interface of water and self-assembled monolayer at room temperatures, revealing it to be sensitive to wetting properties, surface roughness and even the direction of heat flux. These observed dependencies are potentially useful in microscale thermal devices but are poorly understood from a theoretical perspective.

Literature on theoretical and numerical investigations of gaseous slip and temperature jump is extensive, stemming from Maxwell's seminal work. Experimental studies of gaseous slip have largely been confined to flow rate measurements through microconduits, which contain deleterious sources of uncertainties in the measurement of channel height and flow rate. Most liquid slip length measurement techniques are unsuitable for gas flows owing to the low magnitudes of measurable quantities while velocity mapping for gas flows is comparatively less well-established. The viability of the atomic force microscopy (AFM) as a technique for gaseous slip measurements has recently been explored (Maali and Bhushan 2008, Honig et al. 2010).

At present, there is no direct technique that is capable of measuring liquid slip velocity or slip length. Popular experimental measurement techniques include the drainage force and tracer imaging methods. The drainage force method can be used with either the surface force apparatus or atomic force microscope, which possess high resolutions but at the same time are susceptible to experimental artefacts such as cantilever stiffness (Rodrigues et al. 2010) and contamination. Velocity tracking methods have comparatively poorer resolution. The lack of a benchmark has seemingly led to conflicting results being reported (Zhu and Granick 2002b). Slip length measurement uncertainties of 2 nm in drainage force methods have been claimed (Cottin-Bizonne et al. 2005); this is still

somewhat unsatisfactory for smaller slip lengths such as that of water on mica which is roughly 20 nm. There is room for improvement in the areas of resolution and reliability of slip length measurements before any empirical work on boundary slip can be deemed conclusive.

The theory of fluid-solid boundary conditions is currently lacking as most models are incapable of predicting experimentally observed results. Major drawbacks of the present models include the use of phenomenological constants and the use of separate models for gas-solid and liquid-solid interfaces. Some lingering questions that remain unanswered include the non-linear shear rate dependent slip, influence of wetting, near-wall molecular structure and dependence on surface temperature. These shortcomings serve as motivation for this thesis, where we aim to develop unified analytical models that are capable of describing the boundary jump phenomena for both gas and liquid systems.

1.1 Significance

The interfacial boundary condition is not only fundamentally important but also increasingly relevant in a wide range of fields, where it is of paramount interest in modern applications involving MEMS, microfluidic devices, biological systems and colloidal chemistry.

Fluid slip plays a crucial role in myriad applications. One archetypal advantage of slippage is the reduction of flow resistance in microchannels which is also associated with the increase in permeability of porous media. The efficiency and pump head of microscale viscous pumps, used in drug delivery systems and microelectronic cooling, vary with the degree of slip (Sharatchandra et al. 1998, Bataineh and Al-Nimr 2009). Consideration of

slip is important in hard disk drives as the gaseous flow at the slider head-disk interface typically lies in the slip and transitional regime. Due to its nanoscale order of magnitude, fluid slip possibly has unrealised potential applications especially in nanochannels.

The temperature jump finds uses in heat transfer applications like micro-cooling for electronic devices, micro heat-exchangers and fuel cells. In thermal management applications, a low thermal boundary resistance is desirable for increasing heat dissipation in microelectronic cooling while a high resistance could act as a thermal barrier. Large temperature jumps may even have potential novel uses in temperature shielding and as a form of passive temperature control. The recent discovery of the thermal rectification effect shows promise for the development of fluid-based thermal logic components (Murad and Puri 2013).

Majority of the latest studies in this area have been concentrated on investigating the effects of wetting and surface roughness, specifically with the use of superhydrophobic surfaces which are artificially patterned to allow pockets of dissolved gases and also chemically coated to reduce wettability. Such surfaces have the ability to induce high slip velocities and temperature jumps arising from secondary slip processes. A key issue that remains elusive is the true physical mechanism of the boundary jump. This will involve consideration of factors such as molecular interactions, lattice configuration of the substrate and near-wall molecular structure of the fluid. Coupled with the maturing of atomic manipulation techniques, tunable slip and temperature jump on designer lattices may be realised in the near future (Ternes et al. 2008, Gomes et al. 2012).

1.2 Objectives

The aims of this project are as follows:

- To perform a comprehensive survey of the jump boundary condition literature
- To propose a general framework for the discontinuity across an fluid-solid interface
- To develop a model for slip velocity at fluid-solid interfaces based on the general framework and propose other mechanisms for the surface diffusion slip motion
- To develop a unified model for temperature jump at fluid-solid interfaces using the general framework

1.3 Outline

This report presents work on the theoretical modelling of slip flow and temperature jump at fluid-solid interfaces. In Chapter 2, a comprehensive review of current analytical models, experimental techniques and influencing factors is carried out to highlight the current challenges in this area. A general adsorption model is developed in Chapter 3 to describe the interactions between near-wall fluid molecules and solid surface. This model serves as a framework for the theoretical modelling of the boundary jump phenomena. Based on this adsorption model, a new general model for the slip velocity of fluids on solid surfaces is introduced in Chapter 4. Comparisons with existing models and experimental results will be conducted. Next, two alternative mechanisms for molecular slip motion via surface diffusion are proposed in Chapter 5. Slip velocities occurring through these mechanisms are contrasted with that of the existing mechanism suggested in the literature. The problem presented in Chapter 6 involves the development of a new analytical model for the general fluid-solid temperature jump. Results obtained from this model will be validated with available results from the literature. Recommendations for future work are also outlined at the end of the report.

2 A Review of Fluid-Solid Boundary Conditions

The study of fluid-solid boundary conditions has been ongoing for more than a century, starting from gas-solid interfaces and progressing to that of the more complex liquid-solid case. Breakthroughs have been made on the theoretical and experimental fronts but the mechanism behind the phenomena remains a puzzle. This chapter provides a review of the theoretical models, numerical and experimental investigations that have been carried out till date. Probable mechanisms and factors that affect the interfacial discontinuity are also documented.

2.1 Mechanism of Fluid Slip on Solid Surfaces

The physical process of slip remains vague despite the plethora of experimental and theoretical studies. A fairly clear picture of gas-solid slip can be derived within the kinetic theory framework. In liquid-solid slip however, the scattering model is inadequate as the situation is confounded by intertwining of additional interactions with liquid molecules from the bulk flow. At this stage, the contentious influences of surface nanobubbles and wetting in experiments, among other factors, have to be isolated before the primary mechanism(s) can be identified. Nevertheless, several plausible slip models have been put forward.

Scattering Mechanism

In the billiard ball model of collisions between fluid and solid molecules, the nature of reflections governs the efficiency of the net momentum exchanged during the impacts. Maxwell conjectured that the transfer of tangential momentum occurs during diffuse reflections but not in specular reflections, which preserve the original velocity. The notion of diffuse reflections is somewhat fuzzy, but may be thought of as the fluid molecule undergoing several collisions with the solid molecules before escaping at the

same velocity as the solid. Defining the slip velocity as the mean velocity of near-wall particles (usually within a layer thickness of one mean free path), a higher proportion of specular reflections will result in higher slip velocity. This description is appropriate under rarefied conditions as fluid-solid collisions are prevalent in the vicinity of the surface due to the longer mean free paths. For denser fluids with shorter mean free paths, the contribution of scattering to slip is expected to be less dominant as fluid-fluid interactions become more important. The Maxwell model also fails to consider inelastic interactions that are intermediate between specular and diffuse reflections.

Surface Slip

Another model of slip depicts the actual motion of liquid molecules on the bed of solid molecules. This perspective is related to the induced structural ordering of near-wall fluid molecules. Adsorbed fluid molecules that are pinned in the wells of the substrate potential induce the rearrangement of neighbouring fluid molecules due to short-range interactions, forming epitaxial layers next to the surface (Israelachvili 2011). The regular structure is expected to be more significant in crystalline surfaces due to their periodic potential. A solid-like phase of water molecules on a mica surface has been observed experimentally using x-ray reflectivity, revealing density oscillations spanning a few monolayers(Cheng et al. 2001).

On a continuum scale, slip can be visualized as the interfacial fluid layer being dragged along the boundary by adjacent layers under shear. In fact, the evolution of slip should begin at the fluid-fluid interface where the bulk fluid and top-most epitaxial layer meet with the ordered layers beneath being initially locked (Barrat and Bocquet 1999). With increasing shear, the layers start to cleave gradually in a top-down sequence, culminating in the slip of the bottom-most fluid layer past the surface. This represents a macroscale

interpretation of slip. Zooming in further to the molecular details at the interface, the slipping of the interfacial layer can be pictured as surface diffusion with a net drift, comprising of a series of hops by the fluid molecules between substrate lattice sites while being subjected to an external field (Groß 2009).

There is some scepticism about the molecular slip model, as a rough estimate of the shear rate required for slip to develop in this manner far exceeds that attainable experimentally (Lauga et al. 2007). However, adopting the rate theory model where the hopping occurs by thermal vibration shows that it is not necessary for the hydrodynamic force to be greater than the dispersion forces for slip to occur.

A further issue has been brought up with regards to the interpretation of surface molecular motion as a continuum slip condition (Brenner and Ganesan 2000). Distinguishing between conditions at a boundary and boundary conditions, it was advocated that the correct slipping plane congruent with a continuum assumption should be at the edge of the boundary layer where mean molecular motion converges to a bulk effect.

Apparent Slip

Certain microscale phenomena such as the electrical double layer in electrokinetics that exhibit large velocity gradients within a thin boundary layer may also be represented using an apparent slip velocity (Cucchetti and Ying 1996). This approach simplifies the hydrodynamic analysis by allowing the use of continuum governing equations along with effective boundary conditions that account for the mesoscopic slip effect across the interfacial layer. The presence of a less viscous layer sandwiched between the surface and bulk flow has also been suggested as a possible cause of the anomalously high slip

lengths observed in experiments (de Gennes 2002). Possible film types may constitute dissolved gases, coating of nanobubbles or a density-depletion layer, the last of which has recently been disputed (Gutfreund et al. 2011). Though the above forms of apparent slip do not arise from true motion of liquid molecules relative to the surface, they may be exploited as artificial approaches of inducing low interfacial friction.

Non-Newtonian Slip

The slip of non-Newtonian fluids, in particular polymer flows, may be explained using polymer dynamics, which also provides a viable analog for the experimentally observed shear rate dependence of Newtonian fluids (Ala-Nissila et al. 2002). Entanglement states between moving bulk flow polymer chains and surface-grafted chains give rise to three primary slip regimes (Léger et al. 1997). In the no-slip regime of low shear rates, the bulk polymers remain locked to the surface polymers. At the critical shear rate, bound polymers begin to detach from the stretched surface polymers, resulting in the relative sliding of bulk and surface layers. The sliding velocity in this regime increases with increasing shear rate. Upon complete disentanglement, slip reaches its maximum and remains constant thereafter since the bulk flow has effectively disassociated from the surface polymer layer.

2.2 Factors Affecting Slip

The primary mechanism that drives slip may be unresolved but factors displaying an ostensible effect on the measured slip length have been identified through experiments and numerical simulations. Among the most investigated factors is the unusually large slip length of superhydrophobic surfaces which possess high contact angles owing to the combination of patterned roughness and surfactant coating. Another controversial factor is the influence of shear rate, particularly the non-linear change in slip lengths, which could open up more avenues to potential applications. Isolating any individual factor in

experimental studies is a challenging task since some of them might actually be complementary or even originate from identical physics of molecular interactions.

Surface Roughness

Contrary to intuition, roughness does not always act to reduce slip velocities. Richardson (1973) was one of the first to suggest that roughness suppresses slippage and that the macroscopic no-slip boundary condition originated from surface roughness. Experimental work on micro/nano-structured surfaces has produced inconclusive results. While negative slip lengths have been measured on grooved surfaces (Brigo et al. 2008), claims of corrugation-induced drag reduction have also been reported (Bonaccurso et al. 2003, Truesdell et al. 2006). Molecular dynamics simulations by Ziarani and Mohamad (2008) showed that slip velocity decreased monotonically with increasing roughness and that there was no significant change in slip behaviour between different topographic shapes of roughness. Cottin-Bizonne's group (2004) however found that nanometre-scale roughness resulted in reduced friction and were able to formulate a simple expression for the effective slip length of alternating strips of different slip lengths.

Vinogradova and Yakubov (2006) tried to address these discrepancies through their own experimental findings, whereby they concluded that the confusion over roughness's effect on slip arose from different definitions of the wall location prescribed by researchers. They demonstrated that the reduced drag observed in their experiments could be explained by a correction of the gap separation in their model. On the other hand, experimental studies on carbon nanotube coated surfaces revealed that the slip length increased with increasing roughness length scale in the Cassie state but remained constant with minimal slip in the Wenzel state. (The Wenzel state refers to a wetting phase where liquid penetrates the roughness cavities while liquid in the Cassie state sits

above the air pockets. Transition between both states occurs at a critical contact angle θ_c; liquid penetrates and fills the voids to minimise surface energy.) The validity of the Cassie and Wenzel theories has been questioned although it is generally agreed to be applicable under specific conditions (Bartell and Shepard 1953, Extrand 2003, Lauga and Squires 2005, Gao and McCarthy 2007, McHale 2007). Results of a recent study on corrugated hydrophobic surfaces have demonstrated transient slip behaviour, changing from partial slip to no slip after a few hours (Govardhan et al. 2009). This coincides with the transition from a Cassie to Wenzel state as observed from direct visualization of trapped air pockets. Current experimental efforts have been concentrated on biomimetic-inspired superhydrophobic surfaces due to the enhanced slip observed on these artificially structured surfaces (Oner and McCarthy 2000, Lau et al. 2003, Ou et al. 2004, Butt et al. 2006, Choi and Kim 2006).

The effect of surface roughness on slip is hard to quantify in theory since it not only involves the competition between multiple length scales but also the local flow conditions. The difficulty is reduced for macroscopic asperities of a periodic nature in a continuum flow system. Atomic-scale corrugations however necessitate the consideration of the influence of dispersion forces on the near-wall arrangement of the fluid molecules.

Wetting

The initial hypothesis that slippage would only occur on surfaces of low wettability due to the perceived weaker fluid-solid attraction was refuted after several experimental studies showed that slip was also present on completely wetted surfaces (Choi et al. 2003). Ho et al. (2011) presented MD simulation results showing evidence of slip at a wetting boundary and furthermore demonstrated that the slip velocity may even

increase with decreasing hydrophilic contact angle. By manipulating the atomic separation distance of the substrate, it appeared that a water molecule had a higher tendency to migrate to a neighbouring equilibrium site when it was nearer and hence result in large-scale slip.

The Blake-Tolstoi theory (see Section 2.4) predicts the qualitative trend of higher slip velocities with increasing contact angles due to the superior mobilities of liquid molecules on a non-wetting surface (Blake 1990, Ellis et al. 2003). Voronov et al.(2008) carried out a dimensional analysis based on data from MD simulations and realised that different fluid-solid pairs did not share the same slip lengths despite having similar contact angles, as was evident in their earlier work (Voronov et al. 2007). Their results illustrated that slip lengths may not always increase with a greater contact angle and that the relative molecular sizes of the fluid and solid should also be considered.

Near-Wall Fluid Molecular Structure

Early computational work on the epitaxial layering of near-wall fluid molecules has led to the investigation of its relationship with slip (Thompson and Robbins 1990). It should be noted that the near-wall ordering is indirectly linked to molecular-scale roughness, in terms of the potential exerted on the fluid molecules, and wetting, which can be ascribed to fluid-solid affinity. The dependence of slip on molecular structure is not straightforward given the counter-intuitive ability of a solid-like phase to produce stronger slip when fluid-solid molecular interaction is weak (Barrat and Bocquet 1999). Fluid monolayers experience weaker frictional forces compared to the molecules belonging to the bulk phase with the freedom to manoeuvre themselves, causing intermolecular jamming or locking to the substrate (Hall and Martin 1987). Slip can be envisaged to occur via a shear melting mechanism of the monolayers that is typically

observed in confined fluids, beginning from the outermost fluid-fluid layers and eventually propagating to the fluid-solid interface (Hersht and Rabin 1994, Zhu and Granick 2004).

On non-wetting interfaces, a depletion layer of lower local density is thought to be a contributing factor towards apparent slip (Tretheway and Meinhart 2004). Assuming that the viscosity remains constant, the apparent slip length can be estimated by

$$b = \int_{liquid} \left(\frac{\rho_{bulk}}{\rho_s(z)} - 1 \right) dz \tag{2.1}$$

where ρ_{bulk} and $\rho_s(z)$ refer to the liquid densities in the bulk flow and depletion layer.

The thin depletion layer between 5 and 20 Å measured for hexadecane gives a slip length of approximately 5 Å, which fails to account for the large values of up to 350 nm observed for similar interfaces in experiments (Wolff et al. 2008, Gutfreund et al. 2011). Hence, the assumption of depletion-enhanced slip may only hold for strongly hydrophobic surfaces.

Dissolved Gases

Slippage on hydrophobic surfaces has been associated with a thin layer of low viscosity fluid or vapour lying on the surface (Ruckenstein and Rajora 1983, Alexeyev and Vinogradova 1996). Andrienko et al. (2003) suggested that the fluid undergoes a prewetting transition during flow, generating a macroscopically thick gas film at the wall due to phase separation. The discovery of nanobubbles forming on hydrophobic surfaces from direct AFM measurements has lent credibility to this idea (Ishida et al. 2000, Lou et al. 2000, Yang et al. 2003). However, the effective slip in the case of isolated nanobubbles is expected to be smaller than that for a gas layer since the boundary flow is thought to

alternate between regions of complete slip (over the nanobubbles) and no-slip (over the surface). There have been suggestions that nanobubbles could also be responsible for shear-dependent slip (de Gennes 2002). Interestingly, nanobubbles have been detected for water on mica which is a completely wetting interface (Zhang et al. 2004). This might offer an alternative explanation for observed slip on hydrophilic surfaces. Some authors have previously reported lower slippage for degassed liquids which inhibit the growth of such bubbles (Boehnke et al. 1999, Granick et al. 2003). Though nanobubbles are generally undesirable in experimental slip measurements, they may allow for the possibility of controllable apparent slip since the fractional coverage of nanobubbles can be varied by temperature and solvent concentration.

The simple analytical two-phase models by de Gennes (2002) and Tretheway and Meinhart (2004) which consider the presence of a surface gas layer estimate slip lengths of about 7 μm. This result has two ramifications: (i) it may help to explain the atypically large slip lengths observed in certain experiments (Tretheway and Meinhart 2002, Choi and Kim 2006) (ii) the potential to induce enhanced slippage with a low viscosity surface film. It was shown that a fractional surface coverage of nanobubbles of around 40% is sufficient to generate slip lengths lying in the micrometre range.

Shear Rate

Another puzzle that remains to be solved is the dependence of slip behaviour on shear rate. This phenomenon was first discovered by Thompson and Troian (1997) in their MD simulations of Couette flow of a Newtonian liquid. At low shear rates, the results were consistent with the linear Navier slip boundary condition. Beyond a certain shear rate, the slip length began to increase non-linearly with shear-thinning being ruled out as a possible cause. Thus, the assumption of a constant slip length in experimental models

may not apply to the non-linear regime. The shear rates under consideration in MD simulations are generally too high to be realised experimentally. Nonetheless, several researchers have reported evidence of shear-dependent slip, while others have maintained that their results obey the linear Navier expression.

AFM measurements by Craig et al. (2001) exhibited an obvious variation of slip length with the approach velocity (proportional to the surface shear rate) of the colloidal probe towards a planar surface. Furthermore, the no-slip behaviour at low driving rates of the probe offers a plausible reason for the absence of slip flow in previous experiments. Zhu and Granick (2001) obtained similar results at shear rates below the onset of shear-thinning and even observed large slip lengths of up to 2 μm. It should be emphasised that the validity of the constant slip length model as applied in the above experiments is questionable.

It was subsequently suggested by de Gennes (2002) that the reduced hydrodynamic drainage forces leading to interpretations as shear-dependent slip were possibly due to the shear-induced nucleation of nanobubbles on the surfaces. At high shear rates, the nanobubbles may be compressed into a thin film carpeting the solid surface, over which the liquid slips.

Spikes and Granick (2003) had prior to this also proposed their own drainage force slip model pertaining to an assumption that boundary slip manifests only upon exceeding a critical shear stress value and that the ensuing slip length remains constant. Empirical fits revealed that these critical values are typically small and thus may not have been detected in earlier studies. However, their model did not demonstrate an adequate fit at higher shear stress values.

Lauga and Brenner (2004) developed a "leaking mattress" model for effective shear-dependent slippage caused by the formation of surface nanobubbles in surface force measurements. Their first-order model agreed fairly well with the experimental data of Zhu and Granick (2001) but is based on the assumption of 99% surface coverage of nanobubbles.

While the MD simulations of Thompson and Troian (1997) yielded unbounded slip behaviour, Martini et al. (2008a) found that asymptotically limiting slip could be obtained using a different wall model configuration in their MD simulations. The experimental results of Ulmanella and Ho (2008) from nanochannel flow measurements too hints at a limiting value of slip velocity at high shear rates.

2.3 Modelling of Gas Slip

The modelling of gaseous flow in the slip regimes encompasses both intermolecular interactions between gas molecules in the form of governing equations and gas-surface molecular interactions in the form of boundary conditions. Continuum governing equations coupled with appropriate slip conditions are convenient for theoretical analysis but not sufficiently robust to describe slip flow at high Kn due to non-equilibrium effects. In such cases, the statistical Boltzmann equation is able to describe the ballistic fluid behaviour. The prevailing slip models used for gases are the Maxwell-type collision models. Another recent interpretation of the fluid-solid interaction involves the use of gas adsorption concepts.

Maxwell Slip Model

The slippage of gases occurs when the minimum characteristic length scale is comparable to the mean free path of intermolecular collisions ($Kn > 10^{-3}$). In this regime, wall-molecule collisions dictate the gas flow while intermolecular collisions are almost

negligible. Maxwell (1879) proposed that the impact of gas molecules on a wall produces two kinds of collisions – specular and diffuse. In a specular reflection, the tangential momentum of the fluid molecule is conserved while during a diffuse reflection, the equilibrated fluid molecule is re-emitted with a tangential momentum equal to that of the wall. By convention, the fraction of molecules undergoing diffuse reflections is represented by the tangential momentum accommodation coefficient (TMAC) σ, and that of specular reflections by $(1-\sigma)$.

The mean tangential momentum flux p'' at the outer boundary of the Knudsen layer of one mean free path thickness is given by the sum of the incident flux p_i'' and reflected fluxes p_{sp}'' and p_{diff}''

$$p'' = p_i'' + (1-\sigma)\, p_{sp}'' + \sigma p_{diff}'' \tag{2.2}$$

where the specular flux $p_{sp}'' = -p_i''$ and diffuse flux $p_{diff}'' = -p_w'' = 0$.

Eqn. (2.2) is reduced to

$$p'' = \sigma p_i'' \tag{2.3}$$

The momentum flux can be evaluated from the following expression

$$p'' = \iiint v' p\left(c'\right) f_s\left(c'\right) dc' \tag{2.4}$$

where $f_s(c')$ refers to the velocity distribution function and c' denotes the velocity vectors u', v', w'.

By using suitable approximations for the velocity distribution functions, the slip velocity can be obtained as

$$u_s = \frac{2-\sigma}{\sigma}\alpha\frac{du}{dy} + \beta\frac{dT}{dx} \tag{2.5}$$

where the first term on the right represents the slip due to the velocity gradient normal to the surface and the second term is that due to the temperature gradient along the surface, also known as thermal creep.

Alternatively, a less rigorous derivation can be achieved based on the mean tangential velocities of surface gas molecules. The post-collisional tangential velocity u_r can be defined as

$$u_r = \sigma u_w + (1-\sigma) u_i \tag{2.6}$$

Where u_w and u_i are the average tangential wall and incident velocities respectively.

At the wall, half the molecules can be assumed to be reflected while the other half make up the incident population. The average tangential velocity of the gas molecules at the wall u_{av} is hence given by the expression

$$\begin{aligned} u_{av} &= \frac{u_r + u_i}{2} \\ &= \frac{\sigma}{2} u_w + \frac{2-\sigma}{2} u_i \end{aligned} \tag{2.7}$$

Considering that each molecule traverses one mean free path λ between each collision on average, u_i may be expressed as a Taylor expansion of u_{av} (Burgdorfer 1959)

$$u_i = u_{av} + \lambda \left. \frac{\partial u}{\partial y} \right|_{wall} + O\left(\lambda^2\right) \tag{2.8}$$

where y is the coordinate normal to the wall.

Finally, the slip velocity u_s, which is defined as the difference between u_{av} and u_w, is obtained as

$$u_s = \frac{2-\sigma}{\sigma}\lambda \left.\frac{\partial u}{\partial y}\right|_{wall} \tag{2.9}$$

Or in a non-dimensional form:

$$U_s = \frac{2-\sigma}{\sigma} Kn \left.\frac{\partial U}{\partial Y}\right|_{Y=0} \tag{2.10}$$

Variations of the above method such as using higher order expansions and $\frac{2}{3}\lambda$ instead of λ in Eqn. (2.8) have been proposed to improve the accuracy of the model at moderately large Kn numbers. Nevertheless, this continuum approach is not applicable for the transition and free-molecular regimes. It is also noted that the above slip velocity expression contains a singularity in the absence of diffuse reflections which hypothetically occurs on an atomically smooth surface. Other criticisms of the Maxwell formulation include the neglect of inelastic scattering and assumption of a constant TMAC value instead of a local value that should be determined by conditions at the location of impact.

Langmuir Slip Model

An alternative slip model based on the gas-solid interactions as described by Langmuir's theory of adsorption of gases on solids has also been proposed (Bhattacharya and Eu 1987, Myong 2004). One fundamental difference between the Maxwell and Langmuir model lies in the treatment of the wall. In the former, the wall is assumed to be a macroscopic flat surface while the latter considers discrete sites that each interact with a single atom. A TMAC-like parameter s accounts for the fraction of incident interacting gas molecules that are adsorbed and subsequently desorbed at the same velocity as the wall. Correspondingly, the fraction of specular-type interactions is given by $(1-s)$. The mean velocity of surface molecules is

$$u_{slip} = (1-s)u_g + su_w \tag{2.11}$$

s can be obtained from adsorption isotherms such as that of Langmuir

$$s = \frac{\beta p}{1 + \beta p} \tag{2.12}$$

where p is the hydrostatic pressure, $\beta = k/k_B T$ with k being a function of the gas-solid interaction parameters.

The resulting expression for the dimensionless slip velocity is

$$u_{slip} = \frac{1}{1 + \bar{\beta} p} \tag{2.13}$$

where $\bar{\beta} = 1/4\omega Kn$, ω is a function of the equilibrium constant, the local temperature and the heat of adsorption.

Myong (2004) extended the model to consider the dissociative adsorption of diatomic gas molecules which requires two adjacent vacant sites and thus has a second-order dependence on the surface coverage. The Langmuir model exhibited slightly improved agreement with experimental results for nitrogen gas flows as compared to the Maxwell model but it is not mentioned if dissociative adsorption of the nitrogen molecule actually occurs on the surface used in the experiment.

The use of adsorption concepts in boundary slip provides physical meaning to Maxwell's phenomenological accommodation coefficient. However, the assumption of pure scattering and adsorption events using the ideal Langmuir isotherm does not present significantly new ideas with regards to slip behaviour. Extensions to the adsorption model will allow the representation of effects such as non-linear behaviour that has been observed in experiments.

2.4 Modelling of Liquid Slip

Current liquid slip models can be broadly categorised into apparent and molecular slip models. The apparent slip models attempt to provide phenomenological resolution for anomalous empirical findings that do not fit the Navier slip model while the molecular theories describe slip behaviour using finer physical details of molecular interactions that take place at the interface.

Two-Phase Model

The uncharacteristically large slip length that were obtained in experiments, particularly on non-wetting surfaces, led to conjectures that it was due to a less viscous layer sandwiched between the liquid and surface. For a low-viscosity film of thickness δ on the solid surface, the slip length b can be estimated from the matching of shear stress at the fluid-fluid interface as (Vinogradova 1995)

$$b = \delta\left(\frac{\eta}{\eta_s} - 1\right) \tag{2.14}$$

where η and η_s are the bulk and film viscosities.

Alternatively, for a gas layer, De Gennes (2002) considered a kinetic theory expression of the shear stress of a gas and obtained an approximate slip length of

$$b = \frac{\eta}{\rho v_n} \tag{2.15}$$

with ρ and v_n denoting the gas density and thermal velocity component normal to the surface.

Taking into consideration the possibility of slip occurring both at the gas-solid and gas liquid interfaces, Tretheway and Meinhart (2004) worked out the apparent slip length by

applying the gas slip velocity boundary conditions at the two interfaces, showing that the slip velocity was greatly enhanced under such circumstances. However, parameters such as the surface coverage of nanobubbles for intermittent coverage and film thickness are hard to quantify.

Blake-Tolstoi Model

Tolstoi (1952) was among the earliest to adopt a molecular kinetics approach for describing slip behaviour by considering the difference between surface and bulk liquid molecular mobilities. A major contribution of the model was to show a link between slip and surface wettability. His work was later improved by Blake (1990) to overcome its limitations in complete-wetting situations. The Blake-Tolstoi slip length expression reads

$$b = \sigma\left\{\exp\left[\alpha A\gamma_{LV}\left(1-\cos\theta\right)/k_B T\right]-1\right\} \tag{2.16}$$

Where σ is the centre-to-centre molecular separation, α is the fraction of the surface occupied by solid, A is the effective molecular surface area, k_B is the Boltzmann constant, T is the temperature.

The Blake-Tolstoi model provides an adequate qualitative prediction of slip behaviour (Ellis et al. 2003). Two debatable aspects of the theory are the use of a macroscopic form of the activation energy for the molecular mobility and validity of considering a velocity gradient across a one-molecule thick layer. Other shortcomings of the theory include the difficulty in estimation of the surface fraction parameter and the neglect of surface roughness.

Surface Diffusion Model

Ruckenstein and Rajora's (1983) work is often quoted in the literature for their insightful suggestion that a surface gas layer could be a contributing factor towards experimentally

observed magnitudes of slip that otherwise could not be purely explained by their surface diffusion model. Yet, the attempt to associate slip with thermally activated motion of molecules on a substrate lattice deserves more plaudits. Lichter et al. (2007) have suggested a similar surface hopping mechanism in their rate theory model of slip flow. The Arrhenius-type model is conceptually similar to the previously introduced Blake-Tolstoi model but considers tilted potential barriers between adsorption sites of the substrate with the barriers being lower in the direction of the external field. This leads to a net drift velocity which can be considered to be the molecular slip velocity

$$U_{\text{slip}} = \nu_0 \lambda \exp\left(-\frac{E_0}{k_B T}\right) \sinh\left(\frac{\Delta E_{\text{shear}}}{k_{\text{B}} T}\right) \tag{2.17}$$

where ν_0 is the jump rate of each adsorbed molecule, E_0 is the potential energy barrier, ΔE_{shear} is the change in the potential energy barrier due to shear stress exerted on the adsorbed molecules.

Though the slip velocity in Eqn (2.17) appears to show a non-linear dependence on slip, a rough estimate using appropriate parameters revealed that slip remained within the linear regime for the range of experimental shear rates (Bowles et al. 2011); the expression recovers the familiar Navier form when $\Delta E_{\text{shear}} \ll k_{\text{B}} T$. Slight adaptations to the model have also been made to include a critical shear stress criterion and shear-dependent dissipation at high shear rates to improve the match with results from numerical simulations but lack strong physical justifications (Yang 2010, Wang and Zhao 2011).

Variable Density Frenkel-Kontorova Model

The dynamics of liquid molecules at solid surfaces may be modelled classically as a stochastic process using the Langevin equation for a single-molecule description

(Thompson and Troian 1997). More exact models such as the Fokker-Planck equation includes the use of probability density functions of stochastic variables but will have to be solved using numerical means in most cases.

The one-dimensional Frenkel-Kotorova (FK) model has been used to represent the molecular mechanism of slip arising from the interplay of liquid-liquid and liquid-solid interactions (Lichter et al. 2004, Martini et al. 2008b). A modified form of the FK equation was proposed to account for the mass flux in the direction normal to the surface, where the near-wall density is higher due to molecular ordering. Their variable density Frenkel-Kontorova (vdFK) equation reads

$$m\ddot{x}_i = -\frac{2\pi g}{\lambda}\sin\left(\frac{2\pi \dot{x}_i}{\lambda}\right) + k\left(\dot{x}_{i+1} - 2\dot{x}_i + \dot{x}_{i-1}\right) + \eta_{LL}\left(V - \dot{x}_i\right) - \eta_{LS}\dot{x}_i \quad (2.18)$$

where the subscript i is the molecular index, m is the molecular mass, g is the strength of the periodic potential of the substrate, V is the speed of the adjacent fluid layer, η_{LL} and η_{LS} are the liquid-liquid and liquid-solid friction coefficients. The second term on the right hand side represents the stochastic movement of molecules between the surface and adjacent fluid layers

By keeping only the dominant terms in each slip regime, the vdFK equation qualitatively predicts the overall transition of slip: (i) no slip to local slip with isolated molecules performing individual hops to adjacent sites (ii) local to global slip where the fluid molecules forming the surface layer move in tandem (iii) limiting slip at high driving forces.

Realistically, the relative solid-liquid and liquid-liquid affinities are expected to be dissimilar so the stochastic term should instead be represented as an asymmetric random walk with a net drift in the direction of the stronger attractive force.

In summary, the theoretical models described above are only individually capable of predicting slip behaviour under specific circumstances. Ultimately, the aim for theoreticians would be to develop a model which encompasses the various determining factors that have been discovered in experiments. In the next section, we list some of these popular slip measurement techniques.

2.5 Measurement of Liquid Slip

The advent of high resolution measurement systems has boosted the precision that is required in experimental slip flow studies. This has fostered progress in the understanding of liquid slip where extremely fine measurements are involved. Yet, discrepancies may arise due to the highly sensitive nature. Experimental slip lengths have also been found to be generally larger than numerical predictions. Possible sources of experimental errors include the presence of dissolved gases and electrokinetic effects. None of the current techniques can strictly be classified as direct methods – the closest being velocity tracking methods. Instead, the slip variables are inferred from macroscale quantities such as hydrodynamic forces and flow rates. Comprehensive reviews of the present techniques are available in the literature (Neto et al. 2005, Lauga et al. 2007, Bouzigues et al. 2008). Here, the various techniques will be briefly described and assessed.

Surface force methods

The popular surface force methods, using either surface force apparatus (SFA) or atomic force microscopy, transpired from Vinogradova's model for thin film lubrication with the consideration of slip on the two approaching surfaces (Vinogradova 1995). The drainage force methods possess high resolutions, limiting slip length uncertainties to within 2 nm. Additionally, a wide variety of surfaces are possible with AFM. Nevertheless, the SFA technique is known to be susceptible to contamination while the AFM measurements complicated by certain factors like roughness and inertial effects (Neto et al. 2005).

The credibility of AFM measurements have been put into question due to the inconsistency in slip lengths of polar liquids on smooth hydrophilic surfaces that were measured by various researchers (Craig et al. 2001, Bonaccurso et al. 2003, Honig and Ducker 2007). A recent parametric study by Rodrigues et al. (2010) showed that certain experimental factors such as the cantilever stiffness, approach velocity and liquid viscosity may influence the force measurements, thus possibly masking the no-slip boundary condition.

Tracers

The most straightforward way to measure slip is through flow visualisation with the aid of tracer particles. Such studies have been performed using micro particle imaging velocimetry (μPIV), total internal reflection velocimetry (TIRV), total internal reflection using fluorescence recovery after photobleaching (TIR-FRAP), fluorescence cross-correlations and thermal motion of tracers. The imaging techniques suffer from low resolution due to uncertainties in determining the wall and particle positions. Moreover, the accuracy may be hampered by electrophoresis and electrostatic interactions (Lauga 2004).

An interesting method based on the theoretical model of the relationship between the bulk diffusivity of tracers and slip velocity by Lauga and Squires (2005) was employed by Joly et al. (2006). This technique eliminates the need for a flow source and so avoids the influence of gas bubbles. Furthermore, the fact that slip was indirectly observable in the experiments appears to rule out shear rate dependence, although it should be pointed that a more appropriate term for the effect of shear rate from a molecular framework is an external force which for instance can arise in the presence of a chemical potential gradient.

Flow rate measurement

Slip lengths may be evaluated by measuring either the mass flow rate or differential pressure across a micro or nanochannel. Though the experiments are relatively simple to carry out, the method suffers from low resolution. Besides, the extraction of slip length becomes more complex with the consideration of surface roughness and wetting properties.

Other methods

Besides the above methods, slip has also been examined using quartz crystal oscillators (Daikhin et al. 2000, Du et al. 2004, McHale and Newton 2004, Willmott and Tallon 2007), particle sedimentation (Boehnke et al. 1999), increase in potential difference across a capillary containing an electrolyte solution (Churaev et al. 2002). Rheological techniques also offer a convenient means of testing with the use of viscometers (Watanabe et al. 2003, Choi and Kim 2006, Perisanu and Vermeulen 2006, Truesdell et al. 2006) although the unusually large slip lengths of a few hundred micrometres and actual experimental uncertainty as reported by Choi and Kim (2006) have been doubted (Bocquet et al. 2006).

That contrasting slip lengths are obtained for the same liquid-surface configuration using different approaches highlights the work cut out for experimentalists in this field. In fact, inconsistencies exist even within the same technique. Furthermore, current experimental uncertainties are still too large to be able to categorically distinguish between slip and no-slip behaviour. The search remains for a robust and accurate method – achievable by improving the resolution and sieving out interferences in the current methods or devising a new technique altogether.

Numerical Methods

Numerical simulations offer a means of circumventing the complexities and challenges involved in conducting benchtop investigations of slip. The mesoscopic lattice Boltzmann method (LBM), based on the discretisation of the Boltzmann equation on a lattice, has been used for studying slip through simulation of microflows. Though the simulations do not provide molecular-scale insight, the coarser time and length scales are closer to that of experimental conditions and therefore can be understood from a more familiar macroscale perspective. LBM slip studies lack rigor due to the requirement of an *a priori* slip generating mechanism through artificial parameters that account for boundary scattering probabilities, fluid viscosity and interfacial properties (Harting et al. 2010).

To probe the fundamental physics at a fluid-solid boundary, molecular dynamics simulation is the de-facto computational tool employed in slip studies for classical treatment of flows that is based on Newton's equations of motions for a molecular ensemble. A potential model, such as the modified Lennard-Jones potential, determines the intermolecular interaction. This allows the variation of liquid-solid interaction strength and densities so that factors like the wettability can be controlled. In addition, the effect of near-wall molecular structures can also be observed from the simulations.

Evidence of induced epitaxial layering extending a few molecular layers from the wall was found and increased structuring led to smaller slip lengths (Thompson and Robbins 1990, Barrat and Bocquet 1999).

Despite the present-day accessibility to powerful computational resources, MD simulations face restrictions in terms of particle numbers and are only capable of dealing with length and time scales on the nanoscale order. System conditions, for instance, the extremely high shear rates in a Couette flow setup, can neither be replicated in experiments for validation nor translated to the more useful continuum regime. Besides, inherent ambiguities with regards to the specifications of interaction potentials, wall models and thermostatting controls have been shown to affect the trend of slip behaviour (Martini et al. 2008a, Pahlavan and Freund 2011, Yong and Zhang 2012).

2.6 Measurement of Gaseous Slip

The main experimental technique for determination of the gaseous slip coefficient (or TMAC) is flow rate measurement under controlled low-pressure conditions, akin to that used in liquid slip experiments. Measurements of the minute mass flows are sensitive to small variations in temperature and surface corrugations. Slip is also alternatively quantified in the literature by the Poiseuille number $f.Re$, where f is the Fanning friction factor and *Re* is the Reynolds number (Pfahler et al. 1991, Harley et al. 1995).

The spinning rotor gauge, originally developed for vacuum pressure measurements, has also been used for determining the TMAC from the relationship between the torque and angular velocity of the levitated sphere (Bentz et al. 2001). Again, these measurements

are highly sensitive to surface conditions and temperature, which could lead to disagreements between experimental and theoretical results (Bentz et al. 1999).

The surface force technique that is widely employed in liquid slip length experiments has recently been adopted for investigating the slip behaviour of air confined between glass surfaces (Maali and Bhushan 2008). Since the drag forces are much lower for gases, high sensitivity had to be ensured by selecting a cantilever of low stiffness and high quality factor. It is worth noting that the reported uncertainty was higher than those of the well-established mass flow rate measurements (Graur et al. 2009). Nevertheless, this versatile technique is attractive because of its excellent controllability and furthermore avoids the meticulous process of microchannel fabrication.

The direct simulation Monte-Carlo method developed by Bird (1994) is a popular computational tool for simulating rarefied gas flows. In this Boltzmann equation based stochastic approach, molecular motion and collisions are decoupled using an algorithm that samples collisions at every time step to recalculate the new molecular velocities. A caveat of this computationally-efficient method is that the accuracy depends greatly on the collision models being employed.

2.7 Mechanism of Temperature Jump

The imperfect energy accommodation of gas-solid interactions leading to a temperature jump is analogous to that in gaseous slip. The liquid-solid temperature jump is however thought to be due to the transport of heat carriers known as phonons across the interface.

Molecular Scattering Mechanism

The scattering model of temperature jump is similar to the kinetic theory based model of boundary slip flow except that it considers the incomplete exchange of energy between fluid and wall molecules during collisions (Kennard 1938). Again, temperature jump via this mechanism is expected to dominate in gases as a consequence of the longer mean free paths.

Phonon Transmission Mechanism

The existence of a boundary thermal resistance or equivalently a temperature discontinuity has been put down to the interfacial transport of phonons, which are the main carriers of thermal energy arising from the collective vibrations of atoms or molecules in non-metals. Sound typically travels at a velocity that is an order of magnitude higher in solids compared to liquids. Going from one medium to another, the abrupt change in molecular structures as represented by the mismatch in acoustic properties creates a large impedance that prevent incident phonons from propagating freely across the interface (Pollack 1969, Swartz and Pohl 1989, Cahill et al. 2003). This hindered transmission of energy is reflected as a temperature jump. In spite of the qualitative agreement, theoretically predicted thermal resistances are typically much larger than that observed in experiments, which hint that other mechanisms may be at work.

2.8 Factors Affecting Temperature Jump

The same factors that influence slip have also been found to affect the temperature jump behaviour. With the use of MD simulations, the magnitude of the temperature jump shows a dependence on the surface roughness and wettability of the surface.

Surface Roughness

An enhancement in thermal conductance with an increase in nanoscale roughness has been found in non-equilibrium molecular dynamics simulations. This has been intuitively attributed to the larger solid-liquid contact area, evident from the amplified thermal conductance for a sinusoidal roughness geometry compared to grooved corrugations and the smaller temperature jumps for taller nanopillars (Goicochea et al. 2011, Acharya et al. 2012). The problem is compounded by the inclusion of the effect of roughness on wetting characteristics. A larger temperature drop was observed at a rough surface which is hydrophobic but at a smooth surface when it is hydrophilic (Wang and Keblinski 2011).

Wetting

The temperature jump at hydrophobic interfaces has been shown to be larger than that at hydrophilic interfaces (Ge et al. 2006, Goicochea et al. 2011, Wang and Keblinski 2011, Acharya et al. 2012). A smaller thermal resistance is commonly associated with the strong hydrogen bonding between water and surfactant molecules. Shenogina et al. (2009) obtained a simple relationship showing that the thermal conductance was proportional to $(1+\cos\theta)$ with θ being the contact angle. Near a hydrophilic surface, the ordered layer of liquid molecules is thought to minimise the mismatch in structure, hence allowing for more efficient transmission of phonons (Murad and Puri 2008). In addition, Xue et al. (2003) identified an exponential dependence on the solid-liquid bond strength for hydrophobic surfaces whereas hydrophilic surfaces displayed a power law dependence. As the temperature jump in the non-wetting situation is consistently two to three times larger than in wetting situations across several experiments, it was suggested that the disparity could be ascribed to a less dense liquid layer analogous to that in apparent slip flow (Ge et al. 2006).

Direction of Heat Transfer

Interestingly, the thermal conductance has been discovered to be higher when heat flows from the solid to liquid phase and lower in the opposite direction. A possible reason for this phenomenon is the strong temperature dependence of the hydrogen bonds between water molecules that causes a drop in hydrogen bonds as temperature increases (Hu et al. 2009) although the MD results of Shenogina et al. (2009) showed augmented rectification with stronger wetting for the same surface temperature. Murad and Puri (2012) demonstrated that thermal rectification could be controlled by the near-wall liquid molecular structure through either modifying wetting properties or applying an external field. The diode-like behaviour could be promising for nanoscale thermal applications.

2.9 Modelling of Gas-Solid Temperature Jump

von Smoluchowski (1898) developed the earliest theory of temperature jump, drawing inspiration from Maxwell's slip theory. The thermal accommodation coefficient σ_t represents the fraction of reflected or re-emitted molecules possessing the mean energy of gas molecules at the same temperature as the wall (Kennard 1938). It can be expressed as

$$E_i - E_r = \sigma_t \left(E_i - E_w \right) \tag{2.19}$$

where for Γ_m grams of incident gas molecules crossing a unit area per second, E_i refers to the total energy of incident molecules, E_r the energy of reflected and re-emitted molecules and E_w the energy of gas molecules if they were emitted at the wall temperature. An accommodation coefficient of one may be interpreted as a molecule undergoing repeated collisions with the wall and finally getting re-emitted as if it were from a gas at the wall temperature. In contrast, a molecule that is reflected immediately on impact can be thought of as having an accommodation coefficient of zero. In effect,

the accommodation coefficient merely categorises molecules into those that fully equilibrate to the energy of the wall and those that retain their original energy. Temperatures may be used in place of energy although this is not strictly true for polyatomic gases due to their additional internal degrees of freedom.

The terms in bracket on the right of Eqn. (2.19) are given by

$$E_i - E_w = \frac{1}{2} k \frac{\partial T}{\partial n} + \frac{1}{2} \frac{c_v p(\gamma + 1)}{\sqrt{2\pi RT}} (T_0 - T_w) \tag{2.20}$$

Where k is the thermal conductivity of the gas, c_v is the specific heat at constant volume, p is the pressure of the gas at the wall, γ is the ratio of specific heats and R is the specific gas constant. The first term on the right denotes the energy possessed by the incident gas molecules for thermal conduction while the second represents the difference in translational and internal energy carried by gas streams at temperatures T_0 and T_w.

The left-hand side of Eqn. (2.19) represents the energy transferred to the surface and is equivalent to the overall heat conducted by the gas as follows

$$E_i - E_r = k \frac{\partial T}{\partial n} \tag{2.21}$$

Substituting Eqns. (2.20) and (2.21) in Eqn. (2.19) and rearranging, the temperature jump can be expressed as

$$\begin{aligned} T_0 - T_w &= \frac{2 - \sigma_t}{\sigma_t} \frac{1}{\gamma + 1} \frac{k}{c_v p} \sqrt{2\pi RT} \frac{\partial T}{\partial n} \\ &= \frac{2 - \sigma_t}{\sigma_t} \frac{2\gamma}{\gamma + 1} \frac{\lambda}{\mathrm{Pr}} \frac{\partial T}{\partial n} \end{aligned} \tag{2.22}$$

where the Prandtl number Pr and mean free path λ have been introduced.

The accommodation coefficients for the translational and rotational energies have been reported to be much larger than that for the vibrational energy (Schäfer et al. 1942). The above derivation for polyatomic gas molecules does not distinguish between accommodation coefficients for translational, rotational and vibrational energies. A more rigorous approach would be to consider Eqn. (2.19) for each energy component as in the anisotropic scattering model of Dadzie and Meolans (2005).

A classical calculation of the accommodation coefficient by Baule (1914) using the conservation of linear momentum and energy for *n* number of elastic collisions between a monoatomic gas molecule and surface of respective masses m_g and m_w gives the following expression

$$\sigma_t = 1 - \left[\frac{m_g^2 + m_w^2}{\left(m_g + m_w \right)^2} \right]^n \tag{2.23}$$

According to Eqn. (2.23), the accommodation coefficient decreases when the mass of one is much larger than the other. A higher accommodation coefficient occurs for a rough surface, on which a gas molecule may impinge repeatedly before being re-emitted.

For more highly rarefied gases, higher order temperature gradient terms are expected to exert greater influence on temperature jump. Deissler (1964) derived a second-order form of the temperature jump boundary condition, additionally taking into consideration the distributions of molecular velocity and angles of incidence of the impinging gas molecules. It was also proposed that a distinction be made between the mean free path for translational energy exchange and that for internal energy exchange. The fully-developed two-dimensional second-order temperature jump expression is as follows

$$T_0 - T_w = \frac{2 - \sigma_t}{\sigma_t} \frac{2\gamma}{\gamma + 1} \frac{\lambda}{\mathrm{Pr}} \frac{\partial T}{\partial n} - \frac{9}{128} \frac{177\gamma - 145}{\gamma + 1} \lambda^2 \frac{\partial^2 T}{\partial n^2} \tag{2.24}$$

For laminar heat transfer in cylindrical tubes, the first-order and second-order solutions only diverges at $Kn = 0.1$, differing by approximately 15% when $Kn = 0.2$. The second-order terms account for the non-linear constitutive relation between heat flux and temperature gradient when the mean free path is on the order of the characteristic length. In this state, both intermolecular and molecule-wall collisions have to be considered so that the correct solution can only be obtained using molecular-based models. For instance, a closed form solution of the linearised Boltzmann equation has been obtained by Liu and Lees (1960) for the heat transfer of a monoatomic gas between parallel plates

2.10 Modelling of Liquid-Solid Temperature Jump

The two main models of the Kapitza resistance consider phonon interactions at an interface between dissimilar media. In the acoustic mismatch model (AMM) (Mazo 1955), the low-temperature phonon transmission probability is a function of the contrasting acoustic impedances while it depends on the balance of phonon density of states in the diffuse mismatch model (DMM) for the thermal resistance at solid-solid interfaces (Swartz and Pohl 1989). The different derivations originate from the assumptions of fully specular reflections in the AMM and diffuse reflections in the DMM. Both models therefore describe merely the asymptotic cases of interfacial phonon behaviour.

The temperature jump expression is given by

$$\Delta T = R_k \frac{\dot{Q}_{1\to 2}(T_2) - \dot{Q}_{1\to 2}(T_1)}{A} \tag{2.25}$$

Where R_k refers to the Kapitza resistance, A the interfacial area, and $\dot{Q}_{1\to 2}(T)$ the heat current between the two media, which is assumed here to be independent of the

temperature on the other side of the interface to simplify the analysis. In light of the thermal rectification effect observed in MD simulations, this assumption may be invalid.

The heat current comprises the total phonon energy being transmitted across the interface and can be evaluated from the expression

$$\frac{\dot{Q}_{1\to 2}}{A}=\frac{1}{2}\sum_{j}\int_{0}^{\pi/2}\int_{0}^{\omega_1^{max}} N_{1,j}\hbar\omega c_{1,j}\alpha_{1\to 2}\cos\theta\sin\theta d\theta d\omega \tag{2.26}$$

where$N_{1,j}$ is density of phonon states, $\hbar\omega$ the phonon energy, $c_{1,j}$ the phonon velocity with subscript i indicating the medium and j the phonon mode, $\alpha_{1\to 2}$ the transmission probability and θ the incident angle.

The AMM and DMM models differ only in their respective forms of the transmission probability. In the AMM model, the transmission probability for a normal incident angle can be obtained from continuum acoustic theory as

$$\alpha_{1\to 2}=\frac{4Z_2Z_1}{\left(Z_1+Z_2\right)^2} \tag{2.27}$$

Where Z_1 and Z_2 denote the respective acoustic impedance of each medium.

The transmission probability used in the DMM model is based on a Debye approximation for the phonon velocities and density of states

$$\alpha_i\left(\omega\right)=\frac{\sum_j c_{3-i,j}^{-2}}{\sum_j c_{i,j}^{-2}} \tag{2.28}$$

Predictions of the thermal boundary resistance given by the aforementioned models as well as other improved models such as the scattering-mediated AMM by Prasher and Phelan (2001) deviate rather significantly from experimentally observed values (Swartz

and Pohl 1989). The poor agreement may be attributed to the neglected influence of interfacial molecular parameters, the breakdown of the Debye approximation at high temperatures and the assumption that heat transfer in liquids can be adequately described by phonon theory (Bolmatov et al. 2012).

2.11 Measurement of Gas Temperature Jump

The earliest experimental verification of the temperature jump phenomena was performed by von Smoluchowski (1898) through measurements of heat conduction between two parallel surfaces at different temperatures for air and hydrogen. He observed that the temperature jump distance was proportional to pressure, or equivalently the mean free path. His findings were later corroborated by other researchers using nearly similar methods (Devienne 1965).

Other temperature jump or accommodation coefficient measurement techniques include the popular hot-wire method which measures the amount of energy required to maintain an electrically-heated wire immersed in the test gas at a given temperature and determination of thermal conductivity of powder beds in gases (Hall and Martin 1987). These early experimental investigations have been reviewed comprehensively in the literature (Devienne 1965, Saxena 1989). More recently, Trott et al. (2008) employed an updated parallel-plate setup that was housed in a vacuum chamber for two different accommodation coefficient measurement approaches. The first method was to obtain the heat-flux indirectly through temperature difference while the second involved the measurement of gas density profiles by electron-beam fluorescence, which can then be converted to temperature profiles. High-precision instruments were installed to control factors including gas pressure, gas and plate temperature and fluorescence detection.

2.12 Interfacial Thermal Resistance (Temperature Jump)

Experimental work on the temperature discontinuity or the equivalent thermal boundary resistance took off in the mid-20th century after it was proposed that a thermal resistance could exist between liquid helium and a solid surface. Incipient studies on the thermal boundary resistance are chronicled in two review papers (Pollack 1969, Swartz and Pohl 1989). The first reported measurement of temperature drop at a liquid-solid interface was performed by Kapitza (1941) (hence the eponymously termed Kapitza resistance) using a simple technique of measuring the temperature profile around the interfacial region between a copper specimen and liquid helium at temperatures below 1 *K*. As helium is in a superfluid state with negligible thermal conductivity at such temperatures, its temperature could be taken from any location within the liquid while the temperature profile within the copper was extrapolated up to the interface using several thermometers. This bypassed the difficulty of probing the temperatures at both sides of the interface. Later, an indirect approach was developed to evaluate the thermal resistance from the amplitudes of the transmitted and reflected second-sound wave that is incident on a thin metal foil that was immersed within liquid helium. Propagation of heat in superfluid helium occurs through the second-sound. Detection of a reflected sound wave at the interface indicates a finite thermal resistance.

To the best of our knowledge, only one active research group has been conducting experiments on the thermal conductance (the inverse of the thermal resistance) of liquid-solid interfaces at room temperature. In their original experiment, the thermal conductance was obtained from the cooling curves of metallic nanoparticle suspensions which were measured using pump-probe laser spectroscopy (Ge et al. 2004). This method was later realised to be inappropriate for investigating the effect of wetting due to the clustering of hydrophobic particles. Subsequently, time-domain thermoreflectance

was employed to study the thermal conductance of planar interfaces between water and functionalised metal substrates through fitting of an analytical heat transfer model to reflectivity curves (Ge et al. 2006). The drawbacks of this technique include the high experimental uncertainty due to the inaccurate determination of film thickness and heat capacity, as well as additional thermal resistances which could arise from substrate contamination and electron-phonon coupling.

Recent studies on thermal resistance comprise of MD simulations, the bulk of which focus on the role of wetting and surface roughness (Kim et al. 2008, Murad and Puri 2008, Hu et al. 2009, Shenogina et al. 2009, Wang and Keblinski 2011). Apart from the general shortcomings of the MD method listed previously, another criticism lies in its classical nature, thereby not only limiting the accuracy at low temperatures but also the inability to consider the influence of electrons (Cahill et al. 2003).

2.13 Summary and Views

In this chapter, we described the mechanisms that are thought to be the cause of the fluid-solid boundary jump of velocity and temperature. Based on these proposed mechanisms, several theoretical models have been developed but are mostly inadequate in providing accurate predictions of experimentally observed trends. The series of experimental techniques that have been reviewed here show great novelty in overcoming the difficulty of indirect measurements. However, results from these high-resolution methods have to be interpreted with caution as they often contain inherent sources of apparent effects, consequently presenting a misleading picture of the interfacial phenomena. On the other hand, such unintended effects may be useful as a form of artificial control of the jump behaviour in small-scale devices. Molecular dynamics simulations of simple flow and heat transfer systems allow the study of the

relation between molecular behaviour and the macroscopic discontinuity across the interface but outcomes are highly dependent on prescribed input conditions. Besides, simulated variables do not translate to realistic values for practical comparisons.

The confounding information gathered from experiments and simulations deserves to be addressed theoretically in greater detail. In addition, the largely similar characteristics of the respective boundary conditions beg the question of whether the interfacial jump phenomena originates from a common physical mechanism. If so, this would indicate that a single general boundary condition model should apply to both gases and liquids. A critical issue herein is whether observed interfacial behaviour arises from molecular interactions, secondary processes or more likely, a combination of the two.

In the following chapters, we will explore the fundamental mechanisms of the boundary phenomena within the framework of surface science theory. A general adsorption model that describes the interfacial physics is proposed in the next chapter as a foundation for the theoretical modelling of the fluid slip velocity and temperature jump.

3 Interfacial Physics of Fluid-Solid Interaction – A Framework for Slip Velocity and Temperature Jump at Fluid-Solid Interfaces

The state of a fluid molecule upon impact on a surface is governed by interfacial physics and local conditions. In this chapter, a surface physics framework that describes fluid-solid interactions is introduced and built upon in the chapters that follow to develop theoretical models for the velocity slip and temperature jump at the interface.

When a particle comes into contact with the surface, it has a probability of sticking to the surface or scattering away 'immediately' as shown in Fig. 3.1. Within the kinetic theory framework of the Maxwell slip velocity model, the scattering of particles was classified as specular reflections with no change in particle velocity while the diffuse reflection is akin to the particle being desorbed at the same velocity as the wall. While the Maxwell model and subsequent extensions of the model have shown moderate success in the prediction of experimental measurements, we provide an alternative stochastic interpretation of the molecular conditions at the surface and incorporate the physical details of the fluid-solid dynamics.

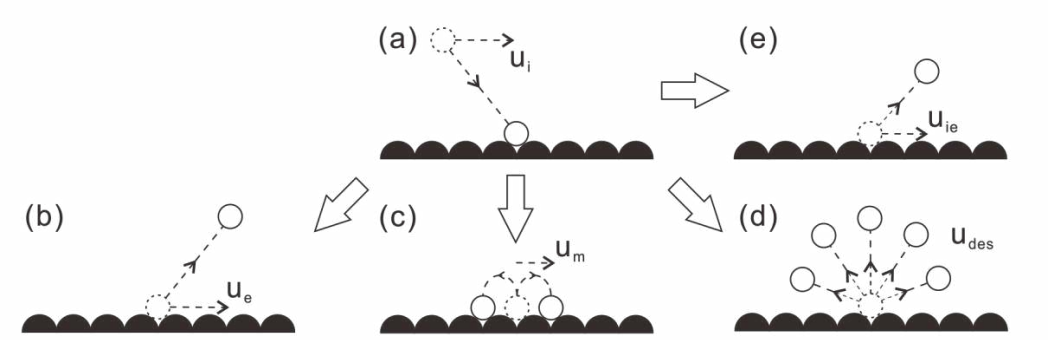

Fig. 3.1 Molecular interactions at a fluid-solid interfaces: (a) incident molecule (b) elastic scattering (c) surface hopping (d) desorption (e) inelastic scattering.

The sticking, termed as adsorption, occurs either by attraction due to van der Waals (vdW) force or chemical bonding when the particle lands on a vacant binding site on the solid lattice. The former is named physisorption while the latter is known as chemisorption (Ibach 2006). The vdW forces, which arise from induced moments in surrounding atoms as a consequence of charge fluctuations of an atom, dominate at large separation distances r, producing an attractive potential with a r^{-6} dependence that adheres the particle to the surface. At shorter separations, the vdW forces are opposed by the Pauli repulsion which is conventionally assumed to vary as r^{-12}. Chemical bonding is much stronger than the vdW force and furthermore is highly directional and site-specific. A transition from activated physisorption to chemisorptions is possible with an increase in temperature (Adamson and Gast 1997). In our model, we do not explicitly distinguish between the two forms of adsorption with the exception of the range of heat of adsorption being considered.

Within each adsorption site, the thermal motion of the solid and particles results in repeated collisions. An adsorbed fluid particle experiences random forces exerted by the solid particles, which effectively act as a heat-bath. Furthermore, as the gas particle equilibrates with the surface, it also experiences damping forces from the solid that eventually causes it to lose memory of its initial velocity. This loss in energy is dissipated throughout the solid and the particle's velocity tends towards that of the surface after a characteristic residence time. The dispersion in velocity by the random forces is mediated by the competing effect of damping, which tries to restore the system to its initial state. It is this competition between the opposing effects that gives rise to the equilibrium distribution. Here, we consider temperatures that are sufficiently high such that quantum effects can be ignored but low enough for the internal degrees of freedom of particles to be neglected.

The evolution of the tangential velocity u_a of the gas particle (atom or molecule) throughout the duration of interaction with the surface may be described by a Markov process

$$P\left(u_a,t\middle|u_0,0\right)\Big|_{t\to 0}=\delta\left(u_a-u_0\right) \tag{3.1}$$

where P is the transition probability from initial state u_0 to u_a at time t, u_0 refers to the initial velocity at the point of impact and t the residence time of the particle on the surface.

As $t\to\infty$, the probability distribution function (pdf) $p\left(u_a,t\right)$ tends toward an equilibrium distribution with mean

$$\begin{aligned}\left\langle u_a\left(t\right)\right\rangle &= \int_{-\infty}^{\infty} u_r\, p\left(u_a,t\right)du_r \\ &= \int_0^t u_a(t')\varphi\left(t'\right)dt'\end{aligned} \tag{3.2}$$

The mean velocity $\left\langle u_a\left(t\right)\right\rangle$ has the characteristics of a continuous-time random walk (CTRW) in velocity space with $\varphi\left(t'\right)$ representing the pdf of the waiting time t between successive velocity jumps.

The tangential velocity of each particle can be modelled classically after the overdamped Ornstein–Uhlenbeck process using the Langevin equation

$$\frac{du}{dt}=-\gamma u+\eta\left(t\right) \tag{3.3}$$

where γ denotes the damping coefficient and $\eta\left(t\right)$ is the noise term that represents the random forces of the solid atoms acting on the gas particle, which conveniently allows us to include the influence of the solid atoms without having to consider the individual

motion of each atom. For random forces taking the form of Gaussian white noise, the mean of the noise term is zero.

$$\langle \eta(t) \rangle = 0 \tag{3.4}$$

The initial condition is given by

$$u(0) = u_0 \tag{3.5}$$

where u_0 is the incident velocity prior to adsorption.

The differential equation in Eqn. (3.3) can be solved together with the initial condition in Eqn. (3.5) to give

$$u(t) = u_0 e^{-t/\tau} + e^{-t/\tau} \int_0^t e^{-t'/\tau} \eta(t')\, dt' \tag{3.6}$$

In Eqn. (3.6) the damping coefficient γ in Eqn. (3.3) has been replaced by the reciprocal of the mean sticking time τ^{-1}.

Finally, by averaging over the ensemble, the noise term drops out based on Eqn. (3.4), resulting in the mean tangential velocity expression

$$\langle u(t) \rangle = u_0 e^{-t/\tau} \tag{3.7}$$

Within the scattering regime, the particle reflects specularly (Fig. 3.1(b)) at its original velocity u_0 without any exchange of energy with the surface. The sticking time τ_e is virtually negligible and can be approximated as (Butt et al. 2006)

$$\begin{aligned} \tau_e &= \frac{2\delta_n}{\langle v_0 \rangle} \\ &\approx \frac{2\delta_n}{\sqrt{k_B T / m}} \end{aligned} \tag{3.8}$$

where δ_n is the normal penetration distance of the particle into the surface and $\langle v_0 \rangle$ is the normal velocity of the particle which may also be expressed in terms of its thermal energy. Typical room temperature sticking times in this regime for molecular-scale δ_n are on the order of 10^{-13} s (Butt et al. 2006). Inelastic scattering could occur in individual collisions but this is not expected to affect the equilibrium distribution of the velocity since collisions in which the particles lose energy are cancelled out by those with a gain in energy (Rice and Raw 1974).

Adsorbed particles reside for longer durations of time, during which it interacts with neighbouring solid atoms. For sticking times beyond the mean sticking time τ_s, most of the gas particles completely thermalise with the surface before being desorbed (Fig 3.1(d)), emerging with velocity u_{des} with the tangential component equivalent to that of the wall. Here, we consider a velocity frame of reference relative to the wall such that the desorbed particle leaves with a zero mean relative velocity. This may be termed correspondingly as the fully inelastic regime since the particle retains no trace of its original velocity, having had its initial energy fully dissipated through the solid atoms.

The mean sticking time is given by the Frenkel Equation

$$\tau_s = \tau_{vib} \, \mathrm{e}^{\Delta H_{ads} / k_B T} \tag{3.9}$$

where τ_{vib} is the inverse of the surface bond vibration frequency and ΔH_{ads} is the heat of adsorption.

$$\Delta H_{ads} = H_{ads} - H_g \tag{3.10}$$

where H_g and H_{ads} are the enthalpies of the gas and adsorbed phase respectively.

Physisorption takes place typically at around ΔH_{ads} = 40 kJ/mol with a residence time above 10^{-12} s (Butt et al. 2006). The sticking times for chemisorption are many orders higher due to the larger heats of adsorption lying in the range of $\Delta H_{ads} \geq 100$ kJ/mol and so adsorbed particles remain indefinitely on the surface.

An adsorbed particle may also remain mobile in a metastable phase while still being physically bound to the surface if it loses sufficient energy to prevent immediate desorption. In this mobile state (Fig 3.1(c)), the particle is able to hop to neighbouring sites with a mean drift velocity u_m before eventually escaping back into the bulk gas or being chemically adsorbed under the right conditions. There is also a probability that an adsorbed particle may escape before reaching thermal equilibrium with the surface (Fig 3.1(e)), leaving prematurely at velocity u_{ie} with a portion of its energy dissipated. The partially inelastic regime has an intermediate timescale that ranges between the elastic and mean sticking time.

Next, we will proceed to consider the probabilities of each interaction type between the fluid and solid particles based on the corresponding rates of the nature of adsorption.

3.1 Rate Balance Equation

The composition of particles departing from the surface comprises those that have undergone either elastic or inelastic interactions. In order to derive the mean condition of particles that leave the surface, the relative rates of sticking and non-sticking events must first be known. The various adsorption processes that take place are dependent on the potential energy landscape of the substrate as well as the energetic conditions of the particles. Figs. 3.2 and 3.3 illustrate the respective potential energy curves for non-activated and activated adsorption.

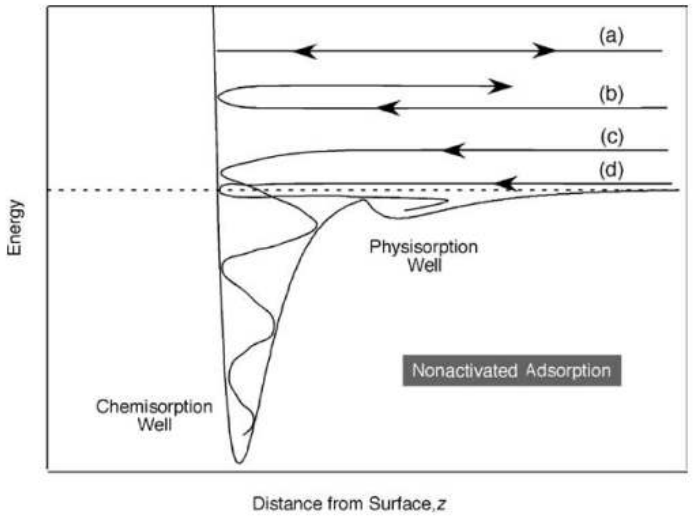

Fig. 3.2 One-dimensional representation of potential energy curve for non-activated adsorption: (a) elastic scattering (b) inelastic scattering (c) chemisorption (d) physisorption. Reproduced from (Kolasinski 2008).

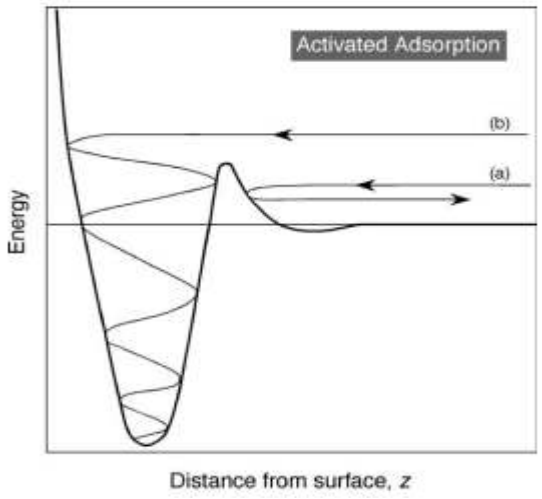

Fig. 3.3 One-dimensional representation of potential energy curve for activated adsorption: (a) low energy trajectory (b) high energy trajectory. Reproduced from (Kolasinski 2008).

The rate of incident particles R_i may be broken down into the rates of adsorption R_{ads} and elastic scattering R_e as follows

$$R_i = R_{ads} + R_e \tag{3.11}$$

where R_{ads} and R_e can be expressed in terms of R_i using the sticking probability p_s that represents the fraction of incident particles being adsorbed

$$R_{ads} = p_s R_i \tag{3.12}$$

$$R_e = (1 - p_s) R_i \tag{3.13}$$

The sticking probability is a function of factors such as the surface coverage, temperature, activation energy in the case of activated adsorption and the energy characteristics of the incident particle in non-activated adsorption. In our analysis, p_s will be assumed as a constant parameter, which is valid under the condition of steady-state equilibrium.

Particles that do not scatter upon collision get adsorbed due to energy dissipated during the impact, preventing them from returning to the bulk phase. Among the adsorbed particles, a fraction p_m is loosely trapped but remains mobile in a precursor state while the remaining $(1 - p_m)$ reside in the potential wells in a physisorbed state, with a possibility of transitioning to the chemisorption state if the temperature rises. At elevated temperatures, the precursor state is unfavourable, giving way to direct adsorption followed by desorption.

Though the mobile particles do not possess sufficient kinetic energy in the normal direction to escape, their tangential energy component allows them to hop from one site in search of another, following which they may desorb after either gaining energy from solid atoms or internally through other degrees of freedom, get adsorbed on an available site or continue hopping. The rate of adsorption of particles R_{ads} may thus be expressed as

$$R_{ads} = R_{m,1|ads} + R_{s,1|ads} \tag{3.14}$$

where $R_{m,1|ads}$ represents the rate of adsorbed particles that enter the precursor state and $R_{s,1|ads}$ the rate of adsorbed particles in the stable state.

$$R_{m,1|ads} = p_m R_{ads} \tag{3.15}$$

$$R_{s,1|ads} = \left(1 - p_m\right) R_{ads} \tag{3.16}$$

Next, the mobile particles consist of those that remain mobile while others get momentarily adsorbed after landing on an available site. Assuming that all particles in the stable adsorbed state are similar in character and that adsorbed particles are eventually desorbed, $R_{m,i|ads}$ during the ith hop is given by the recurring expression

$$R_{m,i|ads} = R_{m,i+1|ads} + R_{s,i+1|ads} \tag{3.17}$$

where the subscript i+1 indicates the state of the particle after the ith hop.

Adsorbed particles can be segregated into two categories – those that manage to escape while still possessing parallel momentum with probability p_e and those that undergo desorption with probability $\left(1 - p_e\right)$. The rate of stable adsorption $R_{s,i+1|ads}$ is given by

$$R_{s,i|ads} = R_{ie|s,i|ads} + R_{s|s,i|ads} \tag{3.18}$$

where $R_{ie|s,i|ads}$ represents the rate of adsorbed particles that escape prematurely and $R_{s|s,i|ads}$ the rate of those that are desorbed after overcoming the energy barrier.

$$R_{ie|s,i|ads} = p_e R_{s,i|ads} \tag{3.19}$$

$$R_{s|s,i|ads} = \left(1 - p_e\right) R_{s,i|ads} \tag{3.20}$$

Eqns(3.11) to (3.20) describe the overall rate balance of incident and departure fluxes and can be used in evaluating the mean condition of fluid molecules at the surface.

3.2 Assumptions

In order to focus on the fundamental essence of adsorption theory in the jump boundary conditions, we will limit the scope of our study to a steady-state reversible equilibrium

process in which the rate of adsorption is matched by the rate of particles being removed from the surface. Furthermore, it is assumed that particles, once stably adsorbed, be it immediately after initial contact with the surface or transitioning from a precursor state, are not physically unique in that they obey similar desorption dynamics. Factors such as lateral interactions between adsorbed particles and more elaborate forms of adsorptions like multi-layered adsorption will also be ignored but will be briefly discussed at the end of this thesis.

The foregoing rate balance analysis presented in this chapter portrays the complete dynamics of fluid particle interactions with a surface. Using this adsorption framework, we may proceed to derive the mean velocities and temperature of the near-wall fluid particles by prescribing the corresponding transport quantities to the respective adsorption states.

4 A New Model for Fluid Velocity Slip on a Solid Surface

The slip boundary condition at a fluid-solid interface has hitherto been considered separately for gases and liquids. In this chapter, we show that the slip velocity in both gases and liquids originates from dynamical adsorption processes at the interface. A unified analytical model that is valid for both gas-solid and liquid-solid slip boundary conditions is proposed based on surface science theory. Corroboration with experimental data extracted from the literature shows that the proposed model is superior to existing analytical models.

4.1 Mean Velocity of Fluid Molecules at a Solid Surface

The velocity of particles at the surface can be assessed based on the relative rates of scattering, adsorption and desorption, which can be translated to the probabilities of the respective velocities of each dynamical state.

Firstly, the tangential velocity u_e (Fig 3.1(b)) of an elastically scattered particle remains unchanged after collision with the surface and is given by

$$u_e = u_i \tag{4.1}$$

For particles in the precursor state, their hops can be represented as an asymmetrical random walk. Limiting the motion to one-dimensional uniform jumps and neglecting the influence of other factors such as site vacancy, non-nearest neighbour jumps, correlated jumps etc., the velocity u_m (Fig 3.1(c)) can be approximated as the drift velocity with the

bias being the difference between rates of hops in the flow direction $R_{m,f}$ and that in the opposite direction $R_{m,b}$.

$$u_m = a\left(R_{m,f} - R_{m,b}\right) \tag{4.2}$$

where a refers to the mean hopping distance.

The velocity of particles that escape while in the precursor state is dependent upon the duration of adsorption; the dissipation of tangential energy increases with increasing number of collisions with the solid and relative sliding against adjacent fluid atoms. The partially inelastic desorption velocity u_{ie} (Fig 3.1(e)) for a particle takes the form

$$u_{ie}\left(t\right) = u_i \varphi\left(t\right) \tag{4.3}$$

where $\varphi\left(t\right)$ denotes the sticking time distribution.

Fully thermalised particles that have spent an average residence time τ_s within the wells can be assumed to share the same tangential velocity as the wall upon desorption and therefore emerge with tangential velocity u_{des} (Fig 3.1(d)) given as

$$u_{des} = 0 \tag{4.4}$$

where the velocity of each particle is taken in a frame of reference relative to the wall.

Table 1 summarises the probabilities and velocities of the escaping particles. In brief, the velocities are composed of that due to probability $\left(1 - p_s\right)$ of elastic scattering, probability $p_s p_m$ of surface hopping in a trapped state and probability $p_s p_e \left(1 - p_m\right)$ of escape during the precursor phase. The desorbed particles play no part in the resultant mean velocity which is stipulated to be relative to the surface.

Table 1 Tangential component of escape velocities for different adsorption processes

Adsorption State	Probability	Velocity
Scattering	$(1-p_s)$	u_e
Precursor Mobile	$p_s p_m$	u_m
Escape	$p_s p_e (1-p_m)$	$u_0 e^{-t/\tau_s}$
Physi/Chemi-sorption	$p_s (1-p_e)(1-p_m)$	0

Finally, putting together the probabilities of the various adsorption states discussed in Eqns. (3.11) to (3.20) and their corresponding velocities in Eqns. (4.1) to (4.4), the mean velocity of surface particles has the following expression

$$\begin{aligned} u_s &= (1-p_s)u_e + p_s p_m u_m + p_s p_e (1-p_m) u_{ie} + p_s (1-p_m)(1-p_e) u_{des} \\ &= (1-p_s)u_e + p_s p_m u_m + p_s p_e (1-p_m) u_{ie} \end{aligned} \tag{4.5}$$

Eqn. (4.5) represents the mean velocity of a fluid particle on a solid surface. Whether it is equivalent to the macroscale boundary condition is a recent point of contention (Brenner and Ganesan 2000). Notwithstanding, the interfacial molecular velocity is still relevant in the derivation of a slip velocity on a larger length scale, for instance, by considering a layer of one mean free path thickness as in the treatment of gaseous slip flow. The new boundary condition is applicable to both gas-solid and liquid-solid interfaces although the dominant mechanism of energy or momentum exchange is expected to occur via scattering in gases but not in liquids owing to the magnitudes of mean free path. This may offer a plausible reason for the lower slip velocities of liquids, which are mainly due to adsorbed molecules in the precursor state. In the following section, the probabilities and velocities are acquired from surface physics theory to arrive at a functional form of the slip velocity.

4.2 General Slip Boundary Condition

In this section, the respective velocities are embellished with physical parameters, with the eventual aim of deriving the general slip velocity expression.

Scattering Velocity

The incident velocity of a particle before it arrives at the surface can be linearly approximated by the velocity after its last collision, which in the kinetic theory framework is taken as that from a distance of one mean free path λ away.

$$u_i \approx u_s + \lambda \dot{\gamma}_s \tag{4.6}$$

$\dot{\gamma}_s$ denotes the shear rate of the fluid at the surface. Eqn. (4.6) is valid in the range of low Knudsen numbers $0.001 < Kn < 0.1$ lying in the slip regime (Karniadakis et al. 2005). The concept of mean free paths does not readily translate to liquids due to the presence of intermolecular bonds. An alternative parameter that has been suggested as a replacement is the intermolecular bond length.

Surface Diffusion Velocity

In the mobile precursor state, the surface hopping velocity can be modelled after an activated rate process in which case the forward and backward rates takes on the Arrhenius form (Ruckenstein and Rajora 1983)

$$\begin{aligned} R_f &= \nu_0 \exp\left(-\frac{E_{a,m} - \Delta E_{\text{shear}}}{k_{\text{B}} T} \right) \\ R_b &= \nu_0 \exp\left(-\frac{E_{a,m} + \Delta E_{\text{shear}}}{k_{\text{B}} T} \right) \end{aligned} \tag{4.7}$$

where ν_0 is the rate prefactor that has been erroneously identified as the frequency of hopping attempts or vibration frequency in the literature (Ibach 2006), $E_{a,m}$ is the

activation energy for surface diffusion and ΔE_{shear} refers to the change in the potential barrier due to an externally applied shear, which can be approximated as

$$\Delta E_{\text{shear}} \approx \frac{1}{2}\mu A_{eff} a \dot{\gamma}_s \tag{4.8}$$

with μ being the dynamic viscosity of the fluid and A_{eff} the effective cross-sectional area of a particle under shear. The factor of $\frac{1}{2}$ indicates the lowering of the activation barrier in the direction of shear stress and rise in the opposite direction as illustrated in Fig. 4.1.

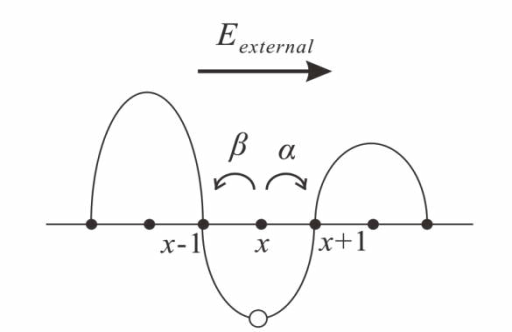

Fig. 4.1 The activated rate process model of surface diffusion in an external field, shown here as a one-dimensional asymmetric random walk on a regular lattice of unit spacing with the probabilities in the forward and backward directions given by α and β.

Hence, from Eqn. (4.2), the surface hopping velocity is given by

$$\begin{aligned} u_m &= a\left(R_{m,f} - R_{m,b}\right) \\ &= u_h \sinh\left(\frac{\dot{\gamma}_s}{\dot{\gamma}_0}\right) \end{aligned} \tag{4.9}$$

where the free surface diffusion velocity $u_h = \nu_0 a \exp\left(-\frac{E_{a,m}}{k_B T}\right)$ and characteristic shear rate $\dot{\gamma}_0 = \left(\frac{\mu A_{eff} a}{2k_B T}\right)^{-1}$.

Substitution of appropriate values for the parameters reveals that $\dot{\gamma}_0$ is typically on the order of 10^{11} Pa.s for gases and 10^9 Pa.s for liquids, which is at least five orders of magnitude larger than that attainable experimentally for $\dot{\gamma}_s$. Under such conditions, the

hyperbolic sine term tends to a first-order function of $\dot{\gamma}_s$. Hence, surface diffusion does not actually contribute to the non-linear dependence on shear rate in practical situations except at highly exaggerated shear rates such as those investigated in the MD simulations of Wang and Zhao (2011). In their study, it was shown that Eqn. (4.9) provided a fairly good prediction of their MD results at shear stress values of up to 100 MPa although the curve-fitting details were not elaborated. Returning to Eqn. (4.9), in the limit $\dot{\gamma}_s \ll \dot{\gamma}_0$, the surface diffusion velocity can be approximated as

$$u_m \approx \frac{u_h}{\dot{\gamma}_0}\dot{\gamma}_s \tag{4.10}$$

In Chapter 5, we also explore other mechanisms by which molecular slip may occur, producing slip velocities of higher magnitudes than in the surface diffusion model.

Escape Velocity

The escape velocity while the particle is in the precursor state can be expressed by considering its net change in the tangential component of energy as follows

$$\begin{aligned} u_{ie} &= \sqrt{u_e^2 - \frac{2}{m_m}\Delta E} \\ &= \sqrt{u_e^2 - 2\mu_u \delta u_e} \\ &= \sqrt{(u_e)(u_e - 2\mu_u \delta)} \end{aligned} \tag{4.11}$$

where ΔE represents the mean tangential energy loss during the period of sticking in the precursor state, μ_u the effective friction coefficient, δ the average distance traversed. The energy dissipation arises from interactions with the substrate as well as adjacent fluid particles within the bulk flow and can be approximated as velocity-dependent friction based on the relative velocity of the adsorbed particle and the surrounding environment (Krim 2012).

Substituting the velocity expressions in Eqns. (4.6), (4.10) and (4.11) into Eqn. (4.5), the following quadratic expression for the slip velocity can be obtained after rearrangement

$$\begin{aligned}&\left(1-c_1\right)u_s^2-2\left[\left(c_1+c_2\lambda\right)\dot{\gamma}_s-c_2\mu_u\delta\right]u_s+\left[\left(c_1^2-c_2\lambda^2\right)\dot{\gamma}_s^2+2c_2\mu_u\delta\lambda\dot{\gamma}_s\right]=0\\&c_1=\frac{1-p_s}{p_s}\lambda+\frac{p_m u_h}{\dot{\gamma}_0},\ c_2=p_e{}^2\left(1-p_m\right)^2\end{aligned}\tag{4.12}$$

where coefficients $c_1\geq 0$ and $0\leq c_2\leq 1$ have been introduced.

Solving Eqn(4.12) for u_s gives

$$\begin{aligned}&u_s=C_1\dot{\gamma}_s-C_2\pm\sqrt{\frac{C_2\left(C_1+\lambda\right)^2}{C_2+\mu_u\delta}\dot{\gamma}_s^2-2C_2\left(C_1+\lambda\right)\dot{\gamma}_s+C_2^2}\\&C_1=\frac{c_1+c_2\lambda}{1-c_2},C_2=\frac{c_2\mu_u\delta}{1-c_2}\end{aligned}\tag{4.13}$$

Since the slip velocity should cease to exist in the absence of an external field ($u_s\big|_{\dot{\gamma}_s=0}=0$), the negative root can be discarded, leaving the final expression

$$u_s=C_1\dot{\gamma}_s-C_2+\sqrt{\frac{C_2\left(C_1+\lambda\right)^2}{C_2+\mu_u\delta}\dot{\gamma}_s^2-2C_2\left(C_1+\lambda\right)\dot{\gamma}_s+C_2^2}\tag{4.14}$$

where it should be emphasised that the coefficients $C_i\left(i=1,2\right)>0$ are representative of the interfacial conditions, adsorption probabilities and properties of the media as follows

$$\begin{aligned}&C_1=\frac{1}{1-p_e^2\left(1-p_m\right)^2}\left[\frac{1-p_s}{p_s}\lambda+\frac{p_m u_h}{\dot{\gamma}_0}+p_e^2\left(1-p_m\right)^2\lambda\right]\\&C_2=\frac{p_e^2\left(1-p_m\right)^2}{1-p_e^2\left(1-p_m\right)^2}\mu_u\delta\end{aligned}\tag{4.15}$$

Eqn. (4.14) is the main result for this chapter and represents a new general slip velocity model for fluid-solid boundary conditions derived based on the theory of interfacial physics, specifically adsorption and desorption processes. The novelty of this model lies in its applicability to both gas and liquid flows which has thus far been studied independently in analytical models to the best of our knowledge. Furthermore, the slip

velocity expression exhibits non-linearity with respect to the wall shear rate which is in accordance with the prediction of experimental measurements where such phenomena have been observed.

In the following sections, validation of the new model will be performed by comparisons with experimental results extracted from the literature and predictions of the existing gas-solid and liquid-solid slip boundary condition models. Findings from the validation will be discussed at the end of the chapter.

4.3 Validation of Slip Velocity Model for a Gas-Solid Interface

While it is remarkable that Maxwell managed to conceive the accommodation coefficient term to describe the effective gas-surface interactions at a point in time when the realm of surface physics was virtually unknown, the accommodation coefficient reveals little about the physical nature of the inter-molecular interactions and the actual motion of fluid molecules at the interface. Fundamentally, the assumption of elastic scattering represents an ideal situation that disregards the occurrence of inelastic scattering events. The accommodation coefficient, which is analogous to the sticking probability, is also not a constant as it should depend on the characteristics of the incident molecule. It is therefore natural that the slip boundary condition should be modelled instead using adsorption-desorption processes. Even so, it has to be acknowledged that the simple form of the linear slip velocity makes it attractive for use in theoretical studies and to date remains a popular area of research for experimentalists.

The Langmuir model marks the first attempt at deriving the slip velocity based on adsorption concepts (Bhattacharya and Eu 1987, Myong 2004). However, the simple

adsorption model based purely on site vacancy is essentially similar to the Maxwell model with the non-dissociative sticking probability playing a similar role as the TMAC. More importantly, both models are only linearly dependent on the shear rate and thus incapable of explaining experimental results displaying a non-linear trend.

To ensure that our model is physically sound, we compare predictions by our model to experimental and numerical results that are available in the literature. First, the procedure of experimental data extraction is briefly described. Following that, the theoretical curves from both the new and existing models are plotted and compared with the extracted data.

4.3.1 Experimental Data for Gas-Solid Interfaces

The experimental studies selected for comparison involve the measurement of mass flow rates and differential pressure of microchannel gas flows, which can be converted into the slip velocity and wall shear rate for comparison with the new slip boundary condition. In the low Kn slip regime, the velocity profile for Poiseuille flow through a long, straight microchannel of uniform rectangular cross-section with low height-width aspect ratio can be simply worked out by solving for Stokes flow coupled with slip boundary conditions prescribed at the top and bottom walls, giving

$$u = \frac{h^2}{2\mu}\frac{dP}{dx}\left(\frac{y^2}{h^2}-1\right)+u_s \tag{4.16}$$

where $2h$ represents the height of the channel, $\frac{dP}{dx}$ the pressure gradient in the flow direction x. The y coordinate is taken to be in the normal direction to the flow with the origin located in the centre of the top and bottom walls.

Subsequently, the mass flow rate can be obtained from the velocity profile and further rearranging gives the desired slip velocity in terms of the mass flow rate and differential pressure as

$$u_s = \frac{\dot{m}}{\rho w h} - \frac{h^2 \Delta P}{12 \mu l} \tag{4.17}$$

The shear rate of the fluid at the wall ($y = \pm h$) can similarly be determined from differentiating Eqn. (4.16) with respect to y

$$\dot{\gamma}_s = \frac{h \Delta P}{2 \mu l} \tag{4.18}$$

After performing the above conversion, the mass flow rate versus pressure ratio curves can be transformed into curves of slip velocity against wall shear rates for ease of comparison with Eqn. (4.14). The results will be presented in the following section.

4.3.2 Comparison with Experimental Studies for Gas-Solid Interfaces

The new slip model is corroborated with data from four reported studies, which have been extracted and converted into the required variables using the procedure described in the previous section.

First, the mass flow rate measurement data for helium and nitrogen gases in silicon microchannels conducted by Shih et. al. (1996) was used. The 4 mm long channel had a rectangular cross-section 40 µm wide and 1.2 µm high. The converted wall shear rates were on the order of magnitudes of 10^5 to 10^6 s^{-1}, with a slip velocity of up to 0.55 ms^{-1}. This justified the use of the linear approximation for the surface diffusion term as indicated in Eqn. (4.10).

In the second study, we use the results of Arkilic et al. (1997), who performed mass flow rate measurements of rarefied helium gas flows in silicon microchannels measuring 52.25 μm wide, 1.33 μm deep and 7500 μm long in the slip regime with a mean outlet Knudsen number of 0.155. The mass flow rates and differential pressures translated into slip velocities ranging from 0.07 to 0.79 ms^{-1} for wall shear rates between 0.25 x 10^6 and 1.35 x 10^6 s^{-1}.

The third reference was from experimental investigations carried out by Zohar et. al. (2002) on the flows of helium, argon and nitrogen gas in silicon nitride coated microchannels of dimensions 40 μm in width, 4000 μm in length, and 0.53 μm in height. The mean Knudsen number for the experiment ranged from 0.12 to 0.38. The range of slip velocities was 0.03 to 0.60 ms^{-1} and that for wall shear rates was 0.35 x 10^6 to 1.36 x 10^6 s^{-1}.

The final set of results being compared was taken from the non-equilibrium molecular dynamics (NEMD) simulations of Kannam at. al. (2011) for Couette flows of argon and methane in 5.78nm tall grapheme nanochannels. The wall shear rates of 0.85 x 10^8 to 1.60 x 10^{11} s^{-1} were much higher than the above two experiments due to the computational time scales involved. As such, the slip velocities were also several orders larger, starting from 6 ms^{-1}up to a maximum of 8.62 x 10^3 ms^{-1}.

Figs. 4.2 to 4.9 show the plots of slip velocity against wall shear rate from the above sets of extracted data. Also plotted within the same graphs are the best-fit curves using Eqn. (4.14) and that of the existing slip velocity models - jointly represented as a single plot by the simplified linear expression

$$u_s = b\dot{\gamma}_s \tag{4.19}$$

where b is the slip coefficient comprising parameters associated with the individual models as listed in Table 2 below. It should be reiterated that all previous analytical models only possess a first-order dependence on the wall shear rate; the so-called second-order models that build upon the Maxwell model to improve its predictions at moderate Knudsen numbers merely retain the second expansion term of the slip velocity and do not indicate a non-linear relationship with the wall shear rate. For Poiseuille flows, the second derivative of the velocity can therefore be expressed in terms of the wall shear rate while that for Couette flows vanishes. Thus, Eqn. (4.19) was only fitted to the experimental data for low shear rates where the trend remained linear.

Table 2 Slip coefficients of various gas slip models

Model	Coefficient b
Maxwell (1879)	$\frac{2-\sigma}{\sigma}\lambda$
Xue and Fan (2000)	$\frac{2-\sigma}{\sigma}\tanh(Kn)$
Deissler(1964)	$\frac{2-\sigma}{\sigma}\lambda\left(1-\frac{9}{8}Kn\right)$
Karniadakis(2005)	$\frac{2-\sigma}{\sigma}\lambda\left(1-Kn\right)$
Myong (2004)	$\frac{P}{4\omega P_r Kn+P}\lambda$

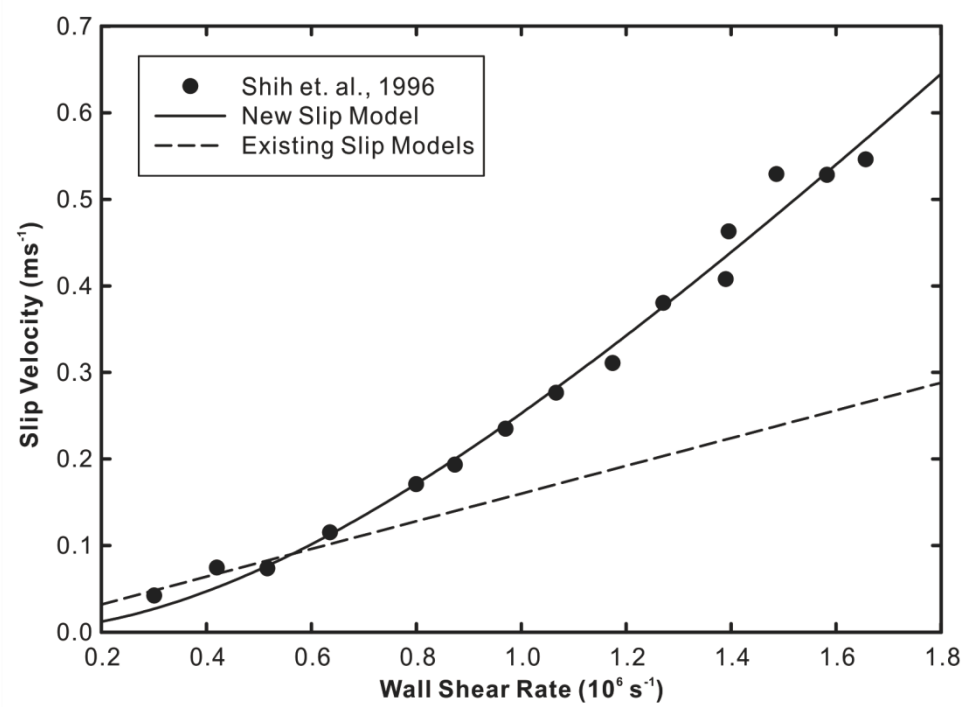

Fig. 4.2 Helium gas flow in silicon microchannel. Symbols: Experimental mass flow rate measurements for Kn = 0.158 (Shih et al. 1996). Solid line: Curve fit using Eqn. (4.14) with C_1 = 5.765 x 10^{-23} m, C_2 = 0.602 ms^{-1}. Dashed line: Curve fit using Eqn. (4.19) with b= 1.6 x 10^{-7} m.

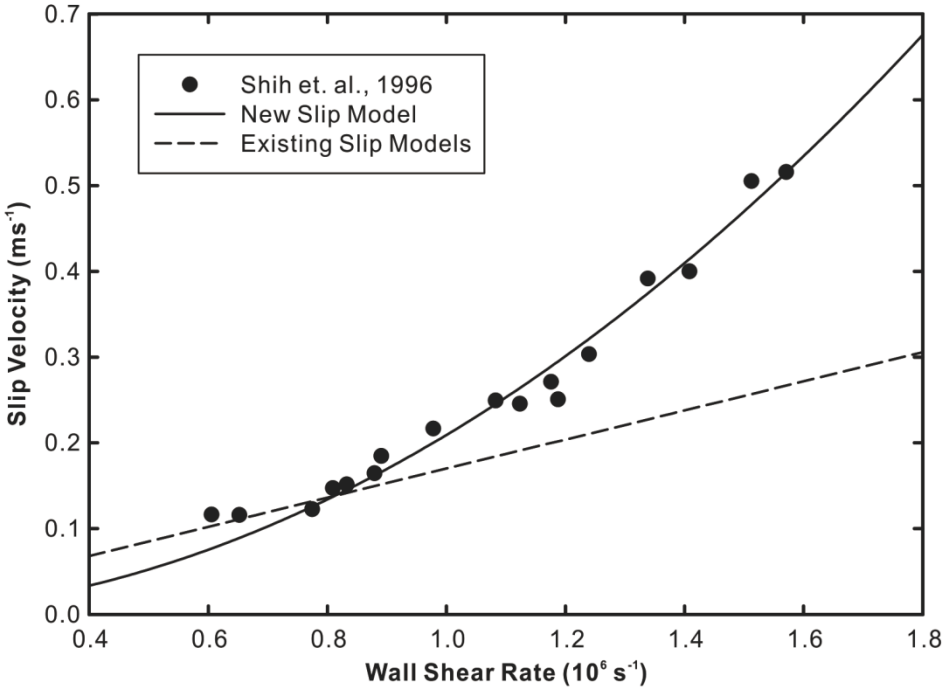

Fig. 4.3 Nitrogen gas flow in silicon microchannel. Symbols: Experimental mass flow rate measurements for Kn = 0.054 (Shih et al. 1996). Solid line: Curve fit using Eqn. (4.14) with C_1 = 1.038 x 10^{-24}m, C_2 = 36.63 ms^{-1}. Dashed line: Curve fit using Eqn. (4.19) with b= 1.7 x 10^{-7} m.

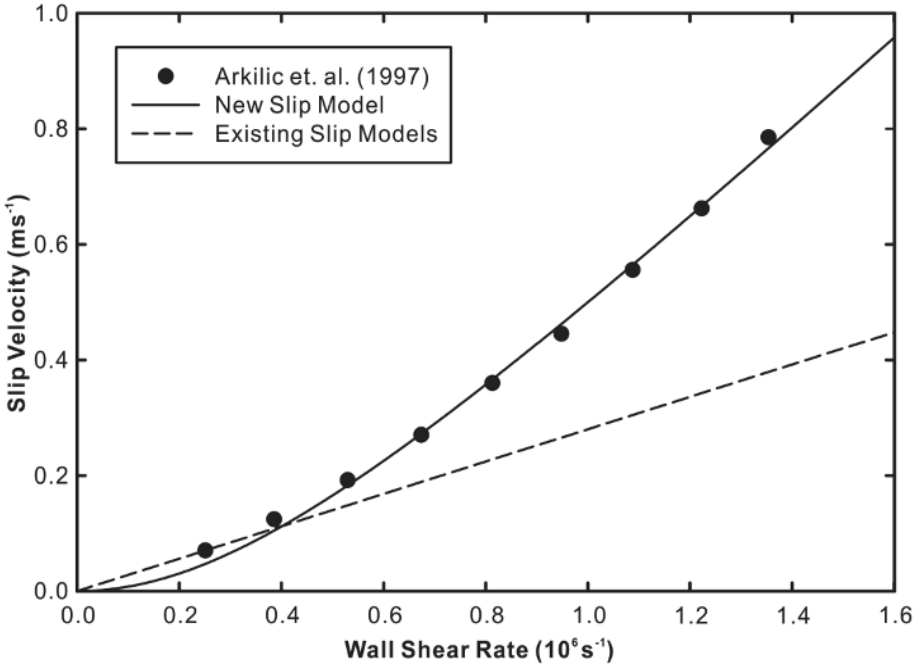

Fig. 4.4 Helium gas flow in silicon microchannel. Symbols: Experimental mass flow rate measurements for Kn = 0.155 (Arkilic et al. 1997). Solid line: Curve fit using Eqn. (4.14) with C_1 = 1.561 x 10^{-24} m, C_2 = 0.432 ms^{-1}. Dashed line: Curve fit using Eqn. (4.19) with b= 2.8 x 10^{-7} m.

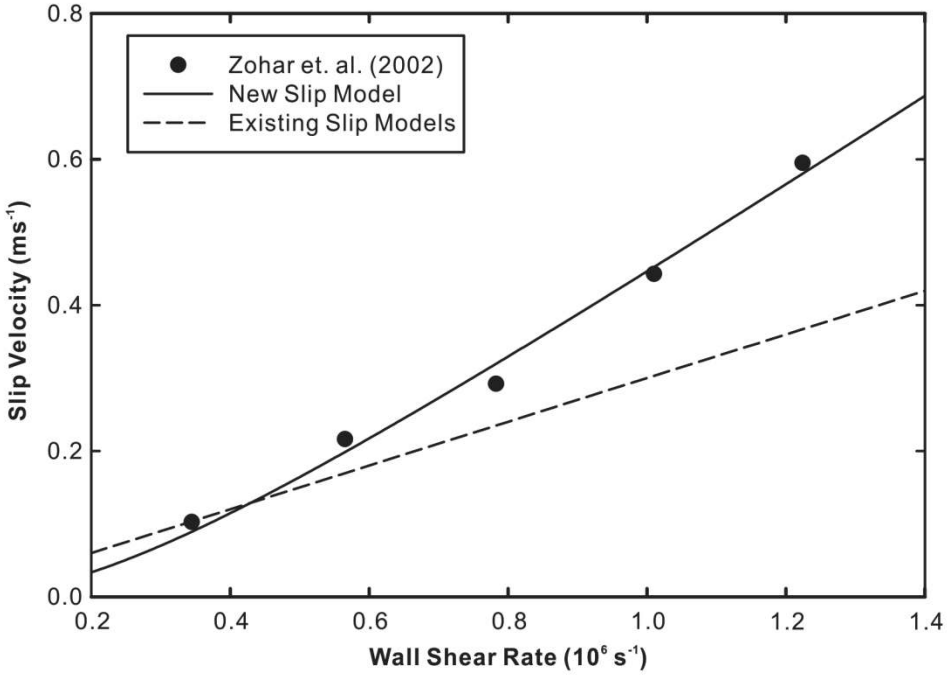

Fig. 4.5 Helium gas flow in silicon nitride microchannel. Symbols: Experimental mass flow rate measurements for Kn = 0.384 (Zohar et al. 2002). Solid line: Curve fit using Eqn. (4.14) with C_1 = 7.537 x 10^{-26} m, C_2 = 0.217 ms^{-1}. Dashed line: Curve fit using Eqn. (4.19) with b= 3.1 x 10^{-7} m.

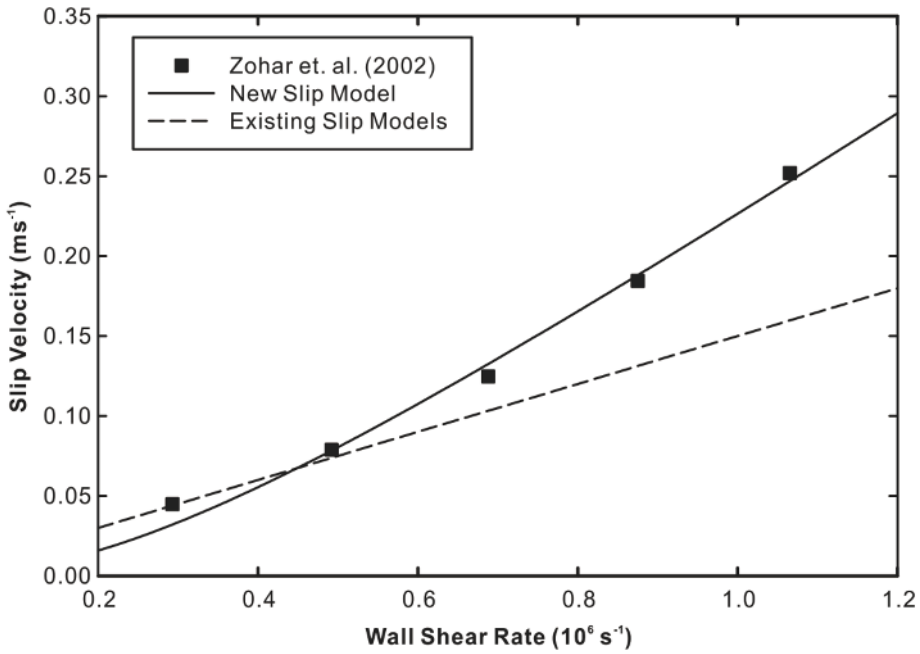

Fig. 4.6 Argon gas flow in silicon nitride microchannel. Symbols: Experimental mass flow rate measurements for Kn = 0.196 (Zohar et al. 2002). Solid line: Curve fit using Eqn. (4.14) with C_1 = 1.536 x 10^{-28} m, C_2 = 0.133 ms^{-1}. Dashed line: Curve fit using Eqn. (4.19) with b= 1.5 x 10^{-7} m.

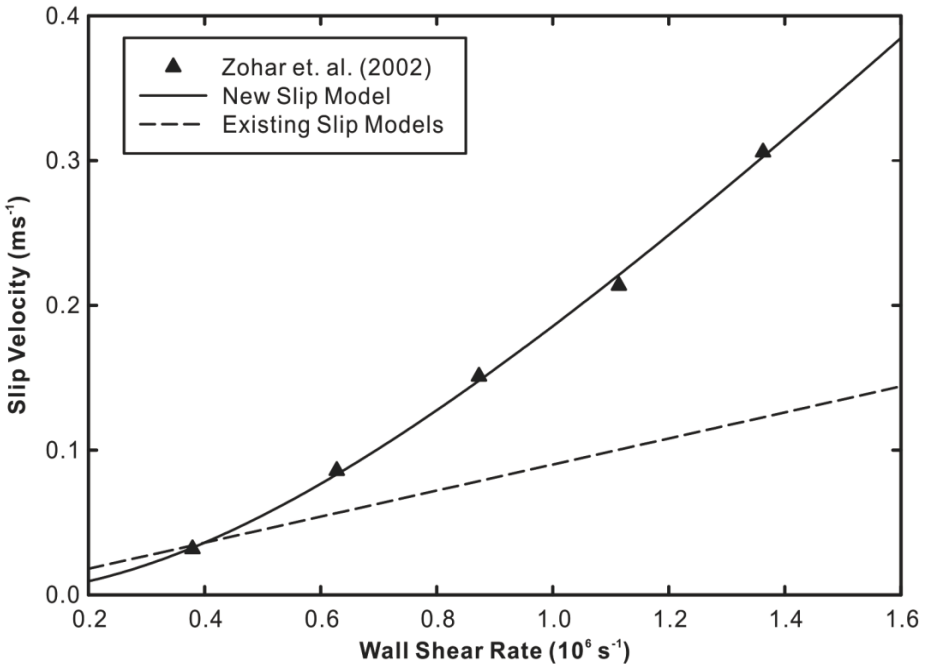

Fig. 4.7 Nitrogen gas flow in silicon nitride microchannel. Symbols: Experimental mass flow rate measurements for Kn = 0.118 (Zohar et al. 2002). Solid line: Curve fit using Eqn. (4.14) with C_1 = 2.616 x 10^{-24}, C_2 = 0.331 ms^{-1}. Dashed line: Curve fit using Eqn. (4.19) with b= 8.9 x 10^{-8} m.

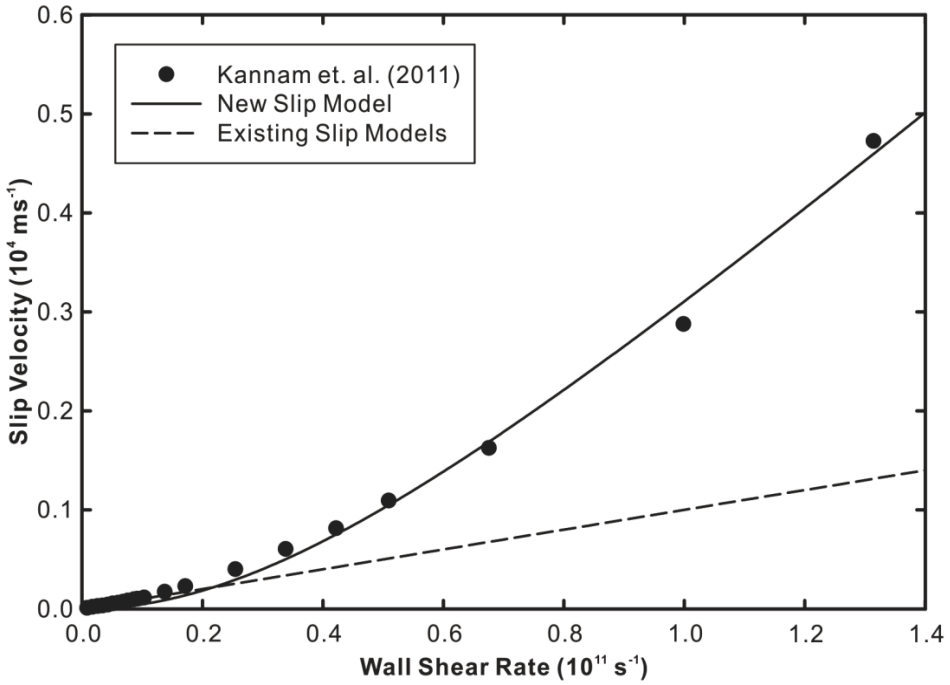

Fig. 4.8 Argon flow in graphene nanochannel. Symbols: NEMD simulation of Couette flow (Kannam et al. 2011). Solid line: Curve fit using Eqn(4.14) with C_1 = 4.29 x 10^{-28} m, C_2 = 2.89x 10^3 ms^{-1}. Dashed line: Curve fit using Eqn. (4.19)b= 9.0 x 10^{-9} m.

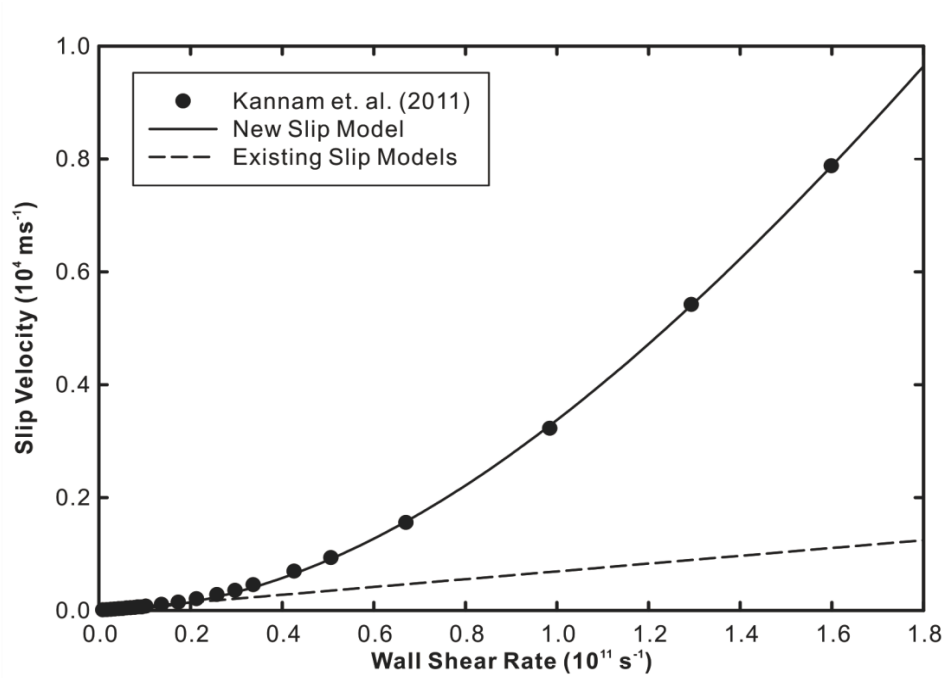

Fig. 4.9 Methane flow in graphene nanochannel. Symbols: NEMD simulation of Couette flow(Kannam et al. 2011). Solid line: Curve fit using Eqn. (4.14) with C_1 = 8.917 x 10^{-24} m, C_2 = 2.186 x 10^4 ms^{-1}. Dashed line: Curve fit using Eqn. (4.19) with b= 6.9 x 10^{-9} m.

The above results will be discussed in Section 4.5. In the next section, we will obtain predictions from the new model of experimental results for liquid slip on solid surfaces.

4.4 Validation of Slip Velocity Model for a Liquid-Solid Interface

For liquid flows on solid surfaces, a survey of the literature reveals a relative lack of analytical models for slip boundary condition. Majority of the experimental works and theoretical studies involving micro and nano-fluidics mostly employ the Navier slip boundary condition, which oversimplifies the problem due to the use of a constant slip length although the deviation from the model is apparent from experimental results. Again, we will use available results in the literature to demonstrate the conformity of predictions using our model.

4.4.1 Experimental Data for Liquid-Solid Interfaces

In the drainage force measurement approach, experimental data is normally plotted as slip length against nominal flow rate. For a surface force apparatus having identical cylindrical probes, the shear rate can be estimated from the expression

$$\dot{\gamma}_{\max} = \sqrt{\frac{27}{128}\frac{R}{h}}\frac{v_{peak}}{h} \tag{4.20}$$

where R refers to the radius of the cylinder, h the film thickness and v_{peak} the peak oscillation velocity for sinusoidal vibrations. Details of the derivation of Eqn. (4.20) are provided in the paper by Horn et al. (2000). Here, the maximum shear rate is used as a rough estimate since the shear rate varies in the region of measurement due to the curved geometry of the probes.

The rest of the experimental and numerical studies being compared did not require any experimental technique-based conversion apart from the straightforward calculation of slip velocity from the slip length and shear rate values provided using the Navier slip boundary condition.

4.4.2 Comparison with Experimental Studies for Liquid-Solid Interfaces

A total of six experimental and MD studies have been chosen for quantitative comparison with our slip model for liquid-solid interfaces. Given the pronounced non-linearity in most of the experimental data, predictions of the linear Navier slip velocity will not be shown in the graphs. Furthermore, the theoretical surface diffusion model of slip remains linear under experimental conditions as discussed previously and hence does not warrant a comparison with our model predictions.

Two of the selected studies were conducted by Zhu and Granick (2001, 2002b), who published a series of experimental findings on the subject of liquid slip with a particular focus on its shear rate dependency. In their experiments, they employed the popular thin film drainage force measurement technique by utilising a surface force apparatus. Slip lengths were inferred from force measurement curves for assorted liquid films of down to 2 nm thickness that were confined between sinusoidally-driven cylindrically-shaped mica probes -each of 2 cm radius of curvature and surfactant-coated. The exponential increase in slip length was apparent throughout most of their experimental results.

Another two sets of results were drawn from the studies of Huang et al. (2006) and Huang and Breuer (2007), who used an imaging technique known as total internal reflection velocimetry (TIRV) to probe the near-wall velocities for pressure-driven flows of tracer-laden deionised water in a 50 μm deep PDMS microchannel at glass surfaces of different wettabilities. In addition to the higher slip lengths measured for the hydrophobic surface (26 to 57 nm and 37 to 96 nm respectively for the hydrophilic and hydrophobic surfaces), it was similarly observed that the slip length was not a constant, increasing with an increase in shear rate.

Ulmanella and Ho (2008) reported mass flow rate slip measurements of liquid flows of isopropanol and n-hexadecane in micro and nanochannels of depths between 350 nm and 5 μm that were fabricated from glass bonded to a silicon substrate. The roughness of the channel walls was controlled by varying the etchant concentration. This allowed them to produce different surface roughness of 0.5 nm and 8.5 nm. Slip flow was clearly enhanced in the smoother channels and was shown to be independent of the channel heights. Non-linear slip behaviour was also evident in their experimental results.

The last study used was from an MD simulation of n-decane in a Couette flow configuration that was carried out by Martini et al. (2008a). Investigating the role of the wall model used in MD simulations and its resultant influence on the shear rate versus slip relationship, they discovered an unbounded increase in slip length with increasing shear-rate for a rigid surface model while that for the flexible surface model remained relatively constant at wall speeds of up to 1000 ms^{-1} for a channel height of 3 nm.

Data from the above studies were converted to values of slip velocity and wall shear rate and reproduced in Figs. 4.10 to 4.18, which also contain the least-squares fit using Eqn. (4.14) to provide verification for our newly derived slip velocity model.

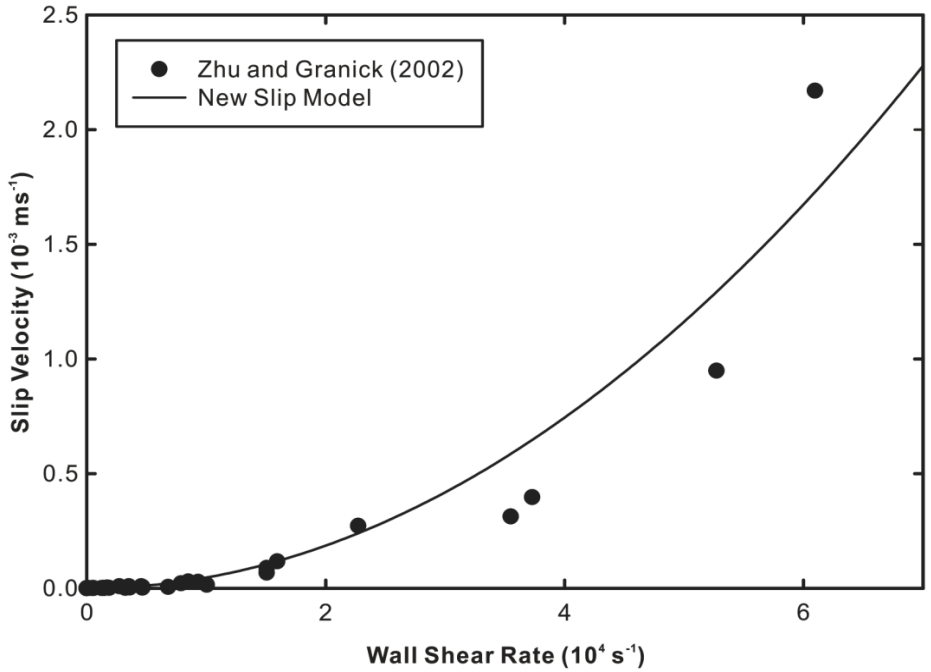

Fig. 4.10 DI water film between mica surfaces coated with polyvinyl alcohol. Symbols: Experimental thin film drainage force measurement using surface force apparatus (Zhu and Granick 2002a). Solid line: Curve fit using Eqn. (4.14) with C_1 = 2.55 x 10^{-11} m, C_2 = 1.19x 10^3 ms^{-1}.

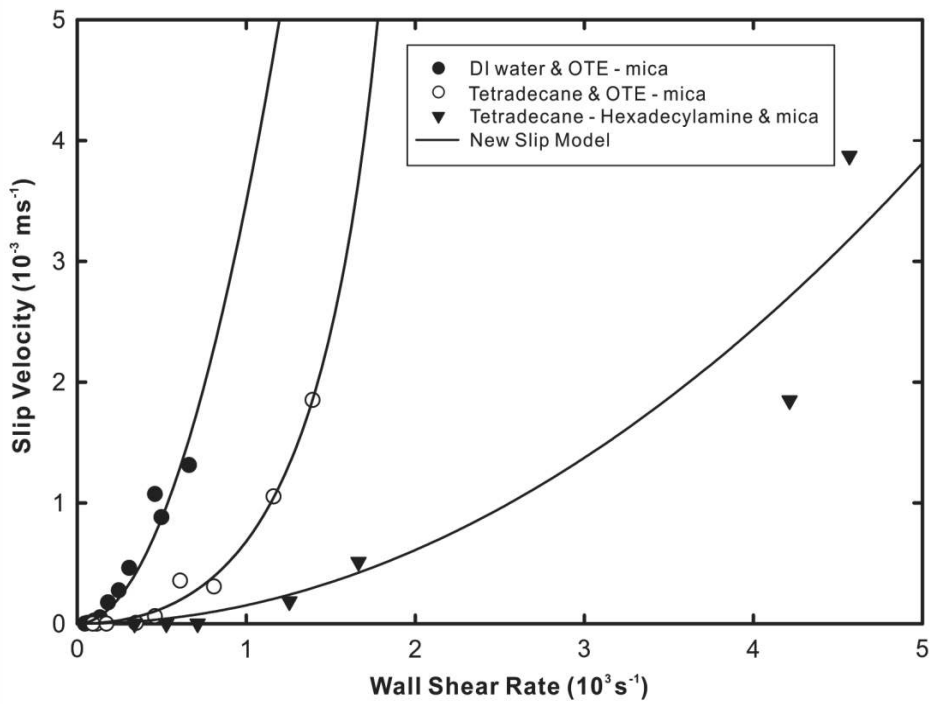

Fig. 4.11 Liquid films between coated mica surfaces (see legend). Symbols: Experimental thin film drainage force measurement using surface force apparatus (Zhu and Granick 2001). Solid line: Curve fit using Eqn. (4.14) with C_1 = 2.59 x 10^{-7} m, C_2 = 35.3 ms^{-1} (DI water - mica), C_1 = 3.83 x 10^{-10} m, C_2 = 7.39 ms^{-1} (Tetradecane & OTE - mica),C_1 = 2.38 x 10^{-10} m, C_2 = 17.4 ms^{-1} (Tetradecane – mica & HDA).

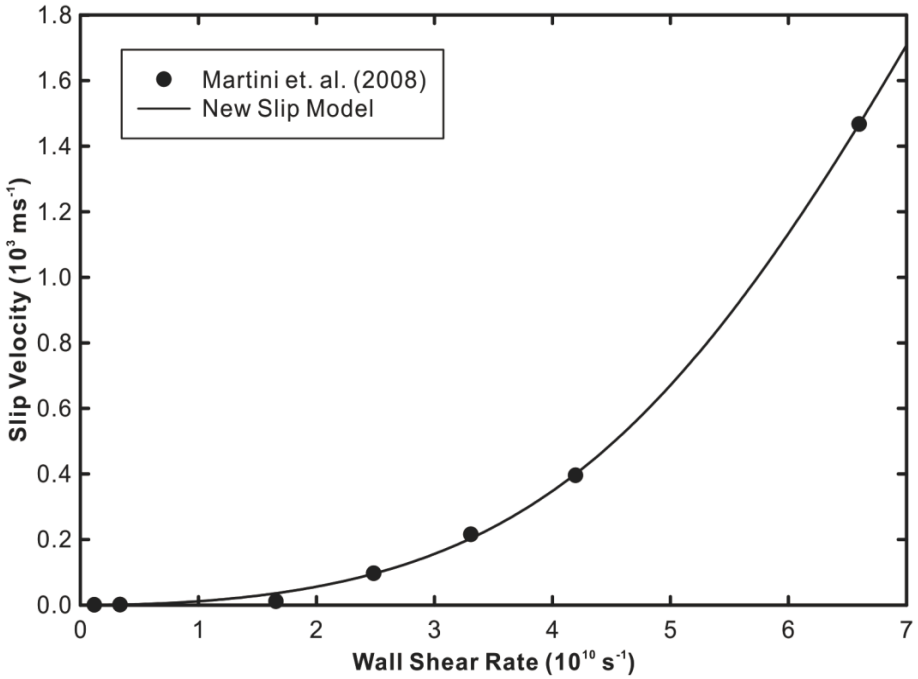

Fig. 4.12 n-decane between 'rigid' walls. Symbols: MD simulation of Couette flow (Martini et al. 2008a). Solid line: Curve fit using Eqn. (4.14) with C_1 = 3.55 x 10^{-8} m, C_2 = 2.267x 10^3 ms^{-1}.

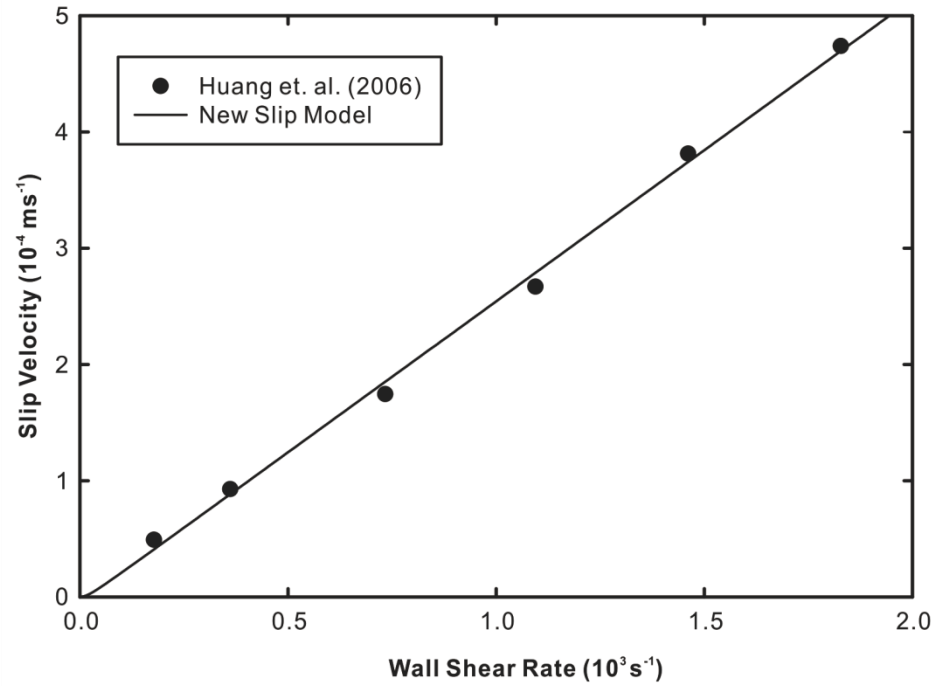

Fig. 4.13 DI water in hydrophilic PDMS microchannel on glass substrate. Symbols: Experimental measurement of liquid velocity using total internal reflection velocimetry (TIRV) technique (Huang et al. 2006). Solid line: Curve fit using Eqn. (4.14) with C_1 = 9.233 x 10^{-27} m, C_2 = 5.6x 10^{-6} ms^{-1}.

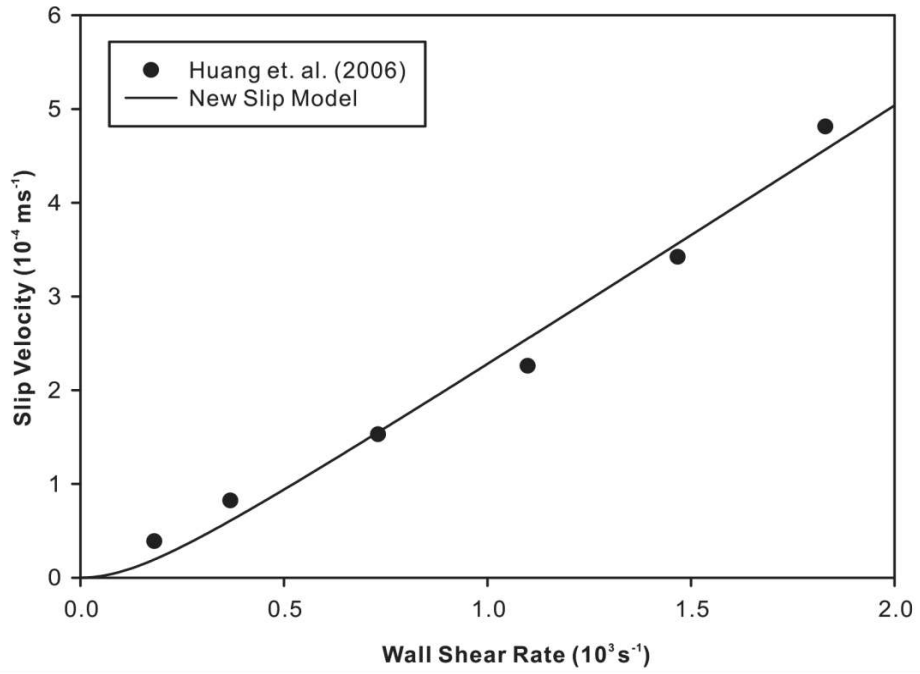

Fig. 4.14 DI water in PDMS microchannel on hydrophobic glass substrate. Symbols: Experimental measurement of liquid velocity using total internal reflection velocimetry (TIRV) technique (Huang et al. 2006). Solid line: Curve fit using Eqn. (4.14) with C_1 = 7.158 x 10^{-22} m, C_2 = 5.60 x 10^{-5} s^{-1}.

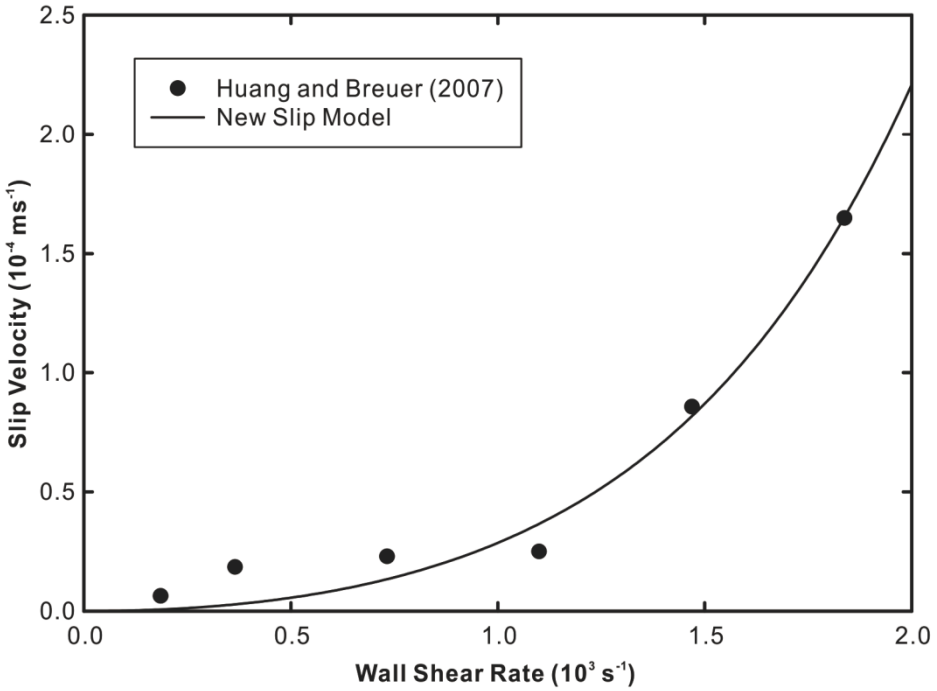

Fig. 4.15 DI water in PDMS microchannel on hydrophobic glass substrate. Symbols: Experimental measurement of liquid velocity using total internal reflection velocimetry (TIRV) technique (Huang and Breuer 2010). Solid line: Curve fit using Eqn. (4.14) with C_1 = 5.867 x 10^{-7} m, C_2 = 1.591x 10^{-3} ms^{-1}.

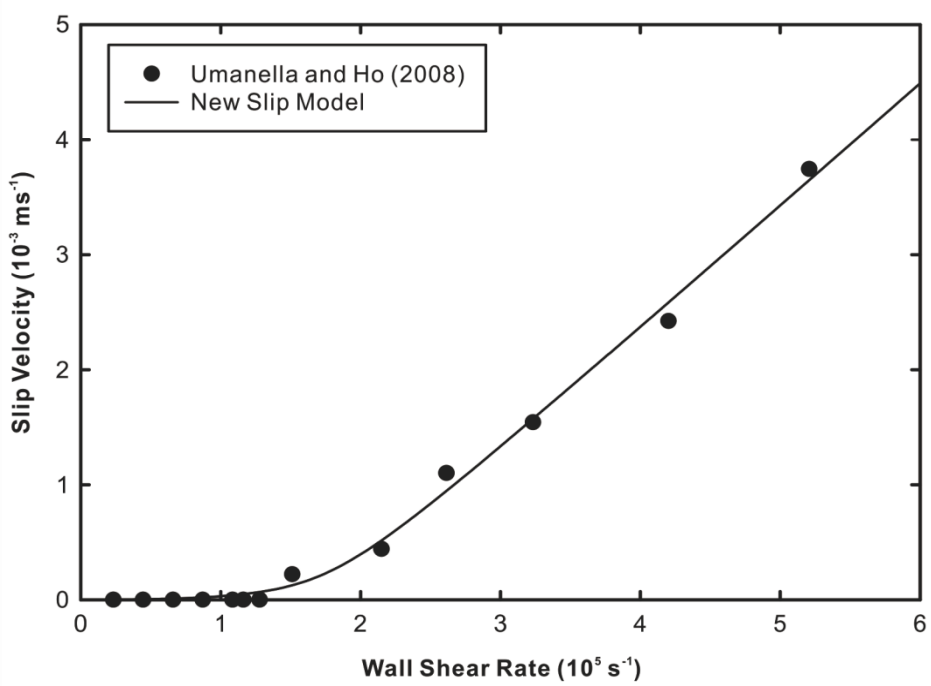

Fig. 4.16 Hexadecane in rough microchannel with glass and silicon walls. Symbols: Experimental flow rate measurement (Ulmanella and Ho 2008). Solid line: Curve fit using Eqn. (4.14) with C_1 = 5.2 x 10^{-9} m, C_2 = 9.93x 10^{-4} ms^{-1}.

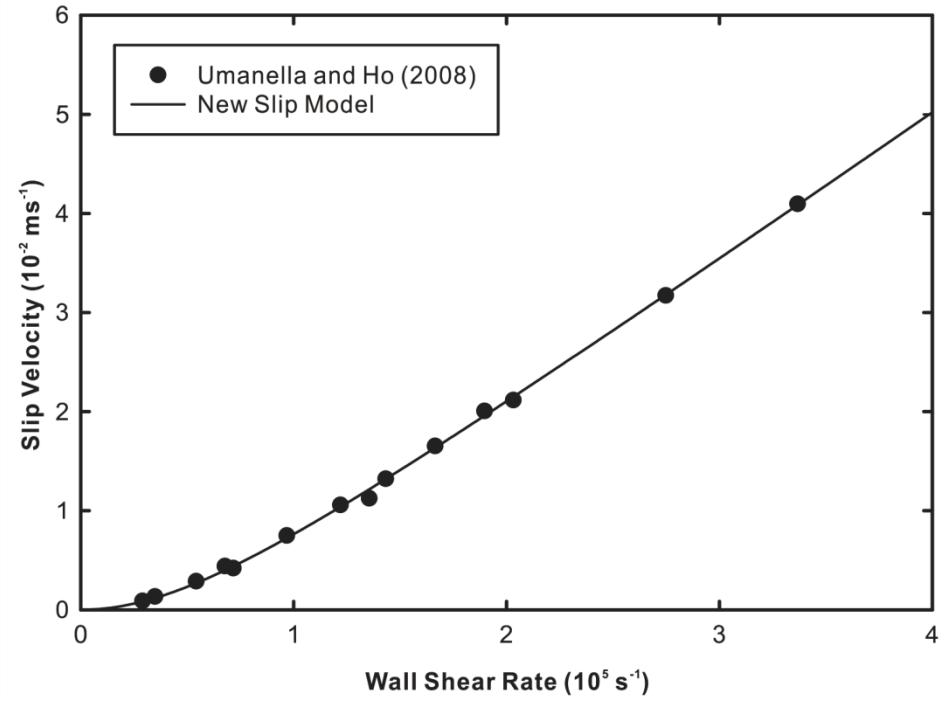

Fig. 4.17 Hexadecane in smooth microchannel with glass and silicon walls. Symbols: Experimental flow rate measurement (Ulmanella and Ho 2008). Solid line: Curve fit using Eqn. (4.14) with C_1 = 4.29 x 10^{-28} m, C_2 = 1.1x 10^{-4} ms^{-1}.

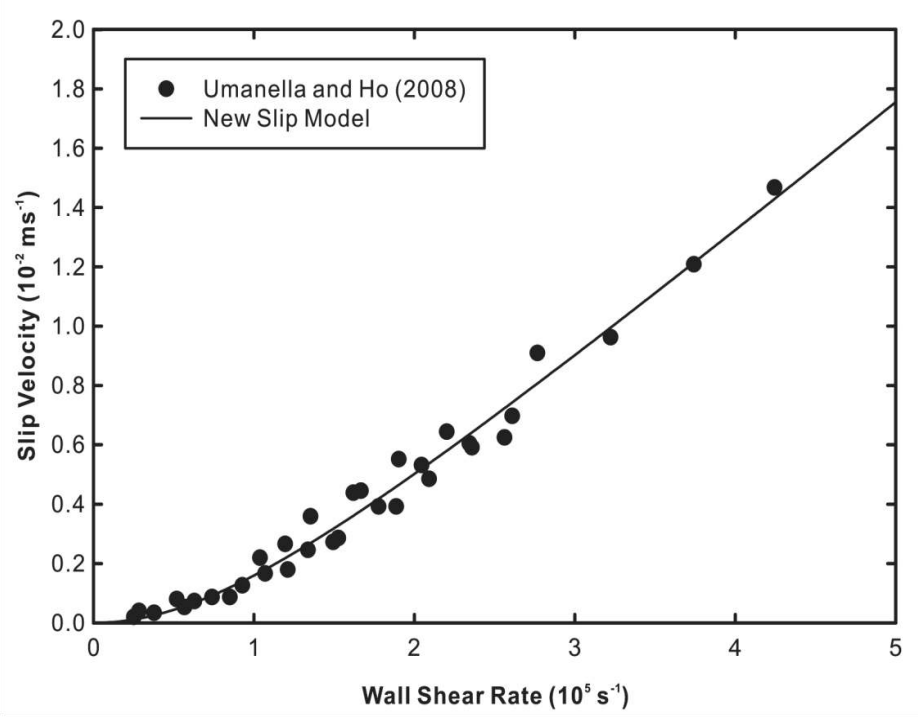

Fig. 4.18 Isopropanol in microchannel with glass and silicon walls. Symbols: Experimental flow rate measurement (Ulmanella and Ho 2008). Solid line: Curve fit using Eqn. (4.14) with C_1 = 2.9 x 10^{-26} m, C_2 = 5.45 x 10^{-5} ms^{-1}.

4.5 Discussion

It is evident from the slip velocity curves for both gases and liquids in Figs. 4.2 to 4.18 that the experimental data exhibit significant non-linearity at elevated wall shear rates which the existing slip boundary condition models fail to predict. By fitting Eqn(4.19) to the data lying within the low shear rate regime using constant slip coefficients, it is found that the analytical curves rapidly deviate from the experimental results as the wall shear rate increases. In contrast, our new model developed here consistently displays obvious improvement in the matching of experimental results, especially at high shear rates.

The poor agreement of existing theoretical models with experimental results for gaseous slip as seen in Figs. 4.2 to 4.9 can be attributed to the simple scattering law adopted in the kinetic-theory based models, which assumes a constant TMAC. Similarly, the elementary adsorption rule applied in the Langmuir approach corresponds to a constant

sticking probability. Conversely, the good agreement between our new model and the experimental results supports the idea of an adsorption-desorption based mechanism of fluid slip. This suggests that near-wall particles are not only limited to pure elastic and diffuse collisions but also various adsorption processes that transpire after impact, among which includes the dissipation of energy during escape from the mobile phase that contributes to the non-linear dependence on shear rate. The non-linear dependence on shear rate is dependent on the value of the coefficient C_2 in Eqn. (4.14), which reverts to a linear function of shear rate when C_2 is zero. Physically, C_2 represents the inelastic contribution of the trapping phase relative to the other adsorption states. As seen in the experiment results of Zohar et al. (2002) in Figs. 4.5 to 4.7 for helium, argon and nitrogen, C_2 increases as the non-linearity becomes more pronounced. In descending order, the values of C_2 are 0.331 ms^{-1} for nitrogen, 0.217 ms^{-1} for helium and 0.133 ms^{-1} for argon, which may be associated with the increasing viscosity of the gases of 1.79 x 10^{-5}Pa.s, 1.99 x 10^{-5}Pa.s and 2.27 x 10^{-5}Pa.s in the same order. The increasing fluid friction between the bulk and surface layers causes a greater dissipation of energy in the trapping phase and results in a lower escape velocity. Consequently, this could indicate that non-linear behaviour is suppressed for gases with higher viscosities.

According to Figs. 4.11, 4.13 and 4.14 which display results for various degrees of wetting, our model accurately reflects the influence of wetting intrinsically through the probability parameters. Qualitatively, the stronger fluid-solid attraction for a hydrophilic surface should lead us to expect a higher value of p_s and lower value of p_e. All other parameters being constant, this results in a higher value of the coefficient C_1. Referring to Fig. 4.11, the contact angles for DI Water and OTE-Mica, Tetradecane and OTE-Mica, and Tetradecane-HAD and Mica are 110^o, 44^o and 22^o respectively in descending order of hydrophobicity. This appears to correspond with the diminishing values of 2.59 x 10^{-7} m,

3.83 x 10^{-10} m and 2.38 x 10^{-10} m obtained for C_1. The experimental results of Huang et. al. (2006) in Figs. 4.13 and 4.14 also show a similar trend with a larger C_1 value of 7.16 x 10^{-22} m for the hydrophobic surface compared to 9.23 x 10^{-27} m for the hydrophilic one. The relationship between C_2 and viscosity that was apparent in the gaseous slip experiments was also evident in the experiments of Zhu and Granick (2001) in Fig. 4.11. Under similar experimental conditions, tetradecane, with a higher viscosity of 2.08 x 10^{-3} Pa s has a lower C_2 value of 3.83 x 10^{-10} ms^{-1} compared to that of water of viscosity 8.9 x 10^{-4} Pa s and C_2 value of 2.59 x 10^{-7} ms^{-1}.

The lack of analytical expressions for the probabilities p_e and p_m confounds the task of obtaining physically sound estimates of their values. One would be tempted to estimate the values of p_s, p_e and p_m based on the best-fit coefficients for each data set. However, this requires approximate values of other parameters such as the free surface diffusion velocity and the friction coefficient for the specific gas-solid pair which are not readily available in most cases. On the other hand, the sticking probability p_s may be estimated but this too requires approximation of certain parameters that will be elaborated upon below.

In activated adsorption, p_s can be evaluated using the expression

$$p_s = f(\theta)\exp\left(-\frac{E_a}{k_B T}\right) \tag{4.21}$$

where E_a is the activation energy and $f(\theta)$ is the surface coverage factor - equivalent to the probability of landing on a vacant site in ideal adsorption. In the case of non-activated adsorption, p_s is a function of the normal component of energy $E_n = E_0 \cos^2 \theta_{in}$ in what is termed as normal energy scaling if the potential energy surface

is only considered one-dimensionally along the normal direction. It was determined through empirical fits of sticking probability data from molecular beam experiments and later theoretically derived that has the sigmodal form (Michelsen and Auerbach 1991, Luntz 2000)

$$p_s = p_{s,sat}\left[1+\mathrm{erf}\left(\frac{E_n - E_{n,c}}{W}\right)\right] \tag{4.22}$$

where $p_{s,sat}$ is the saturation sticking probability, $E_{n,c}$ is the value of E_n at the point of inflection on the curve and W is the width of the potential barrier distribution. However, there is now evidence that the sticking probability could scale with the total kinetic energy rather than just the normal component of energy (Thorman and Bernasek 1981). A possible reason for total energy scaling is due to the presence of corrugation, which introduces a coupling between the parallel and perpendicular components of velocity. Furthermore, it has been suggested that the prevalence of normal energy scaling could be a fortuitous outcome of the collective effects of energetic and geometric corrugations (Darling and Holloway 1994). The sticking probability in total energy scaling varies as $s = s\left(E_n, E_t\right)$ where the parallel component of energy $E_n = E_0 \sin^2\theta_{in}$. Interestingly, total energy scaling will result in higher-order shear rate dependence. Strictly speaking, the sticking probability corresponding to the instantaneous surface coverage should be used. This true value will be different from the initial sticking probability prescribed for an adsorbate-free surface. The initial sticking probability is a function of molecular and steric factors that include the incident angle, kinetic energy, temperature, relative orientation of the adsorbate and substrate particles and the location of collision on the substrate. These factors have a strong influence in activated adsorption, which typically exhibits a low initial sticking probability, but not in non-activated adsorption as the initial sticking probability is near unity.

In the literature, the contribution to molecular slip by adsorbed molecules in the mobile state u_m has been suggested to originate from a surface diffusion mechanism of thermally activated surface hops between adjacent adsorption sites (Ruckenstein and Rajora 1983, Yang 2010, Wang and Zhao 2011). Estimates of the slip velocities occurring from this particular mechanism have been shown to be relatively small compared to experimentally measured values (Bowles et al. 2011). Therefore, this form of molecular slip will account for a smaller fraction of the overall slip velocity compared to the contributions by molecules in the other adsorption states. For slip of liquids on solid surfaces, the mobile adsorbed molecules are expected to make a more significant contribution as the more tightly-packed molecular arrangement diminishes the effect of scattering states. Hence, this may imply that the migration of molecules directly across solid surfaces could arise from other surface diffusion mechanisms. In the next chapter, we propose two alternative mechanisms that are shown to produce enhanced slip velocities compared to surface hopping.

5 Slip of Fluid Molecules on Solid Surfaces by Surface Diffusion

In our unified slip velocity model presented in the last chapter, the fraction of fluid molecules in the mobile state were depicted as undergoing a form of one-dimensional surface diffusion hopping mechanism that was first suggested by Ruckenstein and Rajora (1983). It is intrinsically assumed in this model that individual hopping events are uncorrelated, that is, the time scale of substrate motion (which causes the damping of surface hopping motion) is much shorter than that of the motion of adsorbed fluid molecules. Also, the adsorbed fluid molecules are assumed to remain physically bound to the surface, albeit in a mobile state.

In this chapter, we explore two varying slip motions by surface diffusion that produce contrasting slip velocities. The first is a persistent asymmetric random walk model which considers short-term correlations in molecular motion while the second involves a re-adsorption mechanism that has been proposed as an alternative surface diffusion mechanism for adsorbed liquid molecules on a solid surface. The two proposed molecular slip mechanisms give rise to higher magnitudes of slip velocity that are nearer to experimentally measured values compared to the prevailing basic surface hopping model.

In the one-dimensional surface diffusion mechanism, a fluid molecule is depicted as performing thermally activated unit hops between adjacent adsorption sites on the substrate in the presence of an external force in what is fundamentally an asymmetric discrete random walk with unequal probabilities in both directions as shown in Fig. 5.1.

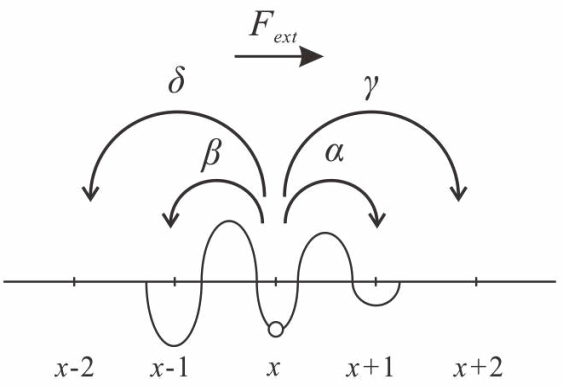

Fig. 5.1 Surface molecular slip motion as an asymmetric random walk

The mean surface velocity of the adsorbed fluid molecules can be obtained as the drift velocity $\langle v \rangle$

$$\langle v \rangle = (\alpha - \beta) a \tag{5.1}$$

where α and β represent the respective rates of hops in the same and opposite directions of the external force, a is the distance between adjacent adsorption sites (assigned as unit spacing in the figure) and τ^{-1} is the hopping frequency.

The nearest neighbour hopping represents the most basic surface diffusion motion. Rough estimates of molecular slip via this process have been shown to be relatively small compared to experimentally obtained values of slip velocity (see Section 3.1.4). An adsorbed fluid molecule is also capable of making longer jumps to adsorption sites that are further away if its energy is not entirely dissipated in a single hop. The energy dissipation for a hopping distance of one lattice spacing can be estimated as (Ala-Nissila et al. 2002)

$$\begin{aligned} \Delta E &= \int_{-a/2}^{a/2} m\eta v(x) dx \\ &= \eta \int_{-a/2}^{a/2} \sqrt{2m\left[E_0 - E(x)\right]} dx \end{aligned} \tag{5.2}$$

where m refers to the molecular mass, η is the friction coefficient per unit mass. The energy terms E_0 and $E(x)$ refer to the total initial energy of the molecule and the instantaneous energy of the moving molecule.

The condition for long jumps is as follows $\Delta E < k_B T$ or from Eqn(5.2)

$$\eta\tau < \frac{k_B T}{E_a \pm E_{ext}} \tag{5.3}$$

where E_a and E_{ext} refer to the activation and external energy.

We may extend the above random walk model to account for longer hops. As a simple example, if hops are limited to two lattice spacing as sketched in Fig. 5.1, the molecular slip velocity can be expressed as (Antczak and Ehrlich 2008)

$$\langle v \rangle = (\alpha + 2\gamma - \beta - 2\delta) a \tag{5.4}$$

Non-nearest-neighbour hops have higher activation energies and are therefore less likely to occur compared to nearest neighbour hops. Assuming that the ratio of forward and backward hops remains constant, the consideration of next nearest neighbour jumps results in a slightly higher slip velocity. This procedure may be extended to longer jumps or even variable jump distances as in the scenario of surface diffusion on non-crystalline surfaces.

The surface diffusion motion of fluid molecules on solid substrates is influenced by fluid-substrate and fluid-fluid interactions. In the Markovian surface hopping model, consecutive hops are assumed to be independent. However, in the real situation, diffusion exhibits temporal behaviour with velocity correlations. The degree of correlation can be estimated based on the relative time scales of surface excitations and

molecular motion. Memory effects may be ignored if the Debye frequency of the substrate is much greater than the vibrational frequency of the adsorbed molecule in a potential well (Ala-Nissila et al. 2002). Single particle velocity correlations result in a variety of diffusion phenomena such as recrossing and multiple hops spanning more than one lattice spacing. In the next section, we will study the effects of correlated hops on the molecular slip velocity arising from surface diffusion.

5.1 Persistent surface diffusion model of molecular slip

To account for memory effects, we include the phenomena of persistence in the asymmetric random walk model of surface hopping diffusion. Here, we will only consider fast-decaying correlations between two consecutive hops as it will allow us to represent the effect of persistence using a single probability factor.

The probabilities of forward and backward hopping motion of the molecules in a discrete, persistent biased random walk, p_F and p_B, may be represented by the following set of recurrence relations

$$\begin{aligned} p_F(x,t) &= p_{F|F}\,p_F(x-a,t-\tau) + p_{F|B}\,p_B(x-a,t-\tau) \\ p_B(x,t) &= p_{B|B}\,p_B(x+a,t-\tau) + p_{B|F}\,p_F(x+a,t-\tau) \end{aligned} \tag{5.5}$$

where the subscripts F and B denote forward and backward directions and probability terms such as $p_{F|B}$ represents the probability that a molecule makes a backward hop followed by a forward hop.

The mean velocity $\langle v(x,t)\rangle$ can be evaluated from the difference equation

$$\begin{aligned}\langle v(x,t)\rangle &= \frac{a}{\tau}\left[\, p_F\left(x+a,t+\tau\right) - p_B\left(x-a,t+\tau\right)\right] \\ &= \frac{a}{\tau}\left[\left(p_{F|F}-p_{B|F}\right)p_F\left(x,t\right) - \left(p_{B|B}-p_{F|B}\right)p_B\left(x,t\right)\right] \\ &= \frac{a}{\tau}\left\{\begin{array}{l}\left(p_{F|F}-p_{B|F}\right)\left[\, p_{F|F}\,p_F\left(x-a,t-\tau\right) + p_{F|B}\,p_B\left(x-a,t-\tau\right)\right] \\ -\left(p_{B|B}-p_{F|B}\right)\left[\, p_{B|B}\,p_B\left(x+a,t-\tau\right) + p_{B|F}\,p_F\left(x+a,t-\tau\right)\right]\end{array}\right\}\end{aligned} \tag{5.6}$$

The probabilities p_F and p_B may be expressed in terms of the probability of a change in hopping direction per unit time (Balakrishnan and Chaturvedi 1988)

$$\begin{aligned} p_F\left(x,t\right) &= \frac{\nu_B}{\nu_B+\nu_F} \\ p_B\left(x,t\right) &= \frac{\nu_F}{\nu_B+\nu_F}\end{aligned} \tag{5.7}$$

where $\nu_B = p_{F|B}/\tau$ and $\nu_F = p_{B|F}/\tau$ represent the rates of directional reversals while moving in the backward and forward directions respectively. The ratio of forward and backward moving durations are in the ratio ν_B/ν_F .

The mean drift velocity in the steady-state is therefore

$$\langle v\rangle = \frac{\nu_B-\nu_F}{\nu_B+\nu_F}\frac{a}{\tau} \tag{5.8}$$

Eqn. (5.8) represents the contribution to the slip velocity by the biased random walk motion of molecules on the substrate with the inclusion of short-term correlations. To aid the comparison of the molecular slip velocities from a persistent, biased random walk and that from a purely biased random walk, we may approximate the reversal rates in Eqn. (5.8) by the probabilities $p_{F|B}$ and $p_{B|F}$, which can be expressed in terms of the independent effects of persistence and the external field

$$\begin{aligned} p_{F|B} &= \frac{r\alpha}{r\alpha + t\beta} \\ p_{B|F} &= \frac{r\beta}{t\alpha + r\beta} \end{aligned} \tag{5.9}$$

where the persistence terms, transmittance t represents the probability of the molecule making two consecutive hops in a similar direction and reflectance r the probability that the molecule reverses its hopping direction during the next hop. We will assume that the transmittance and reflectance are constant at individual adsorption sites such that $t + r = 1$. The forward and backward probabilities α and β arising from the external field retain the same meaning as that used previously in the asymmetric random walk.

Substitution of Eqn. (5.9) into Eqn. (5.8) gives the molecular slip velocity as

$$\begin{aligned} \langle v \rangle &= \left[\frac{p_{F|B} - p_{B|F}}{p_{F|B} + p_{B|F}} \right] \frac{a}{\tau} \\ &= \frac{t(\alpha - \beta)}{t + 2\alpha\beta(1 - 2t)} \frac{a}{\tau} \end{aligned} \tag{5.10}$$

As a simple check, we may substitute the values $t = r = 1/2$ to remove the effect of correlations, which reverts the above drift velocity expression to that of the biased random walk. Next, we will compare the molecular slip behaviour of a persistent, bias nature with that of the original bias form.

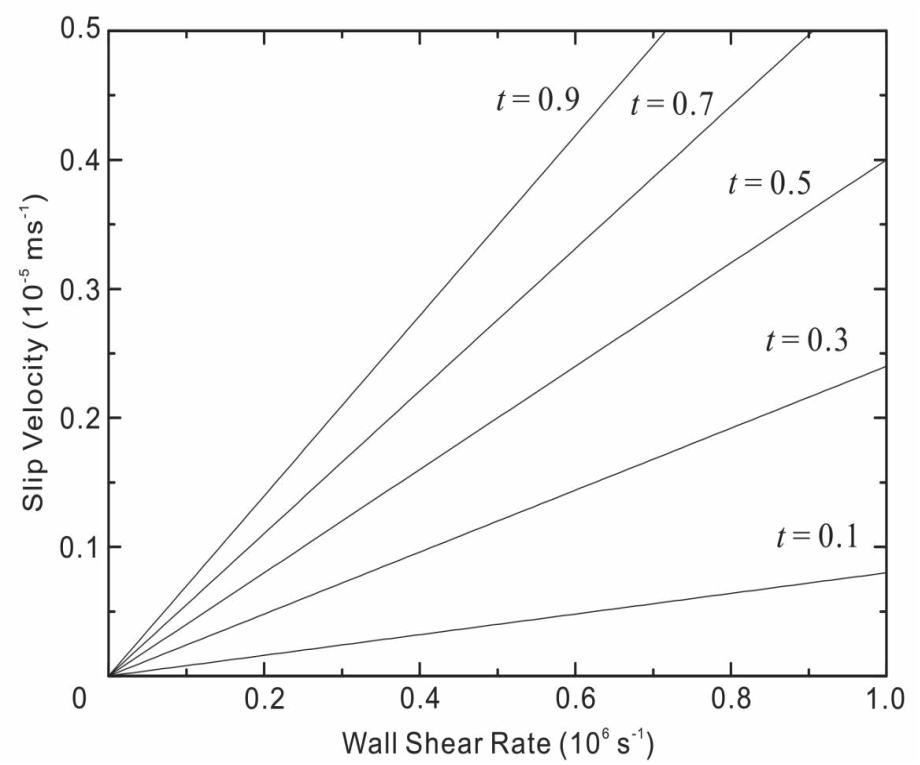

Fig. 5.2 Molecular slip velocity as a function of wall shear rate for a persistent biased random walk for different values of transmittance t. The curve for $t = 0.5$ is that of the basic biased random walk without memory effects

5.2 Discussion

We investigate the effect of persistence for different values of the transmittance using typical values of the forward and backward hopping rates for parameters corresponding to an interface between water and mica substrate as described in Chapter 3. With driven flow of the water, we expect the forward probability to be higher than that in the backward direction. The inclusion of correlations between two consecutive hops affects the overall drift velocity and displays some intriguing behaviour. As illustrated in Fig. 5.2, the molecular slip velocity in the range of $t < 0.5$ is smaller than that of the memoryless biased random walk ($t = 0.5$). For a decreasing value of transmittance i.e. the molecules have a higher tendency of making hops in the reverse direction, memory effects dominate the molecular slip behaviour, weakening the influence of the external field. In the extremely low range, the persistence virtually neutralises the external bias, bringing the system closer to that of a symmetric random walk with a very low drift velocity. On the other hand, molecular slip velocities are higher for correlated motion ($t > 0.5$) compared to the purely asymmetric case. The persistence augments the hopping rates in the direction of the external field, although it should be noted that there has to be a directional bias for this enhancement to be effective.

In physical terms, persistence arises from weak liquid-solid interactions where the internal friction between the substrate atoms and mobile adsorbed molecule is not large enough for the energy to be dissipated in a single hop. From a molecular perspective of slip flow on solid surfaces, the relative time-scales of substrate and adsorbed molecule should then be an important consideration in obtaining desired slip behaviour.

Here, we note that only rapidly-decaying correlations have been considered such that they are only limited to two consecutive hops and that the degree of correlation is

uniform throughout the substrate. This allowed us to represent the memory effects using constant probability factors while still providing adequate insight into the phenomena. For non-crystalline substrate lattices, the transmittance for individual sites should be expected to be different. Correlated motion spanning more than two hops can be analysed using correlation functions (Ala-Nissila et al. 2002).

Apart from the surface hopping mechanism, experimental and theoretical studies have identified other different mechanisms of surface diffusion. The migration of an adsorbed molecule across the surface may also occur through: (i) exchange mechanism in which the adsorbed molecule switches places with a substrate atom (ii) quantum tunneling of a molecule of small mass under low temperature conditions (iii) vacancy migration when the surface adsorption coverage is high (iv) cluster diffusion in adsorbed molecules adhere to form a stable group due to lateral interactions and move together as an island (Oura et al. 2003). In the next section, we describe a molecular slip mechanism due to a different surface diffusion phenomenon that results in superdiffusive behaviour and consequently larger slip velocities.

5.3 Bulk-mediated mechanism of molecular slip motion on solid surfaces

An interesting non-Fickian self-diffusion mechanism of liquid molecules at an interface termed as bulk-mediated effective surface diffusion was proposed by Bychuk and O'Shaughnessy (1995). The mechanism consists of repeated adsorption-desorption of a fluid molecule on the surface. The process begins with the adsorption of a near-surface molecule from the bulk liquid, following which it gets desorbed after a certain waiting time. During this period of desorption, the molecule rejoins and undergoes diffusion within the bulk liquid. Subsequently, the molecule gets readsorbed at a different

adsorption site when it is within the attraction range of the substrate, after having travelled a certain distance in the bulk. The continuous cycle of adsorption and desorption effectively results in an interfacial self-diffusion process. This mechanism is unique in that the surface diffusion conforms to a Levy process instead of the usual Fick's law, exhibiting superdiffusive behaviour with displacement $r \propto t$ instead of the familiar $r \propto \sqrt{t}$.

The bulk-mediated model above describes the self-diffusion of liquid molecules in a quiescent liquid. Here, we will consider a flowing bulk liquid, or in other words, an external force which drives the desorbed molecule in the direction of the force when it returns to the bulk phase before being readsorbed. The bulk-mediated diffusion process in the presence of a driven flow is sketched in Fig. 5.3. Intuitively, this should produce a faster molecular slip velocity compared to the surface hopping mechanism.

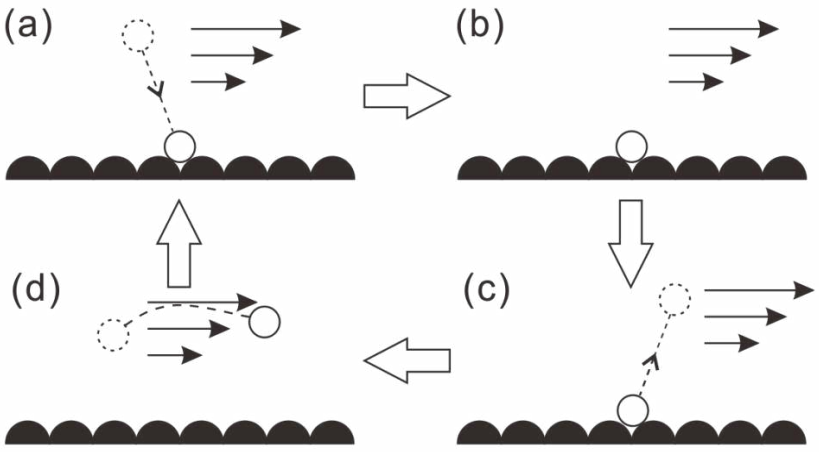

Fig. 5.3 Desorption mediated mechanism of molecular fluid slip: (a) adsorption/re-adsorption from bulk flow (b) adsorbed phase of duration t_{surf} (c) desorption into bulk flow (d) bulk excursion of duration t_{bulk}.

Molecules lying within the surface attraction region of height λ normal to the surface are adsorbed at a rate Q_{ads}. The characteristic time scale of readsorption t_{ads} can be estimated from the displacement in the normal direction which occurs via diffusion

$$t_{ads} = \frac{D}{\left(Q_{ads}\lambda\right)^2} \tag{5.11}$$

where D represents the bulk diffusivity.

From the survival probability $S(\tau) \propto \tau^{-1/2}$, the readsorption time distribution $\psi(\tau)$ can be expressed as

$$\begin{aligned} \psi(\tau) &= -\frac{dS}{d\tau} \\ &= \frac{t_{ads}^{1/2}}{\tau^{3/2}} \end{aligned} \tag{5.12}$$

which is valid in the range $\tau > t_{ads}$

The total duration of time spent in the bulk liquid t_{bulk} by an adsorbed molecule after n cycles of adsorption-desorption is

$$\begin{aligned} t_{bulk} &= \int_{t_{ads}}^{t_{bulk}} n\tau\psi(\tau)d\tau \\ &= n^2 t_{ads} \end{aligned} \tag{5.13}$$

The total residence time t_{surf} is

$$t_{surf} = nQ_{des}^{-1} \tag{5.14}$$

where Q_{des} is the desorption rate

Hence, the total time t_{total} during which the molecule undergoes bulk-mediated diffusion is

$$t_{total} = t_{surf} + t_{bulk} \tag{5.15}$$

In general, the bulk-mediated diffusion dominates when $t_{total} \ll t_{ret}$, where t_{ret} is termed as the surface retention time

$$t_{ret} = \frac{1}{Q_{des}^2 t_{ads}} \tag{5.16}$$

In other words, surface diffusion via this mechanism takes place when the time between desorption events is longer than the readsorption time. This indicates a strongly adsorbing system in which the molecules are repeatedly readsorbed at a different adsorption site after getting desorbed without being permanently retained in the bulk phase. Molecules are lost to the bulk phase at times exceeding the surface retention time.

Following from the above analysis, the molecular slip in bulk-mediated surface diffusion can be obtained as the total displacement of the adsorbed molecule in the direction parallel to the surface $n\langle x\rangle$ per unit time for the total duration of time spent in the bulk-mediated diffusion process

$$\langle v\rangle = \frac{n\langle x\rangle}{t_{total}} \tag{5.17}$$

When a molecule is temporarily desorbed into the bulk flow, it gets driven by the shear flow which is assumed in this case to be linear without loss of generality. The driving force can be approximated by

$$F_{shear} = \mu A\dot{\gamma} \tag{5.18}$$

where μ refers to the dynamic viscosity of the liquid, A the effective molecular surface area and $\dot{\gamma}$ the shear rate of the liquid near the surface.

The net displacement of the molecule during each desorption-readsorption cycle can be estimated kinematically as

$$\langle x\rangle = \frac{1}{2m} F_{shear} t_{bulk}^2 \tag{5.19}$$

Where m refers to the mass of the molecule.

Combining Eqns. (5.13) to (5.19), the molecular slip velocity is eventually obtained as

$$\begin{aligned} \langle v \rangle &= \frac{\mu A}{2m}\left(\frac{n t_{bulk}^2}{t_{surf}+t_{bulk}}\right)\dot{\gamma} \\ &\approx \frac{\mu A}{2m} n^3 t_{ads}^2 Q_{des}\dot{\gamma} \end{aligned} \tag{5.20}$$

The only unknown parameter in Eqn. (5.20) is the number of desorption-readsorption cycles n. In Fig. 5.4, we compare the theoretical predictions of interfacial molecular slip from bulk-mediated diffusion in Eqn. (5.20) and surface hopping diffusion in Eqn (4.10) against two sets of experimental data from the literature for slip velocity measurements of DI water in hydrophilic and hydrophobic microchannels conducted by Huang et al. (2006). The parameters used in Eqn. (5.20) are as follows: $\mu = 9\times10^{-4}$ Pa.s , $A = 1.617\times10^{-19}$ m^2 (Bowles et al. 2011), $m = 3\times10^{-23}$ kg , $t_{ads} = 10^{-13}$ s (Butt et al. 2004), $Q_{des}t_{ads} = 10^{-6}$ (Bychuk and O'Shaughnessy 1995). n was used as a fitting parameter for matching of the experimental results. Parameters for the surface hopping model are as previously described.

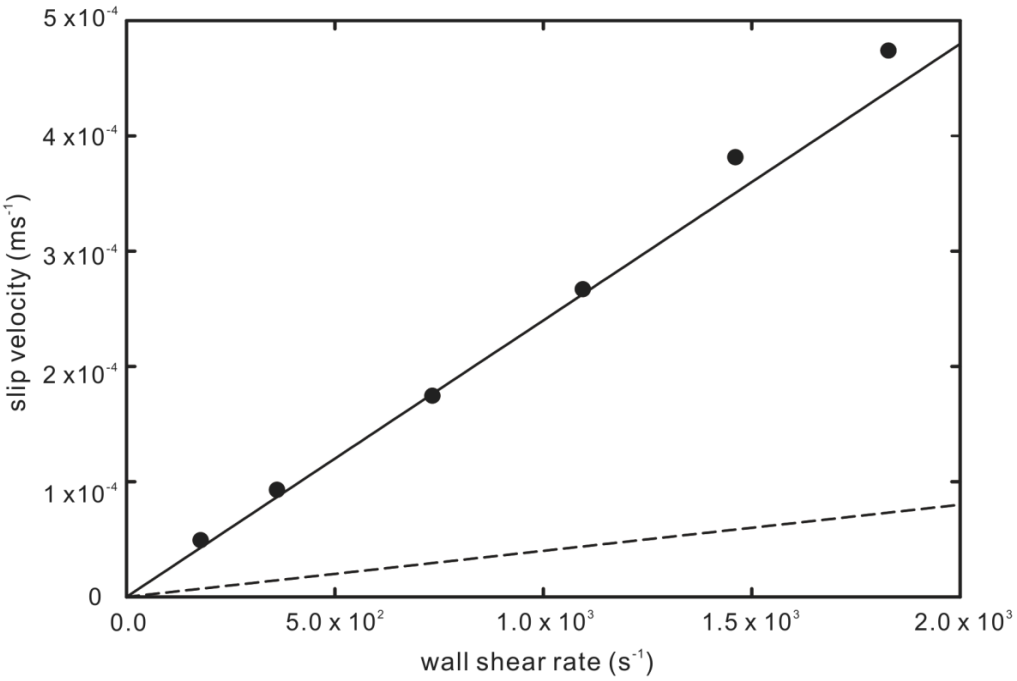

Fig. 5.4 Slip velocity as a function of surface shear rate. Solid line: theoretical prediction from desorption mediated diffusion mechanism for n = 10^4. Dashed line: theoretical prediction from surface hopping mechanism. Symbols: experimental data for DI water in hydrophilic PDMS microchannel (Huang et al. 2006).

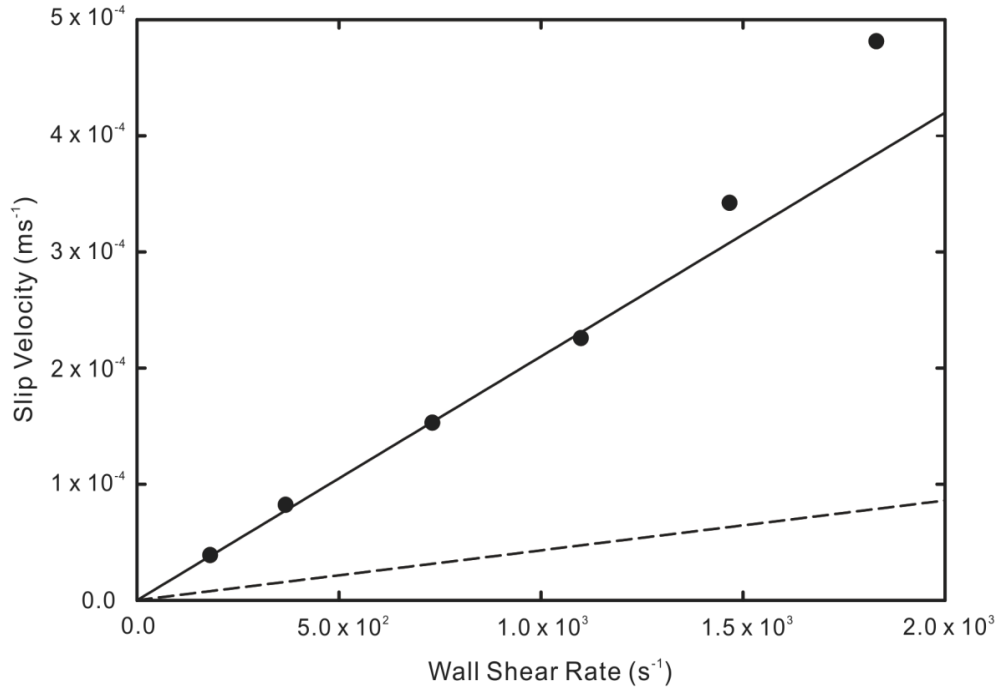

Fig. 5.5 Slip velocity as a function of surface shear rate. Solid line: theoretical prediction from desorption mediated diffusion mechanism for n = 9.5 x 10^3. Dashed line: theoretical prediction from surface hopping mechanism. Symbols: experimental data for DI water in hydrophobic PDMS microchannel (Huang et al. 2006)

5.4 Discussion

It can be observed from Figs. 5.4 and 5.5 that the bulk-mediated surface diffusion mechanism of molecular slip is capable of producing much higher molecular slip velocities compared to the surface hopping diffusion model. However, this is subjected to the number of 'bulk excursions' n that the adsorbed molecule performs while in midst of the desorption-readsorption phase.

The theoretical prediction of molecular slip velocity exhibits a good match with the experimental data of Huang et al. (2006) using a value of $n = 10^4$ and $n = 9.5 \times 10^3$ for the hydrophilic and hydrophobic microchannels respectively. These values of n are on the same order of magnitude as that used in the numerical simulations of Bychuk and O'Shaughnessy (1995). Furthermore, the values of n are consistent with the surface wettability. For a hydrophilic surface, the stronger liquid-solid affinity can be expected to result in a higher number of readsorption events as opposed to a hydrophobic surface. In contrast, the surface hopping diffusion model greatly under-estimates the slip velocity, indicating that this mode of molecular motion is less likely to occur on the liquid-solid pair studied in the experiments. The large disparity between the two models can be attributed to the higher drift velocity due to superdiffusive phenomenon in bulk-mediated surface diffusion.

Intriguingly, the stronger effect of bulk-mediated diffusion mechanism of slip on hydrophilic surfaces suggests that large slip velocities are possible on wetting surfaces since they fulfil the criteria of strong adsorbers due to their high affinity for liquid molecules. In this way, the slip velocity could be much higher than surface molecular motion via the surface hopping mechanism. Altering of the surface chemistry through artificial methods may also promote this mechanism of slip.

At increased surface shear rates however, the deviation of the theoretical prediction from experimental data is palpable. The bulk-mediated surface diffusion model is linear in nature and therefore inadequate at the onset of non-linear slip behaviour. Nevertheless, the model presented here may be used in conjunction with the general slip velocity model presented in Chapter 3 to improve predictions at higher shear rates.

The type of surface diffusion mechanism undergone by the adsorbed molecules will be dictated by the liquid-substrate pair, depending on the nature of the fluid-substrate interactions, surface chemistry and relative time scales of both solid and fluid molecular motion. Bulk-mediated surface diffusion is only possible for fluid-substrate pairs possessing characteristics of strong adsorbers. Surface retention times should typically be much higher than the desorption times so that each molecule spends more time on the surface than in the bulk and furthermore goes through a prolonged series of readsorption events without being instantly relinquished to the bulk phase upon desorption. Yet, if the surface binding energy is too high, desorption events become rarer and the bulk-mediated diffusion becomes ineffective.

In summary, two different mechanisms of direct molecular motion on the substrate have been explored in this chapter. The persistent biased random walk model introduces short-term correlations between individual hopping events while the bulk-mediated diffusion model considers a sequence of periodic readsorption. These forms of molecular slip motion display higher slip velocities under specific conditions compared to the thermal surface diffusion model considered previously. However, these models have to be used with the general slip model in order to represent non-linear slip behaviour.

Based on the adsorption framework for fluid-solid interactions presented in Chapter 3, we will develop a model for the temperature jump of a fluid at a solid surface in the next chapter by studying the energy balance of fluid molecules that interact with the surface.

6 A New Model for Temperature Jump at a Fluid-Solid Interface

Like the slip boundary condition, the temperature jump at a fluid-solid interface has a long history since its discovery by Smoluchowski. The study of temperature jump in rarefied gases was largely popular during the 1950s and 1960s. Meanwhile, the presence of an interfacial thermal resistance, known as the Kapitza resistance, was experimentally detected for liquid helium in a superfluid phase. Little attention has been placed on the phenomena for liquid-solid interfaces until recently when the accessibility of micro and nanoscale fabrication and molecular simulations motivated researchers to explore the feasibility of temperature jump occurring under room conditions.

Theoretical work in the area of fluid-solid temperature jump has seen little progress in recent years. For gas-solid interfaces, the existing temperature jump models largely follow from the kinetic theory derivation of the slip velocity with the use of the thermal accommodation coefficient. The thermal accommodation coefficient is assumed to be a constant in most studies but experimental measurements have reflected a dependence on the wall temperature. Existing theoretical models of the liquid-solid temperature jump adopts the continuum phonon-scattering formulation but is only valid at extremely low temperatures and neglects the influence of molecular interactions at the boundary. To the best of our knowledge, there are no analytical models that provide accurate predictions of the temperature jump for both gas and liquid systems. In this chapter, a unified model for the fluid-solid temperature jump will be developed based on our adsorption model of the interfacial interactions.

6.1 Interfacial Temperature Jump from Fluid-Solid Molecular Interactions

We will consider a quiescent fluid layer that resides on a solid surface in the presence of an externally applied temperature gradient or heat source. In the absence of corrugations, this restricts the interactions to the components of kinetic energy normal to the surface since the parallel components effectively cancel out for an equilibrium distribution.

6.1.1 Mean Kinetic Energy of Surface Fluid Particles

Without driven flow, the particles in the mobile and inelastically desorbed states can be jointly grouped into the precursor state where the probability of a particle being in this state is p_p. In the absence of an external force, the surface hopping of the mobile particles has the characteristics of a symmetrical random walk with a zero mean drift. A schematic illustration of the adsorption and desorption states is shown in Fig.6.1.

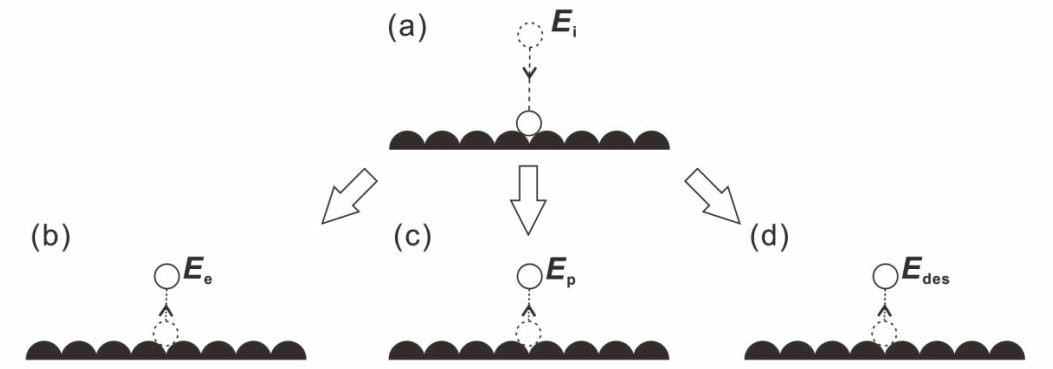

Fig.6.1 Energies of particles in the following states: (a) incident (b) elastic scattering (c) pre-cursor (d) desorped

The mean kinetic energy of the surface fluid particles E_s can be expressed as

$$E_s = (1-p_s)E_e + p_s p_p E_p + p_s (1-p_p) E_{des} \tag{6.1}$$

where E_e , E_p and E_{des} refer to the respective kinetic energy of particles that are elastically scattered, in the precursor and desorbed states.

Elastically scattered particles retain their incident kinetic energy prior to impact E_i

$$E_e = E_i \tag{6.2}$$

Particles that are trapped in the precursor state experience a loss in energy upon impact that is sufficiently large to prevent them from escaping back to the bulk fluid immediately while still preventing them from falling into the bottom of the potential well. We introduce the coefficient of restitution ε that represents the ratio of pre- and post-impact thermal velocities. Hence the kinetic energy of a particle in the precursor state is given by

$$\begin{aligned} E_p &= \varepsilon^2 E_{i,\perp} \\ &= \varepsilon^2 \frac{1}{\pi} \int_{-\pi/2}^{\pi/2} \cos^2\theta E_i d\theta \\ &= \frac{\varepsilon^2}{2} E_i \end{aligned} \tag{6.3}$$

where θ is defined with respect to the normal to the surface in a two-dimensional plane.

The desorbed particles, having spent a residence time longer than that required for equilibration, attain thermal equilibrium with the surface and therefore emerge with kinetic energy that is characteristic of particles possessing the temperature of the surface

$$E_{des} = E_w \tag{6.4}$$

where E_w denotes the kinetic energy of particles at the temperature of the solid surface.

Putting all the energy terms together, we can replace the kinetic energy terms by the temperatures as well as temperature gradients to derive the final functional form of the temperature jump expression.

6.1.2 General Temperature Jump Boundary Condition

Substitution of Eqns. (6.2) to (6.4) into Eqn. (6.1) and rearranging allows us to obtain the following form for the energy balance

$$\begin{aligned} E_i - E_s &= p_s \left[\left(E_i - E_w \right) - p_p \left(\frac{\varepsilon^2}{2} E_i - E_w \right) \right] \\ &= p_s \left[\left(1 - p_p \frac{\varepsilon^2}{2} \right) \left(E_i - E_w \right) + p_p \left(1 - \frac{\varepsilon^2}{2} \right) E_w \right] \end{aligned} \tag{6.5}$$

The difference in kinetic energy between the incident and surface particles on the left-hand side of Eqn. (6.5) can be expressed in terms of the thermal energy conducted between the fluid and solid

$$E_i - E_s = kA\tau \left. \frac{dT}{dn} \right|_s \tag{6.6}$$

where k is the thermal conductivity of the fluid, A is the effective surface area of thermal conduction and τ is the characteristic sticking time.

The kinetic energy difference in the first-term on the right can be approximated by

$$\begin{aligned} E_i - E_w &\approx E_s + \lambda \left. \frac{dE}{dn} \right|_s - E_w \\ &= \alpha k_B \left[\left(T_s - T_w \right) + \lambda \left. \frac{dT}{dn} \right|_s \right] \end{aligned} \tag{6.7}$$

where α is a factor that accounts for the number of molecular degrees of freedom being considered i.e. translational, rotational or vibrational. For instance, α takes on a value of 2 for pure translational motion if the rotational and vibrational degrees of freedom are neglected (Kennard 1938).

Substitution of the kinetic energy terms in Eqns. (6.6) and (6.7) into Eqn. (6.5) gives the final form of the temperature jump as

$$\begin{aligned} T_s - T_w &= \left[\frac{kA\tau}{\alpha k_B p_s \left(1-\frac{1}{2} p_p \varepsilon^2\right)} - \lambda \right] \left. \frac{dT}{dn} \right|_s - \frac{p_p \left(1-\frac{1}{2}\varepsilon^2\right)}{1-\frac{1}{2} p_p \varepsilon^2} T_w \\ &= C_1 \left. \frac{dT}{dn} \right|_s - C_2 T_w \end{aligned} \tag{6.8}$$

where the coefficients C_1 and $0 \le C_2 \le 1$ represent the interfacial conditions, adsorption probabilities and properties of the media.

The temperature jump expression in Eqn. (6.8) marks a new model for the temperature discontinuity at a fluid-solid interface that has been derived based on adsorption theory. Though the general trend of the temperature jump behaviour with respect to the temperature gradient remains largely similar, the temperature jump coefficient C_1 differs slightly from the original model for gas-solid interfaces by Smoluchowski (and other adaptations) due to the introduction of a trapping phase. Molecular interactions are also explicitly considered in the new model, unlike the acoustically based Kapitza resistance models for liquid-solid interfaces. The inclusion of a precursor state also produces an additional dependence on the surface temperature T_w, the second term on the right hand side of Eqn. (6.8), which may explain experimental observations of the surface temperature dependence of the thermal accommodation coefficient as well as thermal rectification effects found in simulations of heat transfer of liquid-solid systems that have been reported in the literature.

In the next section, experimental results for temperature jump measurements at gas-solid and liquid-solid interfaces will be extracted from the literature and used as validation of Eqn. (6.8).

6.2 Validation of New Temperature Jump Boundary Condition

A review of the literature shows that few experimental temperature jump studies have been carried out in recent years. The main difficulty lies in measurement of temperatures of the solid and fluid at the interface within enclosed setups, which researchers have attempted to circumvent using indirect measurement techniques. Using modern apparatus, researchers have revisited traditional temperature jump experimental setups for gases to acquire higher-resolution measurements of the thermal accommodation coefficients. In the study of liquid-solid thermal boundary resistance, molecular dynamics simulation is the preferred tool of choice with only one experimental measurement of room-temperature liquid being reported till date.

In this section, we use our newly developed model to obtain predictions of existing experimental and numerical studies, focusing on the influence of wall temperature which has yet to be fully addressed analytically.

6.2.1 Experimental Measurement of Gas-Solid Temperature Jump

For gas-solid interfaces, two experimental studies have been selected based on the findings of wall temperature dependent temperature jump coefficients which cannot be predicted using the conventional temperature jump model due to the assumption of a constant thermal accommodation coefficient.

Hall and Martin (1987) obtained values of thermal accommodation coefficients from measurements of the thermal conductivity of UO_2 beds that were packed between two concentric cylinders and filled with the test gases. The diameter of the UO_2 microspheres was 82.9 µm with a volume fraction of 0.646. Heat flux was applied via a central heater from the inner to the outer cylinder and temperatures were measured using embedded thermocouples. Working temperatures were controlled between 100 to 700°C at a constant pressure of 0.1 MPa. The temperature jump coefficients were used as fitting parameters for the curves of thermal conductivity.

Recently, Yamaguchi et al. (2012) measured the heat flux in a refined setup of the traditional coaxial cylinder system (Fig. 6.2) under rarefied conditions to perform updated measurements of thermal accommodation coefficients. The inner and outer cylinders were comprised of a thin platinum wire of radius R_i 25 µm placed within the centre of a Pyrex glass tube with an inner radius R_o of 6 mm. Joule heating was used to control the surface temperature of the inner cylinder T_i, which was varied between 357.76 K and 590.79 K. These temperatures were indirectly obtained from the change in its electrical resistance. The temperature of the external cylinder T_o was measured using a thermocouple and was kept relatively constant in the range of 249.9 K to 296.49 K. The external cylinder was filled with Argon gas at test pressures of 0.002 Pa to 30 Pa, which lie in the transitional and free molecular regimes. Heat fluxes were evaluated based on electrical power consumption. The values of thermal accommodation coefficients were used as adjustable parameters in best-fit curves of heat flux versus degree of rarefaction.

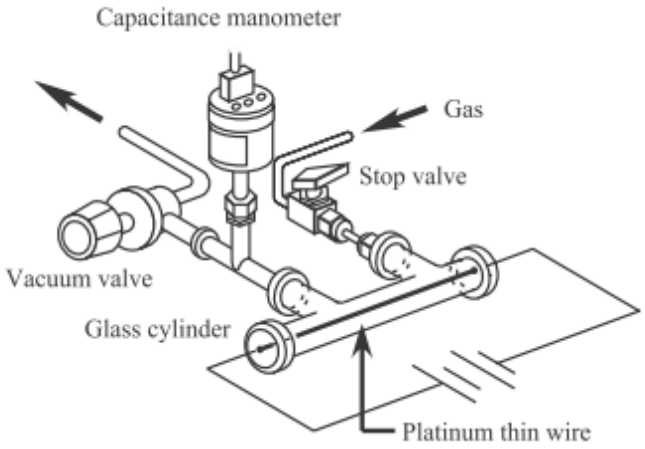

Fig. 6.2 Schematic diagram of the experimental setup of Yamaguchi et. al. (2012)

Next, the procedure of comparing our analytical model with the extracted data from the above experiments will be described and graphically presented.

6.2.2 Comparison of New Model with Experimental Data for Gas-Solid Interface

Under low rarefied conditions, the following Smoluchowski temperature jump expression was used by Hall and Martin (1987) to extract the values of thermal accommodation coefficients from the heat flux curves.

$$\Delta T = \frac{2-\sigma_T}{\sigma_T}\alpha \left.\frac{dT}{dn}\right|_s \tag{6.9}$$

where $\alpha = \frac{1}{1+\gamma}\frac{k}{c_v p}\sqrt{\frac{2\pi RT}{m}}$ represents the gas properties.

Substituting our new temperature jump expression from Eqn. (6.8) into Eqn. (6.9), we may obtain a prediction of the experimentally measured thermal accommodation coefficient in the following temperature dependent form

$$\sigma_T = \frac{2(\alpha/C_1)}{1+(\alpha/C_1)-\left(C_2/\frac{dT}{dn}\Big|_s\right)T_w} \tag{6.10}$$

where the coefficients C_1 and C_2 are the parameters as in Eqn. (6.8).

In Figs. 6.3 and 6.4, Eqn. (6.10) is fitted to the provided data of the temperature dependent thermal accommodation coefficients for helium and argon gases.

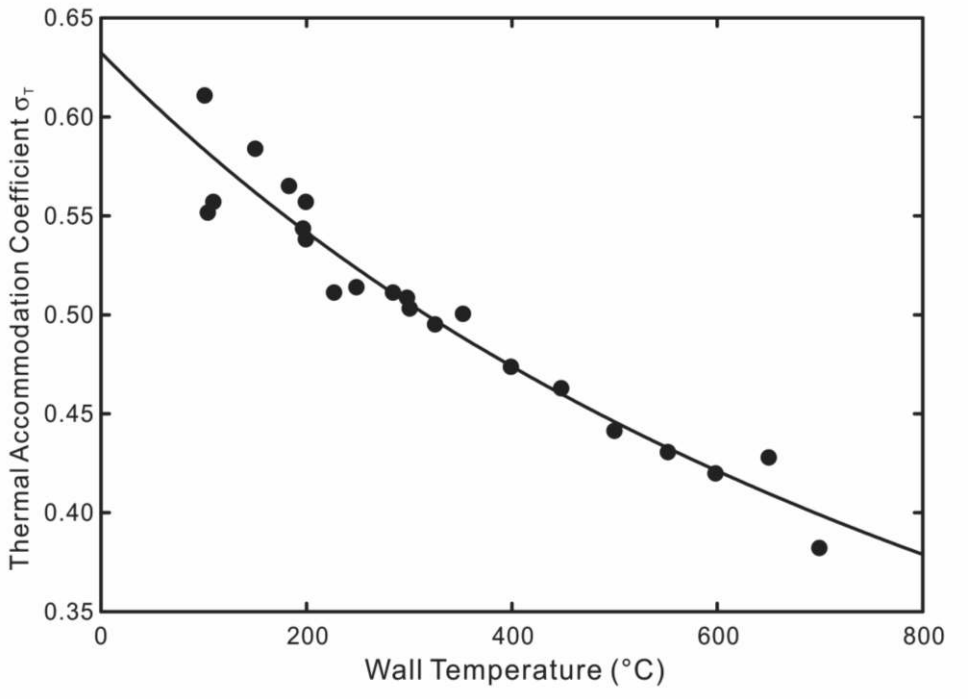

Fig. 6.3 Temperature dependence of thermal accommodation coefficient of UO_2 sphere beds in helium. Symbols: Hall and Martin (1987). Line: Theoretical prediction using Eqn. (6.10) with α/C_1 = 0.462 and $C_2/(dT/dn)$ = 0.001.

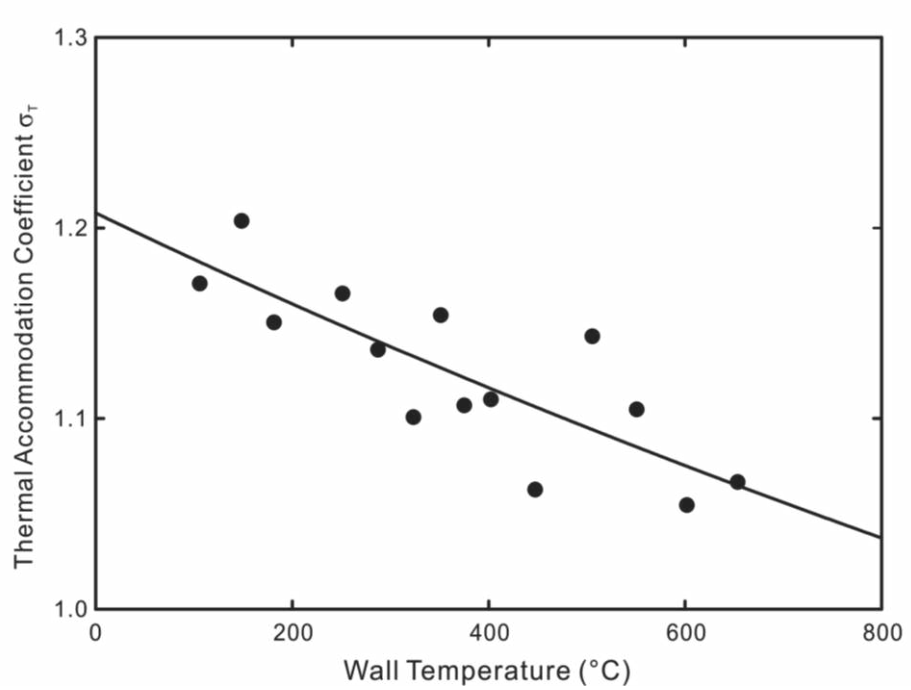

Fig. 6.4 Temperature dependence of thermal accommodation coefficient of UO_2 sphere beds in argon. Symbols: Hall and Martin (1987). Line: Theoretical prediction using Eqn. (6.10) with α/C_1 = 1.525 and $C_2/(dT/dn)$ = 5.19 x 10^{-4}.

In the experiment conducted by Yamaguchi et. al. (2012), the measured heat flux q can be represented using the following expression

$$\frac{1}{q} = \frac{1}{q_{fm}} + \frac{1}{q_c} \tag{6.11}$$

where q_{fm} and q_c are the heat fluxes between the coaxial cylinders for a gas in the free molecular and continuum flow regimes respectively.

The continuum heat flux expression is given by Fourier's law

$$q_c = \frac{k_o\left(T_i - T_o\right)}{R_i \ln\left(R_o/R_i\right)} \tag{6.12}$$

where k_o is the thermal conductivity of the outer glass cylinder.

In the free-molecular limit, the heat flux for a monatomic gas between coaxial cylinders with a thermal accommodation coefficient of unity at the outer radius and σ_T at the inner radii can be expressed as

$$q_{fm} = \frac{\sigma_T}{2}\frac{p\bar{v}}{T}\left(T_i - T_c\right) \tag{6.13}$$

where $\bar{v}$ is the mean molecular speed, p and T refer to the pressure and temperature of the gas in the vicinity of the outer cylinder.

Substituting Eqn. (6.11) into (6.13) and rearranging, the experimental thermal accommodation coefficient is

$$\sigma_T = \frac{2T}{p\bar{v}}\frac{\left(\frac{1}{q} - \frac{1}{q_c}\right)^{-1}}{T_i - T_o} \tag{6.14}$$

where q_c can be evaluated using Eqn. (6.12).

Theoretically, the thermal accommodation coefficient in the free-molecular regime is derived from the expression

$$\sigma_T = \frac{E_i - E_s}{E_i - E_w} \tag{6.15}$$

Substitution of Eqns. (6.5) to (6.8) into the above equation allows us to derive the following form of a temperature-dependent thermal accommodation

$$\begin{aligned}\sigma_T &= \frac{E_i - E_s}{E_i - E_w} \\ &= \frac{kA\tau \left.\frac{dT}{dn}\right|_s}{\alpha k_B \left[\left(T_s - T_w\right) + \lambda \left.\frac{dT}{dn}\right|_s \right]} \\ &= \left(\frac{1}{A\tau p_s \left(1 - \frac{1}{2} p_p \varepsilon^2\right)} + \frac{\alpha k_B p_p \left(1 - \frac{1}{2}\varepsilon^2\right)}{A\tau q_c \left(1 - \frac{1}{2} p_p \varepsilon^2\right)} T_w \right)^{-1} \\ &= \left(a + bT_w\right)^{-1}\end{aligned} \tag{6.16}$$

The theoretical prediction using Eqn. (6.16) of the experimentally measured thermal accommodation coefficients from Yamaguchi et al. (2012) is shown in Fig. 6.5.

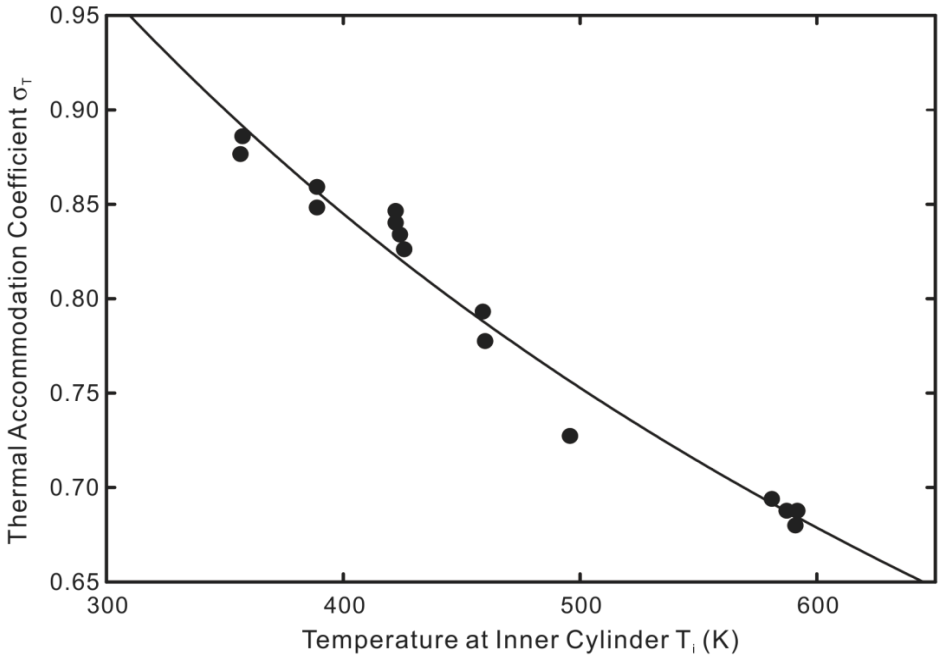

Fig. 6.5 Temperature dependence of the thermal accommodation coefficient for a platinum-argon interface for 10<Kn<250. Symbols: Experimental data (Yamaguchi et al. 2012). Line: Theoretical prediction using Eqn. (6.16) with *a* = 0.604 and *b* = 0.001.

Discussion of the above comparisons between the new theoretical model and experimental data for gases will be presented at the end of the chapter. The following section introduces the liquid-solid temperature jump experiments conducted by several researchers. Using the provided experimental data, we proceed to obtain predictions using our new model as verification.

6.2.3 Measurement of Liquid-Solid Temperature Jump

To the best of our knowledge, only one research group has performed experimental temperature jump measurements for liquid-solid interfaces using a time-domain thermoreflectance technique (Ge et al. 2006). Unfortunately, the lack of temperature jump data in the published report did not allow us to perform any meaningful comparisons. Here, four molecular dynamics simulation studies conducted by separate groups will be used for corroboration of our new temperature jump model.

Kim et al. (2008) performed MD simulations of steady state heat conduction between parallel plates with nanoscale gaps filled with liquid argon. Three different gap separations of 3.24 nm, 6.48 nm and 12.96 nm were investigated with the length and width held constant. The top and bottom plates were maintained at a prescribed temperature of 160 K and 90 K respectively. An empirical fit of their simulation results was suggested using the expression

$$\Delta T = \alpha\left(T_w\right)\left(\frac{\omega_{wall}}{\omega_{fluid}}\right)^4 \exp\left(-1.85\frac{\varepsilon_{wf}}{\varepsilon}\right)\left.\frac{\partial T}{\partial n}\right|_s \tag{6.17}$$

where ε and ε_{wf} denotes the liquid/liquid and liquid/solid interaction strength respectively and $\omega_{wall}/\omega_{fluid}$ the relative thermal oscillation frequency of wall and liquid. The fitting function $\alpha\left(T_w\right)$ was found to have the following form

$$\alpha = 0.0038T_w + 0.672 \tag{6.18}$$

The empirical temperature jump expression coupled with continuum heat conduction equations showed good agreement with simulated temperature distributions.

Shenogina et al. (2009) studied the effect of wetting on thermal conductance for different interfaces of self-assembled monolayers (SAM) and water. A total of seven

neutral head-group chemistries with varying wetting properties ranging from hydrophilic to hydrophobic were represented in their nonequilibrium molecular dynamics simulations. The simulated heat conduction system had a wall surface area of 3.5 nm x 3.5 nm and height of 7 nm. A steady-state heat flux was applied in the direction from the water to SAM. Their results showed that hydrophobic surfaces tended to generate a larger temperature jump for the same heat flux with the increase being congruent with the degree of non-wetting. The relationship between interfacial conductance G and wetting was consistent with the following linear expression

$$G = A\left(1+\cos\theta\right) \tag{6.19}$$

where $\left(1+\cos\theta\right)$ represents the work of adhesion , with θ denoting the contact angle. A is a proportionality constant that was found to have a value of 85 MW/m^{2}K through a fit of Eqn. (6.19) to their simulation results.

Hu et al. (2009) conducted nonequilibrium molecular dynamics heat conduction simulations of a system consisting of self-assembled monolayers bonded to a silica surface that was submerged within a water phase comprising around 3000 molecules. The simulation model had dimensions of 27.2 Å x 28.2 Å x 200Å. For heat current flowing in the direction from SAM to water, the thermal conductance was about 1000 MW/m^{2}K compared to 650 MW/m^{2}k in the opposite direction, revealing a rectification effect. The change in hydrogen bonding characteristics of water with temperature was suggested as a reason for the thermal rectification phenomenon.

The nonequilibrium molecular dynamics simulations of Acharya et al. (2012) involved the study of Kapitza thermal conductance of solid-liquid interfaces between self-assembled monolayers and liquid water for mixed -CF3/-OH SAMs. The simulated system consisted of a SAM bilayer (comprising of two alkane chains anchored to a central sulphur atom)

sandwiched between water layers. Their results indicated that the thermal conductance increased almost linearly with increasing fraction of -OH groups and also with increasing nanoscale roughness. A thermal rectification effect was observed when the direction of heat transfer was reversed - a larger temperature drop was produced when heat flowed from the water to SAM. However, closer examination of the provided temperature distribution revealed that the interface temperatures differed by about 16 K in both cases and therefore could imply a dependence on the wall temperature instead since the gradient of the temperature jump curves remained unchanged.

6.2.4 Comparison of New Model with MD simulation Data for Liquid-Solid Interfaces

The temperature jump versus wall temperature gradient curves from the four sets of MD simulations are replicated in Figs. 6.6 to 6.9. The wall temperature gradients were evaluated using Fourier's heat conduction law for given heat fluxes. On the same graphs, the new temperature jump model in Eqn. (6.8) is plotted fitting of the experimental data with appropriate values of the coefficients C_1 and C_2. Also shown in the figures are predictions obtained using the existing temperature jump model

$$\Delta T = C \left. \frac{dT}{dn} \right|_s \tag{6.20}$$

where C represents the temperature jump coefficient, also referred to as the Kapitza length in the literature. Discussion of the results will be presented at the end of the chapter.

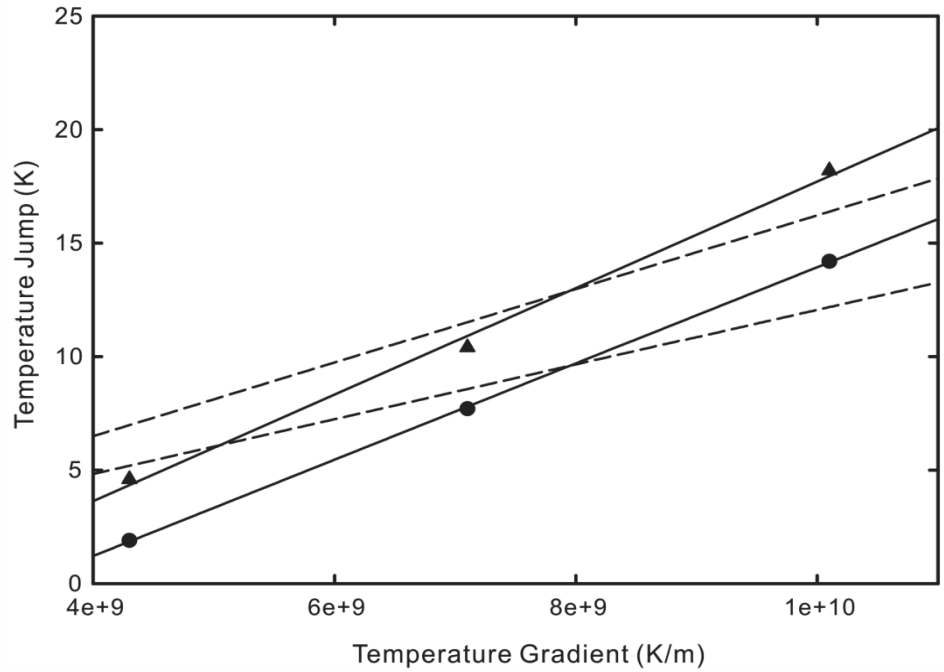

Fig. 6.6 Temperature jump as a function of wall temperature gradient at a solid-liquid argon interface. Symbols: MD simulation results at T_w = 160K (Triangles),T_w= 90K (Circles) (Kim et al. 2008). Solid line: Fit using new temperature jump model from Eqn. (6.8) with C_1 = 2.348 x 10^{-9} and C_2 = 0.036 for T_w = 160K, C_1 = 2.121 x 10^{-9} and C_2 = 0.081 for T_w = 90K. Dashed line: Fit using existing temperature jump model from Eqn. (6.20) with C_1 = 1.623 x 10^{-9} for T_w = 160K, C_1 = 1.207 x 10^{-9} for T_w = 90K.

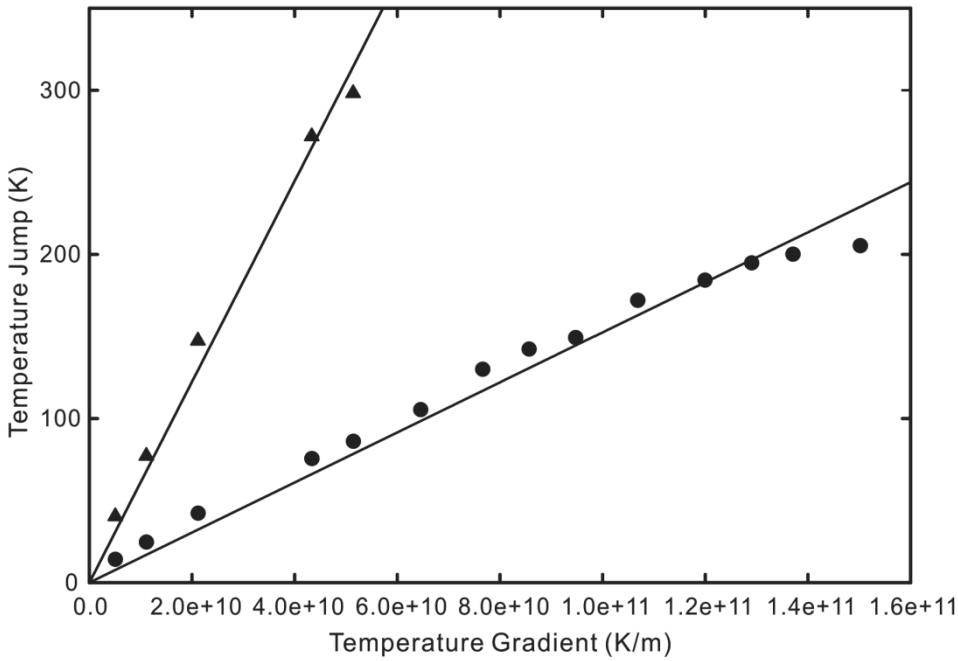

Fig. 6.7 Temperature jump as a function of wall temperature gradient at a SAM-water interface. Symbols: MD simulation results for hydrophobic -CF_3 SAM (Triangles) and hydrophilic –OH SAM (Shenogina et al. 2009). Solid line: Fit using new temperature jump model from Eqn. (6.8) with C_1 = 6.121 x 10^{-9} for -CF_3 SAM at T_w = 300K, C_1 = 1.525 x 10^{-9} for –OH SAM at T_w = 285K.

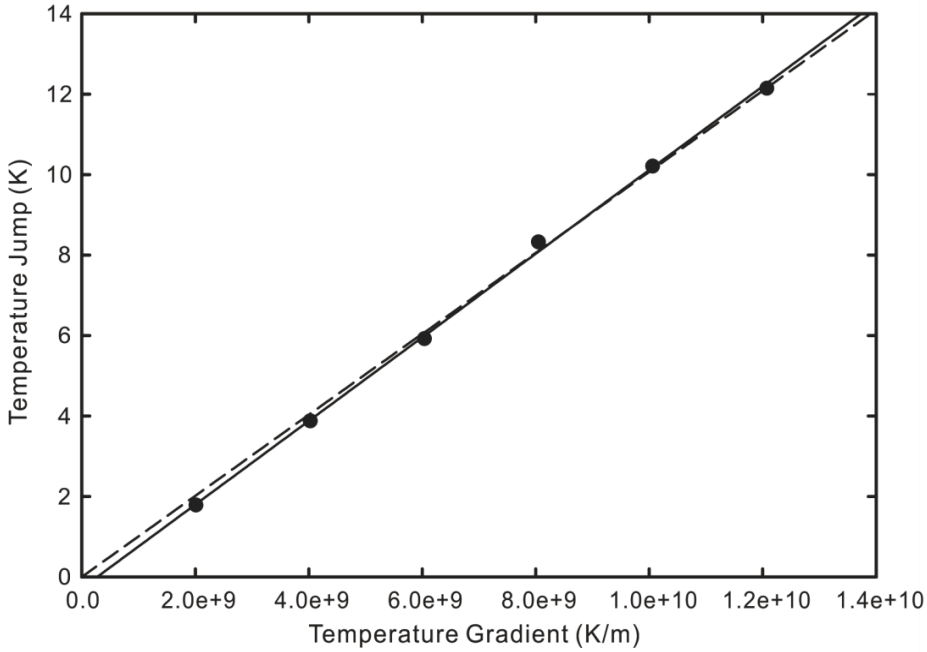

Fig. 6.8 Temperature jump as a function of wall temperature gradient at a silica-SAM-water interface. Symbols: MD simulation results (Hu et al. 2009). Solid line: Fit using new temperature jump model from Eqn. (6.8) with C_1 = 1.04 x 10^{-9} and C_2 = 9.682 x 10^{-4} for T_w = 292K. Dashed line: Fit using existing temperature jump model from Eqn. (6.20) with C_1 = 1.007 x 10^{-9}.

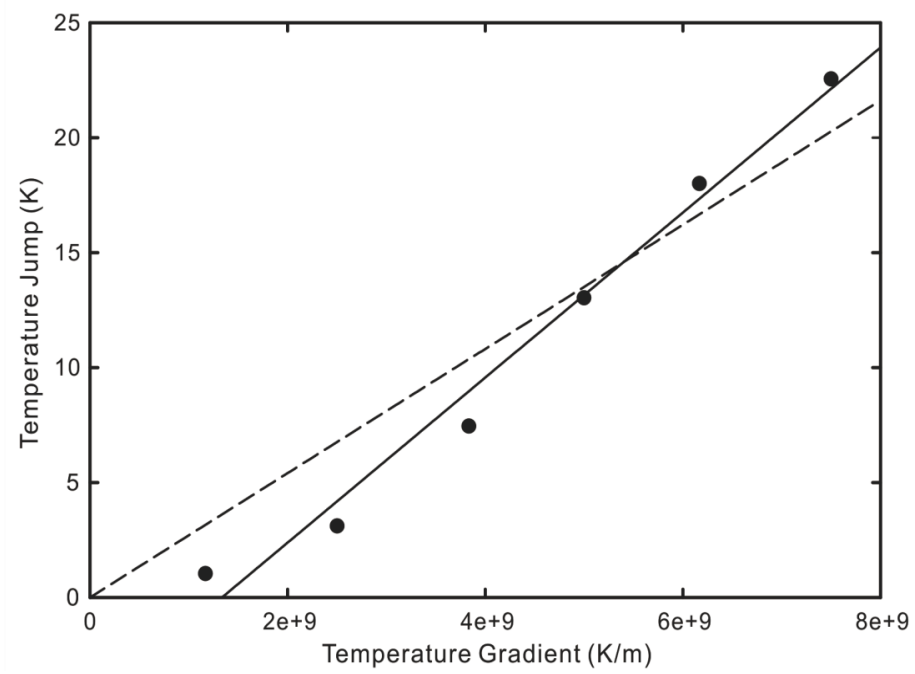

Fig. 6.9 Temperature jump as a function of wall temperature gradient at a silica-SAM-water interface. Symbols: MD simulation results (Acharya et al. 2012). Solid line: Fit using new temperature jump model from Eqn. (6.8) with C_1 = 3.59 x 10^{-9} and C_2 = 0.015 for T_w = 326K. Dashed line: Fit using existing temperature jump model from Eqn. (6.20) with C_1 = 2.704 x 10^{-9}.

6.3 Discussion

As seen in Figs. 6.3 to 6.5, the predictions by the new temperature jump model displays good agreement with results of the two reference experiments for gas-solid interfaces. This is due to the fact that the new model is able to reflect the wall temperature dependent behaviour of the thermal interactions that lead to the temperature discontinuity at the interface whereas the conventional temperature jump models assume a constant thermal accommodation coefficient.

Interestingly, in Fig. 6.4, the measured thermal accommodation coefficients for argon gas are above unity. The authors postulated from a kinetic theory perspective that this over-accommodation could be attributed to surface roughness which promotes more efficient heat exchange between the gas molecules and solid surface due to the higher tendency for the gas molecules to be scattered at larger angles and therefore remain within the vicinity of the surface. Based on the definition of the thermal accommodation coefficient as given in Eqn. (6.15), it connotes that the net energy exchange is greater than the available difference in energy, which appears to violate the second law of thermodynamics. Furthermore, argon is a monatomic gas and therefore should not experience an exchange of energy modes with internal degrees of freedom. This leads to the point that the thermal accommodation coefficient by itself may not provide an adequate description of the molecular interactions at the surface using a straightforward specular and diffuse reflection model. Hence, it should not be inferred from the variation of the thermal accommodation coefficient with temperature that the thermal accommodation coefficient is a function of the temperature. Rather, it could be explained by more complex forms of molecule-surface interactions, such as the precursor adsorption states considered in our model which the gas molecules may assume upon

impacting the surface, consequently contributing to the temperature discontinuity at the interface.

From comparisons of the agreement between the analytical curves and experimental data for liquid-solid interfaces displayed in Figs 6.6 to 6.9, the new temperature jump model described by Eqn. (6.8) ostensibly offers a better prediction over that of the existing model. In particular, it can be observed that the temperature jump in most of the MD simulation results does not vanish when the wall temperature gradient decreases to zero. This suggests that the temperature jump is not merely driven by the wall temperature gradient but also affected by the thermal energy of the solid molecules.

The experimental data of Shenogina et al. (2009) in Fig. 6.7 depicts the contrasting temperature jump behaviours of hydrophilic and hydrophobic surfaces. Granted that the conventional temperature jump model is able to provide a good prediction of the experimental data using different temperature jump coefficients, we can provide a qualitative explanation of the influence of wetting using our new model since the sticking probability is expected to decrease with increasing hydrophobicity. Indeed, for the hydrophobic CF_3 self-assembled monolayer, the best-fit value of C_1 is 6.121 x 10^{-9} while that for the hydrophilic OH self-assembled monolayer is 1.525x 10^{-9}, corresponding to a higher sticking probability with reference to Eqn(6.8). This is also supported by the lower value of C_1 = 3.59 x 10^{-9} for the hydrophilic –$CONH_2$ surface studied by Acharya et al. (2012) in Fig. 6.9.

Examination of the values of C_2 in Figs. 6.6 to 6.9 reveals a dependence on the wall temperature. As seen in the plot of C_2 against the wall temperature in Fig. 6.10, C_2

decreases monotonically with increasing wall temperature. According to Eqn. (6.8), C_2 represents the relative dominance of the precursor state over the other adsorption states. It may be inferred from Fig. 6.10 that the temperature jump dependence on wall temperature approximately vanishes at higher wall temperatures. Indeed, the wall temperature dependence is absent in the experiments of Shenogina et al.(2009) as shown in Fig. 6.7 for wall temperatures of 285 K and 300 K.

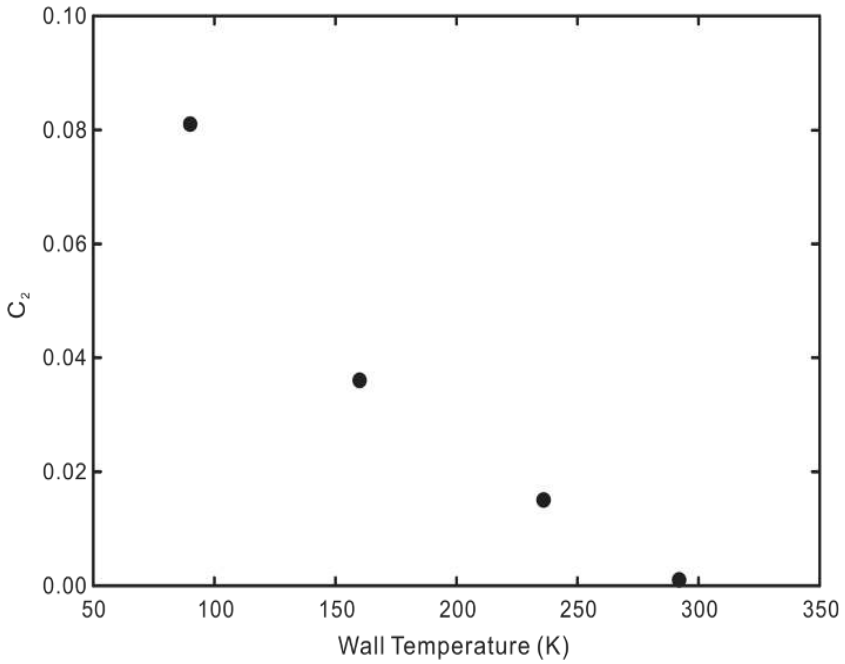

Fig. 6.10 Fitting parameter C_2 in Eqn(6.8) as a function of wall temperature.

At elevated temperature gradients, the experimental data begins to deviate from linear behaviour predicted by both the conventional and new temperature jump models, instead displaying a non-linearly decreasing tail that draws parallels with the shear rate dependence of the slip length at increased wall shear rates. It is noted that only one other group has reported similar non-linear findings from their MD simulations of a silicon-water system (Murad and Puri 2008). However, in their case, the temperature jump increases non-linearly with increasing heat flux. Owing to the paucity of available data, the non-linear behaviour warrants further investigation.

Molecular dynamics simulation of heat transfer across liquid-solid interfaces have unveiled a thermal rectification effect, whereby the magnitude of the temperature jump changes with the direction of the heat flux for the same absolute value. Our new model reflects this phenomenon which has several potential uses such as thermal diodes or temperature cloaks. The thermal rectification effect is graphically depicted in Fig. 6.11 using similar values for the wall temperature in Eqn. (6.8). It can be observed that a heat current flowing from the liquid phase to solid phase diminishes the magnitude of the temperature jump while reversing the direction results in an augmented temperature jump. Closer inspection of the temperature distributions in certain MD simulations purporting this rectification property reveals a difference in wall temperatures when the direction of heat flux is altered. For example, the wall temperatures differ by 23 K and 16 K respectively in the simulations of Hu et al. (2009) and Acharya et al. (2012). However, we note that the temperature jump in the case of the former increases at a steeper rate when the direction of heat flux points from the solid to liquid. According to our model, this wall temperature disparity may possibly give rise to an apparent rectification effect since the magnitude of the temperature jump is affected by the boundary temperature. Stricter control of the interfacial temperature will be necessary in order to rule out its influence on the resulting temperature jump. The temperature jump data of Kim et al. shown in Fig. 6.6 provides evidence of this wall temperature dependence for two wall temperatures of 160 K and 90 K, though the authors did not claim to have observed the rectification effect.

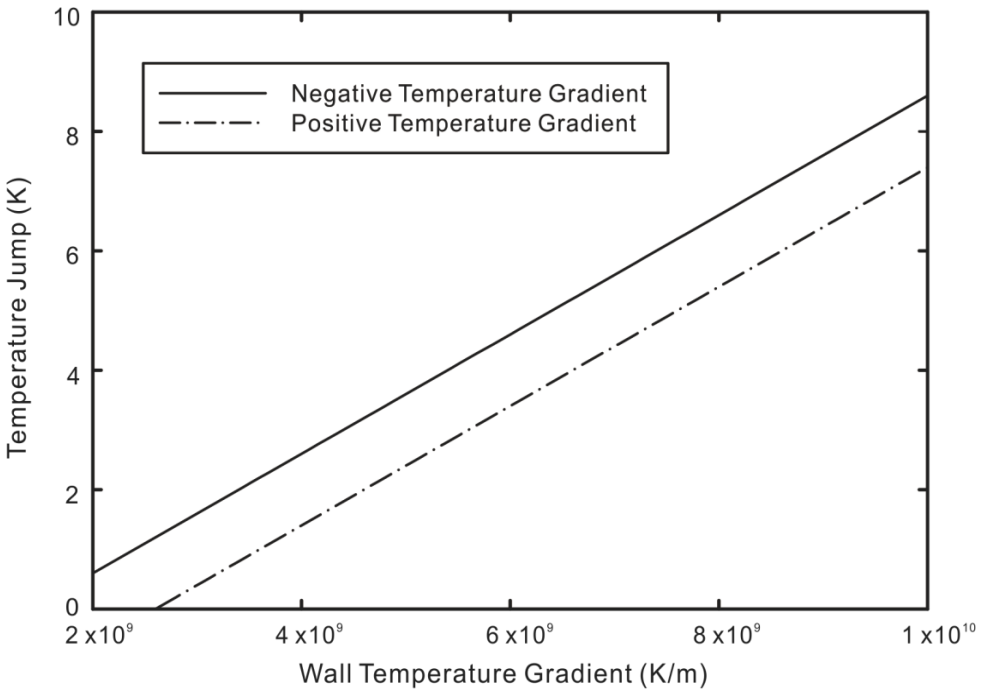

Fig. 6.11 Thermal rectification effect with a change in direction of heat flux. A negative temperature gradient refers to decreasing fluid temperatures with increasing normal distance from the solid surface and vice versa for a positive temperature gradient.

In summary, we have developed a general model that is capable of describing the temperature discontinuity across a fluid-solid interface based on the energy balance of fluid molecules in various adsorption states. The applicability of the model to both fluid and liquid systems is substantiated by the good agreement with experimental data from the literature. In particular, the wall temperature dependence of the thermal accommodation coefficient, which is assumed to be constant in majority of the gaseous temperature jump studies, is well-represented by the model. Improved predictions of experimental measurements of liquid-solid temperature jump were also obtained using the new model.

In the concluding chapter that follows, we will provide a summary of the findings from this thesis and highlight the major contributions. Possible extensions of the current work are also suggested.

7 Conclusion

The discontinuity of transport quantities across a fluid-solid interface is pronounced in micro and nanoscale transport phenomena but poor understanding of the actual mechanism limits the proper use of the boundary conditions. Adding to the puzzle is the perplexing influence of several affecting factors that have been discovered in experiments. In view of these uncertainties, theoretical work grounded in the fundamental behaviour of the fluid-solid interactions is crucial in elucidating the physics behind this phenomenon.

New analytical models for the slip and temperature jump of fluids at solid surfaces have been developed in this thesis. Aspects of surface science theory were incorporated in the description of dynamical intermolecular interactions at the interface. Novel ideas in the proposed models include the establishment of an adsorption framework for fluid-solid interactions, its use in the derivation of the boundary discontinuities, and the validity of the models for both gas-solid and liquid-solid interfaces. In addition, the new set of boundary conditions provides viable explanations for observed phenomena that have eluded researchers thus far.

7.1 Summary and Contributions

Our new adsorption model for the fluid slip velocity and temperature jump considers, apart from the usual elastic and diffuse scattering included in the kinetic theory based gas models, precursor phases that comprise of mobile and momentary trapping states. In the mobile state, molecules migrate across the substrate through surface diffusion mechanisms while those that are trapped return to the bulk fluid after a brief surface residence time, during which a certain fraction of their energy is dissipated. The detailed

balance of fluid particles that interact with the surface was accomplished by the prescription of probabilities to each adsorption state. With respect to the intermolecular separation distances and forces, scattering events can be expected to be dominant in gases while the precursor states are likely to be the major cause of slip and temperature jump in liquids.

In the new theoretical model for fluid slip velocity, appropriate velocities were assigned to fluid particles in their respective adsorption states. The final slip velocity expression was obtained as the mean fluid molecular velocity at the surface, made up by the velocities of scattered molecules, mobile molecules that undergo surface diffusion and trapped molecules in the precursor state. Predictions using the new model were corroborated with experimental results for gas and liquid systems from the literature, showing good agreement compared with existing models, namely the Maxwell-type and Langmuir models for gases and Navier slip boundary condition for liquids. The non-linear dependence on shear rate, which cannot be represented using the aforementioned models, was correctly reflected by the new model via the parameter C_2. C_2 exhibits a relationship with the fluid viscosity which can be interpreted as the frictional dissipation due to the relative motion of the surface and bulk fluid molecules in the trapping state. Additionally, the decreasing value of parameter C_1 with decreasing contact angle in the new slip velocity model was shown to be physically consistent with the effect of wettability.

We have also proposed two alternative mechanisms of slip for molecules in the mobile adsorption state that show contrasting behaviour to that of the basic surface hopping mechanism, which predicts surface molecular velocities that are substantially lower than that measured experimentally. The first mechanism was represented using a persistent

asymmetric random walk model that includes correlations between two consecutive surface hops while the second involves a periodic re-adsorption mechanism. For transmittance probabilities greater than 0.5, correlated motion enhances the directional bias by the external field, resulting in a higher surface slip velocity compared to the original uncorrelated case. Surface diffusion slip velocity that arises from a desorption-readsorption process was shown to be significantly higher than that from surface hopping and furthermore matches experimentally measured values. The type of surface diffusion mechanism that takes place will be determined by the interfacial properties of each liquid-substrate pair.

The adsorption framework was also applied to develop a new temperature jump model for fluid-solid interface based on the processes of energy exchange between the adsorbed fluid molecules and substrate. The new model was shown to provide a good match with available experimental data for both gas-solid and liquid-solid interfaces. Furthermore, the additional dependence on the wall temperature in our model supports experimental observations of the variation of thermal accommodation coefficients with surface temperature for a gas-solid interface. For temperature jump at a liquid-solid interface, the model parameter C_1 could be associated with the effect of wettability. The other parameter C_2 showed an interesting dependence on the wall temperature, suggesting that the wall temperature effect vanishes at higher surface temperatures. It was also shown that the model was able to reproduce the thermal rectification effect observed in molecular dynamics simulations of liquid-solid interfaces.

On the whole, the good agreement between the newly developed models and data from the literature shows strong evidence that the slip and temperature jump at a fluid-solid interface may be attributed to adsorption processes.

7.2 Recommendations for Future Work

In this study, certain factors pertaining to aspects of interfacial physics were not considered though it should be stressed that the general fidelity of our model was not compromised. These effects which are listed below can be incorporated as an extension of the model with the drawback of increasing complexity.

Lateral interactions

The interaction of an adsorbed molecule with neighbouring particles and adsorption sites may be taken into account by the addition of the energy of lateral interaction energy to the added energy of adsorption. This could explain the counter-intuitive observation of slip on hydrophilic surfaces through the formation of liquid bridges in MD simulations (Ho et al. 2011). For a two-dimensional lattice, the choice of multiple hopping sites increases the number of traversing paths across the lattice and may be studied using percolation concepts.

Adsorption from solution

The assumption of physisorption is only valid for dilute solutions. For higher concentrations, chemisorptions of ions may take place. Furthermore, the electrostatic forces should also be considered for electrolyte solutions.

Multi-layered adsorption

Experimental evidence of interfacial water ordering that spans a few molecular layers has recently been reported (Cheng et al. 2001). One way to permit adsorption of multilayers within the model is to assume a particular heat of adsorption for the first layer and a common value for subsequent layers (Brunauer et al. 1938). This can affect slip behaviour in two ways: Firstly, the transition from monolayer to multilayer adsorption

results in a dynamic slip mechanism. Secondly, surface diffusion may occur through shearing of adsorbate clusters against an adjacent layer, leading to non-linear slip behaviour. Interfacial ordering should also result in a lowered thermal boundary resistance given the closer proximity of near-wall fluid molecules and increased commensurability between the molecular structures of the solid and fluid.

Corrugations

The presence of corrugations leads to non-specular scattering and possible repeated collisions that result in more efficient exchange of energy. In contrast to an atomically smooth surface, corrugations couple the parallel and perpendicular components of momentum and energy, causing the sticking probability to obey total energy scaling instead of the ideal normal scaling that is usually assumed (Kolasinski 2008). This introduces velocity-dependent and energy-dependent sticking probabilities that translate to higher-order dependence on the transport gradients.

Rotations and Vibrations

At elevated temperatures, the rotational and vibrational degrees of freedom have to be considered in the sticking probability. Rotational velocities will be critical in site-specific chemisorption since an incident particle has to be precisely orientated relative to the binding site in order to achieve adsorption. Hence, higher rotational speeds tend to promote scattering rather than sticking due to the insufficient time allowed for the incident particle to be steered into the right orientation to fit the adsorption site.

References

Acharya, H., N. J. Mozdzierz, P. Keblinski and S. Garde (2012). "How chemistry, nanoscale roughness, and the direction of heat flow affect thermal conductance of solid-water interfaces." Industrial and Engineering Chemistry Research **51**(4): 1767-1773.

Adamson, A. W. and A. P. Gast (1997). Physical chemistry of surfaces, Wiley.

Ala-Nissila, T., R. Ferrando and S. C. Ying (2002). "Collective and single particle diffusion on surfaces." Advances in Physics **51**(3): 949-1078.

Alexeyev, A. A. and O. I. Vinogradova (1996). "Flow of a liquid in a nonuniformly hydrophobized capillary." Colloids and Surfaces A **108**(2-3): 173-179.

Andrienko, D., B. Dunweg and O. I. Vinogradova (2003). "Boundary slip as a result of a prewetting transition." Journal of Chemical Physics **119**(24): 13106-13112.

Antczak, G. and G. Ehrlich (2008). "Asymmetric one-dimensional random walks." The Journal of Chemical Physics **129**(12): 124702-124704.

Arkilic, E. B., M. A. Schmidt and K. S. Breuer (1997). "Gaseous slip flow in long microchannels." Journal of Microelectromechanical Systems **6**(2): 167-178.

Balakrishnan, V. and S. Chaturvedi (1988). "Persistent diffusion on a line." Physica A: Statistical Mechanics and its Applications **148**(3): 581-596.

Barrat, J. L. and L. Bocquet (1999). "Influence of wetting properties on hydrodynamic boundary conditions at a fluid/solid interface." Faraday Discussions **112**: 119-127.

Bartell, F. E. and J. W. Shepard (1953). "Surface roughness as related to hysteresis of contact angles. II. The systems paraffin-3 molar calcium chloride solution-air and paraffin-glycerol-air." Journal of Physical Chemistry **57**: 455-458.

Bataineh, K. M. and M. A. Al-Nimr (2009). "2D Navier-stokes simulations of microscale viscous pump with slip flow." Journal of Fluids Engineering **131**(5): 051105 (051107 pp.).

Baule, B. (1914). "Phenomena in rarefied gases." Annalen der Physik **44**(1): 145-176.

Bentz, J. A., R. V. Tompson and S. K. Loyalka (1999). "Viscosity and velocity slip coefficients for gas mixtures: Measurements with a spinning rotor gauge." Journal of Vacuum Science and Technology A **17**(1): 235-241.

Bentz, J. A., R. V. Tompson and S. K. Loyalka (2001). "Measurements of viscosity, velocity slip coefficients, and tangential momentum accommodation coefficients using a modified spinning rotor gauge." Journal of Vacuum Science and Technology A **19**(1): 317-324.

Bhattacharya, D. K. and B. C. Eu (1987). "Nonlinear transport processes and fluid dynamics: Effects of thermoviscous coupling and nonlinear transport coefficients on plane Couette flow of Lennard-Jones fluids." Physical Review A **35**(2): 821-836.

Bird, G. A. (1994). Molecular Gas Dynamics and the Direct Simulation of Gas Flows, Oxford University Press, Incorporated.

Blake, T. D. (1990). "Slip between a liquid and a solid. D.M. Tolstoi's (1952) theory reconsidered." Colloids and surfaces **47**(1): 135-145.

Bocquet, L., P. Tabeling and S. Manneville (2006). "Comment on "large slip of aqueous liquid flow over a nanoengineered superhydrophobic surface"." Physical Review Letters **97**(10).

Boehnke, U. C., T. Remmler, H. Motschmann, S. Wurlitzer and J. Hauwede (1999). "Partial air wetting on solvophobic surfaces in polar liquids." Journal of Colloid and Interface Science **211**(2): 243-251.

Bolmatov, D., V. V. Brazhkin and K. Trachenko (2012). "The phonon theory of liquid thermodynamics." Scientific Reports **2**.

Bonaccurso, E., H. J. Butt and V. S. J. Craig (2003). "Surface roughness and hydrodynamic boundary slip of a Newtonian fluid in a completely wetting system." Physical Review Letters **90**(14): 144501-144501.

Bouzigues, C. I., L. Bocquet, E. Charlaix, C. Cottin-Bizonne, B. Cross, L. Joly, A. Steinberger, C. Ybert and P. Tabeling (2008). "Using surface force apparatus, diffusion and velocimetry to measure slip lengths." Philosophical Transactions of the Royal Society A **366**(1869): 1455-1468.

Bowles, A. P., C. D. F. Honig and W. A. Ducker (2011). "No-slip boundary condition for weak solid-liquid interactions." Journal of Physical Chemistry C **115**(17): 8613-8621.

Brenner, H. and V. Ganesan (2000). "Molecular wall effects: Are conditions at a boundary “boundary conditions”?" Physical Review E **61**(6): 6879-6897.

Brigo, L., M. Natali, M. Pierno, F. Mammano, C. Sada, G. Fois, A. Pozzato, S. dal Zilio, M. Tormen and G. Mistura (2008). "Water slip and friction at a solid surface." Journal of Physics: Condensed Matter **20**(35): 354016 (354015 pp.).

Brunauer, S., P. H. Emmett and E. Teller (1938). "Adsorption of Gases in Multimolecular Layers." Journal of the American Chemical Society **60**(2): 309-319.

Burgdorfer, A. (1959). "Influence of molecular mean free path on performance of hydrodynamic gas lubricated bearings." Journal of Basic Engineering **81, Series D**(1): 98-100.

Butt, H.-J., K. Graf and M. Kappl (2004). Physics and Chemistry of Interfaces, Wiley-VCH Verlag GmbH & Co. KGaA.

Butt, H. J., K. Graf and M. Kappl (2006). Physics and Chemistry of Interfaces, Wiley.

Bychuk, O. V. and B. O'Shaughnessy (1995). "Anomalous Diffusion at Liquid Surfaces." Physical Review Letters **74**(10): 1795-1798.

Cahill, D. G., W. K. Ford, K. E. Goodson, G. D. Mahan, A. Majumdar, H. J. Maris, R. Merlin and S. R. Phillpot (2003). "Nanoscale thermal transport." Journal of Applied Physics **93**(2): 793-818.

Cheng, L., P. Fenter, K. L. Nagy, M. L. Schlegel and N. C. Sturchio (2001). "Molecular-scale density oscillations in water adjacent to a mica surface." Physical Review Letters **87**(15): 156103/156101-156103/156104.

Choi, C.-H. and C.-J. Kim (2006). "Large slip of aqueous liquid flow over a nanoengineered superhydrophobic surface." Physical Review Letters **96**(6): 066001-066001.

Choi, C.-H., K. J. A. Westin and K. S. Breuer (2003). "Apparent slip flows in hydrophilic and hydrophobic microchannels." PHYSICS OF FLUIDS **15**(10): 2897-2902.

Churaev, N. V., J. Ralston, I. P. Sergeeva and V. D. Sobolev (2002). "Electrokinetic properties of methylated quartz capillaries." Advances in Colloid and Interface Science **96**(1-3): 265-278.

Cottin-Bizonne, C., C. Barentin, E. Charlaix, L. Bocquet and J. L. Barrat (2004). "Dynamics of simple liquids at heterogeneous surfaces: Molecular-dynamics simulations and hydrodynamic description." European Physical Journal E **15**(4): 427-438.

Cottin-Bizonne, C., B. Cross, A. Steinberger and E. Charlaix (2005). "Boundary slip on smooth hydrophobic surfaces: Intrinsic effects and possible artifacts." Physical Review Letters **94**(5): 1-4.

Craig, V. S. J., C. Neto and D. R. M. Williams (2001). "Shear-dependent boundary slip in an aqueous Newtonian liquid." Physical Review Letters **87**(5): 054504-054501.

Cucchetti, A. and S. C. Ying (1996). "Memory effects in the frictional damping of diffusive and vibrational motion of adatoms." Physical Review B **54**(5): 3300-3310.

Dadzie, S. K. S. K. and J. G. J. G. Meolans (2005). "Temperature jump and slip velocity calculations from an anisotropic scattering kernel." Physica A **358**(2-4): 328-346.

Daikhin, L., E. Gileadi, V. Tsionsky, M. Urbakh and G. Zilberman (2000). "Slippage at adsorbate-electrolyte interface. Response of electrochemical quartz crystal microbalance to adsorption." Electrochimica Acta **45**(22): 3615-3621.

Darling, G. R. and S. Holloway (1994). "The role of parallel momentum in the dissociative adsorption of H2 at highly corrugated surfaces." Surface Science **304**(3): 461-467.

de Gennes, P. G. (2002). "On fluid/wall slippage." Langmuir **18**(9): 3413-3414.

Deissler, R. G. (1964). "An analysis of second-order slip flow and temperature-jump boundary conditions for rarefied gases." International Journal of Heat and Mass Transfer **7**(6): 681-694.

Devienne, F. M. (1965). Low Density Heat Transfer. Advances in Heat Transfer. J. James P. Hartnett and Thomas F. Irvine, Elsevier. **Volume 2:** 271-356.

Du, B., I. Goubaidoulline and D. Johannsmann (2004). "Effects of laterally heterogeneous slip on the resonance properties of quartz crystals immersed in liquids." Langmuir **20**(24): 10617-10624.

Ellis, J. S., G. McHale, G. L. Hayward and M. Thompson (2003). "Contact angle-based predictive model for slip at the solid-liquid interface of a transverse-shear mode acoustic wave device." Journal of Applied Physics **94**(9): 6201-6207.

Extrand, C. W. (2003). "Contact angles and hysteresis on surfaces with chemically heterogeneous islands." Langmuir **19**(9): 3793-3796.

Fukui, S. and R. Kaneko (1988). "Analysis of ultra-thin gas film lubrication based on linearized Boltzmann equation: first reports - derivation of a generalised lubrication equation including thermal creep flow." Journal of Tribology **110**(2): 253-262.

Gad-el-Hak, M. (2003). "Comments on "Critical view on new results in micro-fluid mechanics"." International Journal of Heat and Mass Transfer **46**(20): 3941-3945.

Gao, L. and T. J. McCarthy (2007). "How Wenzel and Cassie were wrong." Langmuir **23**(7): 3762-3765.

Ge, Z., D. G. Cahill and P. V. Braun (2004). "AuPd Metal Nanoparticles as Probes of Nanoscale Thermal Transport in Aqueous Solution." The Journal of Physical Chemistry B **108**(49): 18870-18875.

Ge, Z., D. G. Cahill and P. V. Braun (2006). "Thermal Conductance of Hydrophilic and Hydrophobic Interfaces." Physical Review Letters **96**(18): 186101.

Goicochea, J. V., M. Hu, B. Michel and D. Poulikakos (2011). "Surface functionalization mechanisms of enhancing heat transfer at solid-liquid interfaces." Journal of Heat Transfer **133**(8).

Gomes, K. K., W. Mar, W. Ko, F. Guinea and H. C. Manoharan (2012). "Designer Dirac fermions and topological phases in molecular graphene." Nature **483**(7389): 306-310.

Govardhan, R. N., G. S. Srinivas, A. Asthana and M. S. Bobji (2009). "Time dependence of effective slip on textured hydrophobic surfaces." PHYSICS OF FLUIDS **21**(5): 052001 (052008 pp.).

Granick, S., Y. Zhu and H. Lee (2003). "Slippery questions about complex fluids flowing past solids." Nature Materials **2**(4): 221-227.

Graur, I. A., P. Perrier, W. Ghozlani and J. G. Méolans (2009). "Measurements of tangential momentum accommodation coefficient for various gases in plane microchannel." PHYSICS OF FLUIDS **21**(10).

Groß, A. (2009). Theoretical Surface Science [electronic resource] : A Microscopic Perspective / by Axel Groß, Berlin, Heidelberg : Springer-Verlag Berlin Heidelberg, 2009.

Gutfreund, P., M. Wolff, M. MacCarini, S. Gerth, J. F. Ankner, J. Browning, C. E. Halbert, H. Wacklin and H. Zabel (2011). "Depletion at solid/liquid interfaces: Flowing hexadecane on functionalized surfaces." Journal of Chemical Physics **134**(6).

Hall, R. O. A. and D. G. Martin (1987). "The evaluation of temperature jump distances and thermal accommodation coefficients from measurements of the thermal conductivity of UO2 packed sphere beds." Nuclear Engineering and Design **101**(3): 249-258.

Harley, J. C., Y. Huang, H. H. Bau and J. N. Zemel (1995). "Gas flow in micro-channels." Journal of Fluid Mechanics **284**: 257-274.

Harting, J., C. Kunert and J. Hyväluoma (2010). "Lattice Boltzmann simulations in microfluidics: Probing the no-slip boundary condition in hydrophobic, rough, and surface nanobubble laden microchannels." Microfluidics and Nanofluidics **8**(1): 1-10.

Hersht, I. and Y. Rabin (1994). "Shear melting of solid-like boundary layers in thin liquid films." Journal of Non-Crystalline Solids **172-174**(PART 2): 857-861.

Ho, T. A., D. V. Papavassiliou, L. L. Lee and A. Strioloa (2011). "Liquid water can slip on a hydrophilic surface." Proceedings of the National Academy of Sciences of the United States of America **108**(39): 16170-16175.

Honig, C. D. F. and W. A. Ducker (2007). "No-slip hydrodynamic boundary condition for hydrophilic particles." Physical Review Letters **98**(2).

Honig, C. D. F., J. E. Sader, P. Mulvaney and W. A. Ducker (2010). "Lubrication forces in air and accommodation coefficient measured by a thermal damping method using an atomic force microscope." Physical Review E **81**(5): 056305 (056311 pp.).

Horn, R. G., O. I. Vinogradova, M. E. Mackay and N. Phan-Thien (2000). "Hydrodynamic slippage inferred from thin film drainage measurements in a solution of nonadsorbing polymer." Journal of Chemical Physics **112**(14): 6424-6433.

Hu, M., J. V. Goicochea, B. Michel and D. Poulikakos (2009). "Thermal rectification at water/functionalized silica interfaces." Applied Physics Letters **95**(15).

Huang, P. and K. S. Breuer (2007). "Direct measurement of slip length in electrolyte solutions." Physics of Fluids (1994-present) **19**(2): 028104.

Huang, P. and K. S. Breuer (2010). "Direct measurement of slip length in electrolyte solutions." SOCAR Proceedings **2010**(2): 81-85.

Huang, P., J. S. Guasto and K. S. Breuer (2006). "Direct measurement of slip velocities using three-dimensional total internal reflection velocimetry." Journal of Fluid Mechanics **566**: 447-464.

Huang, W., D. B. Bogy and A. L. Garcia (1997). "Three-dimensional direct simulation Monte Carlo method for slider air bearings." PHYSICS OF FLUIDS **9**(6): 1764-1769.

Ibach, H. (2006). Physics of Surfaces and Interfaces, Berlin, Heidelberg : Springer-Verlag Berlin Heidelberg, 2006.

Ishida, N., T. Inoue, M. Miyahara and K. Higashitani (2000). "Nano bubbles on a hydrophobic surface in water observed by tapping-mode atomic force microscopy." Langmuir **16**(16): 6377-6380.

Israelachvili, J. N. (2011). Intermolecular and surface forces / Jacob N. Israelachvili, Burlington, MA : Academic Press, 2011.
3rd ed.

Joly, L., C. Ybert and L. Bocquet (2006). "Probing the nanohydrodynamics at liquid-solid interfaces using thermal motion." Physical Review Letters **96**(4): 046101-046101.

Kannam, S. K., B. D. Todd, J. S. Hansen and P. J. Daivis (2011). "Slip flow in graphene nanochannels." Journal of Chemical Physics **135**(14).

Kapitza, P. (1941). "The study of heat transfer in helium II." J. Phys.(USSR) **4**(3): 181-210.

Karniadakis, G., A. Beskök and N. R. Aluru (2005). Microflows and nanoflows : fundamentals and simulation. New York, NY, Springer.

Kennard, E. H. (1938). Kinetic Theory of Gases. New York, McGraw Hill Book Company.

Kim, B. H., A. Beskok and T. Cagin (2008). "Molecular dynamics simulations of thermal resistance at the liquid-solid interface." Journal of Chemical Physics **129**(17).

Kolasinski, K. W. (2008). Surface science : foundations of catalysis and nanoscience / Kurt W Kolasinski, Chichester, England ; Hoboken, NJ : Wiley, c2008.
2nd ed.

Krim, J. (2012). "Friction and energy dissipation mechanisms in adsorbed molecules and molecularly thin films." Advances in Physics **61**(3): 155-323.

Lamb, H. (1932). Hydrodynamics. Cambridge [Eng.], The University Press.

Lau, K. K. S., J. Bico, K. B. K. Teo, M. Chhowalla, G. A. J. Amaratunga, W. I. Milne, G. H. McKinley and K. K. Gleason (2003). "Superhydrophobic carbon nanotube forests." Nano Letters **3**(12): 1701-1705.

Lauga, E. (2004). "Apparent slip due to the motion of suspended particles in flows of electrolyte solutions." Langmuir **20**(20): 8924-8930.

Lauga, E. and M. P. Brenner (2004). "Dynamic mechanisms for apparent slip on hydrophobic surfaces." Physical Review E **70**(2): 26311-26311.

Lauga, E., M. P. Brenner and H. A. Stone (2007). Microfluidics: The No-Slip Boundary Condition. Springer Handbook of Experimental Fluid Mechanics. C. Tropea, A. L. Yarin and J. F. Foss. Berlin, Springer**:** 1219-1240.

Lauga, E. and T. M. Squires (2005). "Brownian motion near a partial-slip boundary: a local probe of the no-slip condition." PHYSICS OF FLUIDS **17**(10): 103102-103101.

Léger, L., H. Hervet, G. Massey and E. Durliat (1997). "Wall slip in polymer melts." Journal of Physics Condensed Matter **9**(37): 7719-7740.

Lichter, S., A. Martini, R. Q. Snurr and Q. Wang (2007). "Liquid slip in nanoscale channels as a rate process." Physical Review Letters **98**(22).

Lichter, S., A. Roxin and S. Mandre (2004). "Mechanisms for liquid slip at solid surfaces." Physical Review Letters **93**(8): 086001-086001-086001-086004.

Liu, C. and L. Lees (1960). Kinetic theory description of plane compressible Couette flow.

Lou, S.-T., Z.-Q. Ouyang, Y. Zhang, L. Xiao-Jun, H. Jun, L. Min-Qian and Y. Fu-Jia (2000). "Nanobubbles on solid surface imaged by atomic force microscopy." Journal of Vacuum Science and Technology B **18**(5): 2573-2575.

Luntz, A. C. (2000). "Simple model for associative desorption and dissociative chemisorption." Journal of Chemical Physics **113**(16): 6901-6905.

Maali, A. and B. Bhushan (2008). "Slip-length measurement of confined air flow using dynamic atomic force microscopy." Physical Review E **78**(2): 027302 (027304 pp.).

Martini, A., H. Hua-Yi, N. A. Patankar and S. Lichter (2008a). "Slip at high shear rates." Physical Review Letters **100**(20): 206001-206001.

Martini, A., A. Roxin, R. Q. Snurr, Q. Wang and S. Lichter (2008b). "Molecular mechanisms of liquid slip." Journal of Fluid Mechanics **600**: 257-269.

Maxwell, J. C. (1879). "On stresses in rarefied gases arising from inequalities of temperature." Philosophical Transactions of the Royal Society Part 1 **170**: 231-256.

Mazo, R. M. (1955). Theoretical studies on low temperature phenomena, Yale University.

McHale, G. (2007). "Cassie and Wenzel: Were they really so wrong?" Langmuir **23**(15): 8200-8205.

McHale, G. and M. I. Newton (2004). "Surface roughness and interfacial slip boundary condition for quartz crystal microbalances." Journal of Applied Physics **95**(1): 373-380.

Michelsen, H. A. and D. J. Auerbach (1991). "A critical examination of data on the dissociative adsorption and associative desorption of hydrogen at copper surfaces." Journal of Chemical Physics **94**(11): 7502-7520.

Murad, S. and I. K. Puri (2008). "Thermal transport across nanoscale solid-fluid interfaces." Applied Physics Letters **92**(13).

Murad, S. and I. K. Puri (2012). "Communication: Thermal rectification in liquids by manipulating the solid-liquid interface." Journal of Chemical Physics **137**(8).

Murad, S. and I. K. Puri (2013). "A thermal logic device based on fluid-solid interfaces." Applied Physics Letters **102**(19): 193109-193104.

Myong, R. S. (2004). "Gaseous slip models based on the Langmuir adsorption isotherm." PHYSICS OF FLUIDS **16**(1): 104-117.

Navier, C. (1823). "Memoirs de l'Academie." Royale des Sciences de l'Institut de France **1**: 414-416.

Neto, C., D. R. Evans, E. Bonaccurso, H. J. Butt and V. S. J. Craig (2005). "Boundary slip in Newtonian liquids: A review of experimental studies." Reports on Progress in Physics **68**(12): 2859-2897.

Oner, D. and T. J. McCarthy (2000). "Ultrahydrophobic surfaces. Effects of topography length scales on wettability." Langmuir **16**(20): 7777-7782.

Ou, J., B. Perot and J. P. Rothstein (2004). "Laminar drag reduction in microchannels using ultrahydrophobic surfaces." PHYSICS OF FLUIDS **16**(12): 4635-4643.

Oura, K., V. G. Lifshits, A. A. Saranin, A. V. Zotov and M. Katayama (2003). Surface Science: An Introduction. Berlin ; New York, Springer.

Pahlavan, A. A. and J. B. Freund (2011). "Effect of solid properties on slip at a fluid-solid interface." Physical Review E (Statistical, Nonlinear, and Soft Matter Physics) **83**(2): 021602 (021607 pp.).

Perisanu, S. and G. Vermeulen (2006). "Curvature, slip, and viscosity in 3He-4He mixtures." Physical Review B **73**(13): 134517-134511.

Pfahler, J., J. Harley, H. Bau and J. N. Zemel (1991). Gas and liquid flow in small channels, Atlanta, GA, USA, Publ by ASME.

Pollack, G. L. (1969). "Kapitza resistance." Reviews of Modern Physics **41**(1): 48-81.

Prasher, R. S. and P. E. Phelan (2001). "A scattering-mediated acoustic mismatch model for the prediction of thermal boundary resistance." Journal of Heat Transfer **123**(1): 105-112.

Rice, B. and C. J. G. Raw (1974). "The assumption of elastic collisions in elementary gas kinetic theory." Journal of Chemical Education **51**(2): 139.

Richardson, S. (1973). "On the no-slip boundary condition." Journal of Fluid Mechanics **59**: 707-719.

Rodrigues, T. S., H. J. Butt and E. Bonaccurso (2010). "Influence of the spring constant of cantilevers on hydrodynamic force measurements by the colloidal probe technique." Colloids and Surfaces A **354**(1-3): 72-80.

Ruckenstein, E. and P. Rajora (1983). "On the no-slip boundary condition of hydrodynamics." Journal of Colloid and Interface Science **96**(2): 488-491.

Saxena, S. C., Joshi, R.K. (1989). Thermal Accommodation and Adsorption Coefficients of Gases. New York, Hemisphere Publishing Company.

Schäfer, K., W. Rating and A. Eucken (1942). "Über den Einfluß des gehemmten Austauschs der Translations‐ und Schwingungsenergie auf das Wärmeleitvermögen der Gase." Annalen der Physik **434**(2‐3): 176-202.

Sharatchandra, M. C., M. Sen and M. Gad-El-Hak (1998). "Thermal aspects of a novel viscous pump." Journal of Heat Transfer **120**(1): 99-107.

Shenogina, N., R. Godawat, P. Keblinski and S. Garde (2009). "How wetting and adhesion affect thermal conductance of a range of hydrophobic to hydrophilic aqueous interfaces." Physical Review Letters **102**(15).

Shih, J. C., C. M. Ho, J. Liu and Y. C. Tai (1996). "Monatomic and polyatomic gas flow through uniform microchannels." American Society of Mechanical Engineers, Dynamic Systems and Control Division (Publication) DSC **59**: 197-203.

Spikes, H. and S. Granick (2003). "Equation for slip of simple liquids at smooth solid surfaces." Langmuir **19**(12): 5065-5071.

Swartz, E. T. and R. O. Pohl (1989). "Thermal boundary resistance." Reviews of Modern Physics **61**(3): 605-668.

Ternes, M., C. P. Lutz, C. F. Hirjibehedin, F. J. Giessibl and A. J. Heinrich (2008). "The Force Needed to Move an Atom on a Surface." Science **319**(5866): 1066-1069.

Thompson, P. A. and M. O. Robbins (1990). "Shear flow near solids: Epitaxial order and flow boundary conditions." Physical Review A **41**(12): 6830-6837.

Thompson, P. A. and S. M. Troian (1997). "A general boundary condition for liquid flow at solid surfaces." Nature **389**(6649): 360-362.

Thorman, R. P. and S. L. Bernasek (1981). "The internal energy distribution of atom-recombination product N[sub 2] desorbing from polycrystalline Fe." The Journal of Chemical Physics **74**(11): 6498-6504.

Tolstoi, D. M. (1952). "Molecular theory of the gliding of liquids on solid surfaces." Doklady Akademii Nauk SSSR **85**(5): 1089-1092.

Tretheway, D. C. and C. D. Meinhart (2002). "Apparent fluid slip at hydrophobic microchannel walls." PHYSICS OF FLUIDS **14**(3): L9-L12.

Tretheway, D. C. and C. D. Meinhart (2004). "A generating mechanism for apparent fluid slip in hydrophobic microchannels." PHYSICS OF FLUIDS **16**(5): 1509-1515.

Trott, W. M., D. J. Rader, J. N. Castaneda, J. R. Torczynski and T. A. Abe (2008). Measurement of gas-surface accommodation, USA, AIP.

Truesdell, R., A. Mammoli, P. Vorobieff, F. van Swol and C. J. Brinker (2006). "Drag reduction on a patterned superhydrophobic surface." Physical Review Letters **97**(4): 044504-044501.

Ulmanella, U. and C.-M. Ho (2008). Molecular effects on boundary condition in micro/nanoliquid flows, 2 Huntington Quadrangle, Suite N101, Melville, NY 11747-4502, United States, American Institute of Physics.

Vinogradova, O. I. (1995). "Drainage of a thin liquid film confined between hydrophobic surfaces." Langmuir **11**(6): 2213-2213.

Vinogradova, O. I. and G. E. Yakubov (2006). "Surface roughness and hydrodynamic boundary conditions." Physical Review E **73**(4): 45302-45301.

von Helmholtz, H. and G. von Piotrowski (1860). "Über Reibung tropfbarer Flüssigkeiten." Sitz. Math.-Naturwiss. Kl. Akad. Wiss. Wien **40**: 607-658.

von Smoluchowski, M. S. (1898). "Ueber wärmeleitung in verdünnten gasen." Annalen der Physik **300**(1): 101-130.

Voronov, R. S., D. V. Papavassiliou and L. L. Lee (2007). "Slip length and contact angle over hydrophobic surfaces." Chemical Physics Letters **441**(4-6): 273-276.

Voronov, R. S., D. V. Papavassiliou and L. L. Lee (2008). "Review of fluid slip over superhydrophobic surfaces and its dependence on the contact angle." Industrial and Engineering Chemistry Research **47**(8): 2455-2477.

Wang, F.-C. and Y.-P. Zhao (2011). "Slip boundary conditions based on molecular kinetic theory: The critical shear stress and the energy dissipation at the liquid-solid interface." Soft Matter **7**(18): 8628-8634.

Wang, Y. and P. Keblinski (2011). "Role of wetting and nanoscale roughness on thermal conductance at liquid-solid interface." Applied Physics Letters **99**(7).

Watanabe, K., T. Takayama, S. Ogata and S. Isozaki (2003). "Flow between two coaxial rotating cylinders with a highly water-repellent wall." AIChE Journal **49**(8): 1956-1963.

Willmott, G. R. and J. L. Tallon (2007). "Measurement of Newtonian fluid slip using a torsional ultrasonic oscillator." Physical Review E **76**(6): 066306-066301.

Wolff, M., B. Akgun, M. Walz, A. Magerl and H. Zabel (2008). "Slip and depletion in a Newtonian liquid." EPL **82**(3).

Xue, H. and Q. Fan (2000). "A new analytic solution of the Navier-Stokes equations for microchannel flow." Microscale Thermophysical Engineering **4**(2): 125-143.

Xue, L., P. Keblinski, S. R. Phillpot, S. U. S. Choi and J. A. Eastman (2003). "Two regimes of thermal resistance at a liquid-solid interface." Journal of Chemical Physics **118**(1): 337-339.

Yamaguchi, H., K. Kanazawa, Y. Matsuda, T. Niimi, A. Polikarpov and I. Graur (2012). "Investigation on heat transfer between two coaxial cylinders for measurement of thermal accommodation coefficient." Physics of Fluids (1994-present) **24**(6): 062002.

Yang, F. (2010). "Slip boundary condition for viscous flow over solid surfaces." Chemical Engineering Communications **197**(4): 544-550.

Yang, J., J. Duan, D. Fornasiero and J. Ralston (2003). "Very small bubble formation at the solid-water interface." Journal of Physical Chemistry B **107**(25): 6139-6147.

Yong, X. and L. T. Zhang (2012). "Slip in nanoscale shear flow: mechanisms of interfacial friction." 1-10.

Zhang, X. H., X. D. Zhang, S. T. Lou, Z. X. Zhang, J. L. Sun and J. Hu (2004). "Degassing and temperature effects on the formation of nanobubbles at the mica/water interface." Langmuir **20**(9): 3813-3815.

Zhu, Y. and S. Granick (2001). "Rate-dependent slip of Newtonian liquid at smooth surfaces." Physical Review Letters **87**(9): 961051-961054.

Zhu, Y. and S. Granick (2002a). "Apparent slip of Newtonian fluids past adsorbed polymer layers." Macromolecules **35**(12): 4658-4663.

Zhu, Y. and S. Granick (2002b). "Limits of the hydrodynamic no-slip boundary condition." Physical Review Letters **88**(10): 1061021-1061024.

Zhu, Y. and S. Granick (2004). "Superlubricity: A paradox about confined fluids resolved." Physical Review Letters **93**(9): 096101-096101-096101-096104.

Ziarani, A. S. and A. A. Mohamad (2008). "Effect of wall roughness on the slip of fluid in a microchannel." Nanoscale and Microscale Thermophysical Engineering **12**(2): 154-169.

Zohar, Y., S. Y. K. Lee, W. Y. Lee, L. Jiang and P. Tong (2002). "Subsonic gas flow in a straight and uniform microchannel." Journal of Fluid Mechanics(472): 125-151.